

# Assessment of Dancoff Adjusted Wigner-Seitz Cells for Self-Shielding LWR Lattices

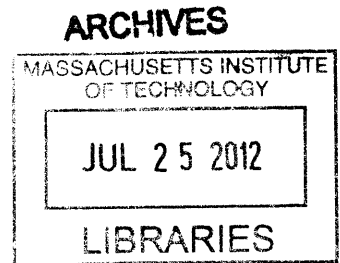
by

Thomas Hayward Roomy

Submitted to the Department of Nuclear Science and Engineering in Partial Fulfillment of the Requirements for the Degree of

Master of Science in Nuclear Science and Engineering

at the  
Massachusetts Institute of Technology  
June 2012



© Massachusetts Institute of Technology, 2012, All rights reserved

Signature of Author: \_\_\_\_\_  
Department of Nuclear Science and Engineering  
May 12, 2012

Certified By: \_\_\_\_\_  
Benoit Forget, Ph.D.  
Assistant Professor of Nuclear Engineering  
Thesis Supervisor

Certified By: \_\_\_\_\_  
Kord Smith, Ph.D.  
KEPCO Professor of the Practice of Nuclear Engineering  
Thesis Reader

Accepted By: \_\_\_\_\_  
Mujid S. Kazimi, Ph.D.  
Chair, Committee on Graduate Students

# Assessment of Dancoff Adjusted Wigner-Seitz Cells for Self-Shielding LWR Lattices

By

Thomas Hayward Roomy

Submitted to the Department of Nuclear Science and Engineering on May 11, 2012, in partial fulfillment of the requirements for the Degree of Master of Science in  
*Nuclear Science and Engineering*

## Abstract

The objective of this thesis was to assess the effectiveness of using a Wigner-Seitz (WS) cell with an adjusted moderator thickness to produce more accurate resonance self-shielded cross sections for light water reactor (LWR) lattices. The WS approximation has been commonly used in lattice physics calculations for many decades regardless that it has been shown to underestimate  $k$ -eff for an infinite LWR lattice by several hundred pcm.

The WS cell moderator thickness was adjusted in order make the WS cell Dancoff correction match that for the square unit cell. It was shown that the effectiveness of this method is sensitive to the Dancoff correction which was being calculated from the real three-dimensional geometry because in practice users commonly employ unconverged values for the Dancoff correction. For an infinite lattice the Dancoff adjusted Wigner-Seitz cell (DAWSC) resulted in small improvements in  $k$ -eff (~20 pcm) and reaction rates when using converged Dancoff corrections, however much larger improvements in values (up to 220 pcm) were seen for unconverged values of Dancoff corrections.

When the DAWSC method was applied to a boiling water reactor (BWR) bundle,  $k$ -eff was worse for the DAWSC cases than for the normal WS cell treatment relative to continuous energy results. Improvements were seen in  $U^{238}$  absorption reaction rates for DAWSC cases in the inner fuel pins of the bundle; however the results were the opposite for fuel pins on the outer edges of the bundle. These results showed that the DAWSC method failed to account for irregularities in the bundle for the Dancoff corrections that were calculated.

The Dancoff correction calculation sequence was evaluated against CASMO4e. Good agreement (-0.34% difference) was seen for infinite lattices, however large variations (+5% to -4%) were seen among neighboring pins in a BWR lattice. These results for Dancoff correction prediction along with the significant improvements seen in  $k$ -eff for infinite lattices using *unconverged* Dancoff corrections implies that the DAWSC method may work if given the correct values for Dancoff corrections. The originally intended use for a Dancoff correction was to adjust the fuel escape probability for a particular energy group. Conversely, the application of DAWSC uses a single Dancoff correction to effectively change the fuel escape probability for all energy groups. A method for calculating an appropriate Dancoff correction for use in the DAWSC method should be investigated.

Thesis: Supervisor: Benoit Forget

Title: Assistant Professor of Nuclear Science and Engineering

# Acknowledgements

I would like to express my sincere appreciation to Ben Forget for allowing me the freedom to tackle the subject of this thesis while at the same time offering constructive advice throughout the process. I'm also very grateful for the financial support that he was able to offer me in the form of a teaching assistantship and through the Nuclear Regulatory Commission's Faculty Development Grant.

Thanks are also due to Kord Smith for serving as the reader for this thesis. His suggestions from classes and for this thesis were generally insightful to the process of validating models and will not be forgotten.

Many thanks are due to members of the group of Scale developers and users at Oak Ridge National Laboratory (ORNL) without whom this research would not have been possible. Particular thanks go to Brad Rearden for setting up my second internship at ORNL in order to begin my work on the subject of this thesis. Thanks are also due to Robert and Jordan Lefebvre for their willingness to and aptitude for answering my many questions regarding the Scale infrastructure, data structures and general computer science knowledge. I'd also like to extend my gratitude to Thomas Miller for spending a significant amount of time teaching me how Scale works among other things. Bruce Patton also deserves thanks for teaching me how to compile and build Scale.

The contributions from officemate and friend Koroush Shirvan also requires thanks due to countless hours of discussing my ideas and the useful criticisms which were developed.

All of the above mentioned people were not only professionally outstanding but were also very pleasant to work with which helped make the past 2 years at MIT and at ORNL very enjoyable. I am very gracious for this.

# Table of Contents

Abstract .....	iii
Acknowledgements .....	iv
List of Figures .....	v
List of Tables .....	viii
Introduction .....	1-1
- Background .....	2-1
2.1 - Slowing Down Theory .....	2-1
2.2 - Slowing Down in Infinite Media .....	2-4
2.3 - Slowing Down in Infinite Media with a Resonate Absorber .....	2-6
2.3.1 - Narrow Resonance Approximation .....	2-7
2.3.2 - Wide Resonance Approximation .....	2-9
2.4 - Equivalence Theory .....	2-9
2.4.1 - An Isolated Fuel Lump .....	2-9
2.4.2 - A Lattice of Fuel Lumps .....	2-13
2.5 - Ultrafine Group Method of Self-Shielding .....	2-14
- Methods .....	3-1
3.1 – Scale6.1 .....	3-1
3.1.1 - BONAMI .....	3-2
3.1.2 - WORKER .....	3-4
3.1.3 - CENTRM .....	3-4
3.1.4 - PMC .....	3-6
3.1.5 - NEWT .....	3-7

3.1.6 - KENO-VI.....	3-7
3.1.7 - MCDancoff.....	3-7
3.2 - MCNP5.....	3-8
3.3 - STEDFAST .....	3-9
– Results and Discussion .....	4-1
4.1 - Analysis of the Wigner-Seitz Cell Approximation.....	4-1
4.2 - Dancoff Factor Adjustments to the Wigner-Seitz Cell.....	4-5
4.3 - Effects of Dancoff Factor Adjustments on Infinite Lattices.....	4-10
4.4 - Effects of Dancoff Factor Adjustments on Irregular Lattices .....	4-14
4.5 - Analysis of Dancoff Corrections .....	4-27
Chapter 5 - Conclusions.....	5-1
Appendix A.....	6-1
MCNP5 Input for a Square Cell.....	6-1
Appendix B .....	7-1
NEWT Input for a Square Cell Using Dan2pitch .....	7-1
KENO-VI Input for a Square Cell Using Dan2pitch .....	7-2
Appendix C .....	8-1
NEWT Input for a BWR Bundle Using Dan2pitch .....	8-1
MCNP5 Input for a BWR Bundle.....	8-10
References.....	9-1



# List of Figures

Figure 1-1: Plot of the KENO continuous energy $U^{238}$ absorption cross section at 293 K in the resolved resonance energy region. The Scale 238 neutron group library is also shown. This plot was generated using Javapeno from the Scale6.1 package. ....	1-2
Figure 1-2 Figure 2: Diagram of a unit cell for an infinite square lattice and an equivalent Wigner-Seitz cell using a white boundary condition .....	1-3
Figure 3-1: Scale flow diagram for a typical calculation used in this study. ....	3-2
Figure 4-1: Percent Difference in Flux in the Fuel for Equivalent Cylindrical Unit Cells Using Reflective and White Boundary Conditions Relative to a Square Unit Cell. All error bars depicted represent a 99% confidence interval. ....	4-2
Figure 4-2: Percent Difference in Flux in the Moderator for Equivalent Cylindrical Unit Cells Using Reflective and White Boundary Conditions Relative to a Square Unit Cell. All error bars depicted represent a 99% confidence interval. ....	4-2
Figure 4-3: Square pin cell and equivalent Wigner-Seitz cell with reflective boundary condition. Same incident direction and location. Taken from [Reference] with permission. ....	4-3
Figure 4-4: Percent difference in flux in the moderator and fuel for a Wigner-Seitz cell using a white boundary condition relative to a square unit cell. All error bars depicted represent a 99% confidence interval. ....	4-4
Figure 4-5: Unit cell geometry for a square lattice element, an equivalent Wigner-Seitz cell and several Dancoff correction adjusted Wigner-Seitz cells with dimensions listed in Table 4-3. Side A depicts the all of the unit cells while Side B shows a close up of the unit cell boundaries. ....	4-6
Figure 4-6: Percent difference in flux in the fuel for a normal Wigner-Seitz cell where the volume of moderator is conserved as well as for three different Dancoff adjusted Wigner-Seitz cells. Percent difference is relative to the actual square unit cell. All error bars depicted represent a 99% confidence interval. ....	4-8
Figure 4-7: $U^{238}$ absorption reaction rates for a normal Wigner-Seitz cell where the volume of moderator is conserved as well as for three different Dancoff adjusted Wigner-Seitz cells. Percent difference is relative to	

the actual square unit cell. All error bars represent 99% confidence intervals.....	4-9
Figure 4-8: $U^{235}$ fission reaction rates for a normal Wigner-Seitz cell where the volume of moderator is conserved as well as for three different Dancoff correction adjusted Wigner-Seitz cells. Percent difference is relative to the actual square unit cell. All error bars represent 99% confidence intervals. ....	4-10
Figure 4-9: Percent difference relative to MCNP5 in $U^{238}$ absorption microscopic cross sections CENTRM using several Dancoff adjusted Wigner-Seitz cell.....	4-12
Figure 4-10: 99% confidence intervals for the percent difference in $U^{235}$ fission reaction rates for a BWR fuel pin with reflective boundary conditions. Four different self-shielded cross section sets are compared and used with KENO-VI. Percent differences are relative to the actual square unit cell which was modeled with MCNP5. ....	4-13
Figure 4-11: 99% confidence intervals for the percent difference in $U^{238}$ absorption reaction rates for a BWR fuel pin with reflective boundary conditions. Four different self-shielded cross section sets are compared and used with KENO-VI. Percent differences are relative to the actual square unit cell which was modeled with MCNP5. ....	4-14
Figure 4-12: The problem geometry used in all simulations. A typical BWR bundle geometry using two fuel pin types with the wide bundle gap on the top and left side of the shroud. This figure was produced using Scale 6.1.....	4-15
Figure 4-13: Unit/universe maps for the lattice before and after pins are grouped by Dancoff correction for a BWR bundle with a void fraction of 40 % for the moderator. Dancoff correction maps using fuel heights of 10 cm, 40 cm, and 160 cm in MCDancoff are shown. All Dancoff correction relative uncertainties are less than 0.15 .....	4-17
Figure 4-14: Pin power from MCNP5 and the percent difference from NEWT. ....	4-19
Figure 4-15: Unit 34 (Inner Fuel Pin) $U^{238}$ reaction rate percent differences among self-shielding models relative to MCNP5 continuous energy results.....	4-21
Figure 4-16: Unit 33 (Inner Fuel Pin with gadolinia) $U^{238}$ reaction rate percent differences among self-shielding models relative to MCNP5 continuous energy results.....	4-21
Figure 4-17: Unit 15 (Side Pins on Narrow Gap) $U^{238}$ reaction rate percent differences among self-shielding models relative to MCNP5 continuous energy results.....	4-22



Figure 4-18: Unit 145 (Side Pins on Wide Gap) $U^{238}$ reaction rate percent differences among self-shielding models relative to MCNP5 continuous energy results. ....	4-22
Figure 4-19: Unit 429 (Corner Pins between Wide and Narrow ) $U^{238}$ reaction rate percent differences among self-shielding models relative to MCNP5 continuous energy results.....	4-23
Figure 4-20: Unit 209 (Corner Pin between Narrow Gaps) $U^{238}$ reaction rate percent differences among self-shielding models relative to MCNP5 continuous energy results.....	4-23
Figure 4-21: Unit 11 (Corner Pin between Wide Gaps) $U^{238}$ reaction rate percent differences among self-shielding models relative to MCNP5 continuous energy results.....	4-24
Figure 4-22: Dancoff correction predictions for a BWR bundle at 40% void fraction using CASMO4e and MCDancoff with several different fuel heights used in the model. ....	4-30
Figure 4-23: Altered reflected unit cells to emphasize the effect of water (left) and Zirc2 (right) on the Dancoff corrections predicted by MCDancoff and CASMO4e.....	4-32
Figure 4-24: Plot of the total cross section for $H^1$ in the resolved resonance region. The one group cross section used by MCDancoff and the 238 group ENDF/B-VI.8 cross sections are shown. This plot was generated using Javapeno from the Scale6.1 package. [Reference Scale6.1] .....	4-34
Figure 4-25: Plot of the total cross section for Zr in the resolved resonance region. The one group cross section used by MCDancoff and the 238 group ENDF/B-VI.8 cross sections are shown. This plot was generated using Javapeno from the Scale6.1 package. [Reference Scale6.1] .....	4-35

# List of Tables

Table 4-1: Model parameters for a UO<sub>2</sub> pin cell modeled in MCNP5 ..... 4-1

Table 4-2: K-eff for the unit cell for the real geometry compared to Wigner-Seitz approximations with white and reflective boundary conditions..... 4-4

Table 4-3: K-eff for the unit cell with the real geometry compared to cells using the Wigner-Seitz approximations with white boundary conditions. Several different Dancoff corrections were used to examine tendencies. Outer radius of moderator is determined by the Dancoff correction..... 4-6

Table 4-4: Differences in k-eff for a BWR fuel pin with reflective boundary conditions among MCNP5, KENO-VI and NEWT using normal Wigner-Seitz models as well as Dancoff adjusted Wigner-Seitz models for self-shielding cross sections. Dancoff corrections were calculated using three different fuel heights in MCDancoff. The radius of the moderator used in CENTRM is also supplied..... 4-11

Table 4-5: Differences in k-eff for a BWR bundle with a void fraction of 40 % from MCNP5, KENO-VI and NEWT using normal Wigner-Seitz models for self-shielding cross sections, and KENO-VI and NEWT using Dancoff adjusted Wigner-Seitz models for self-shielding cross sections. Dancoff corrections were calculated using four different fuel heights in MCDancoff..... 4-18

Table 4-6: Differences in k-eff for a BWR bundle with a void fraction of 40 % from MCNP5 and NEWT using normal Wigner-Seitz models for self-shielding cross sections, and NEWT using Dancoff adjusted Wigner-Seitz models for self-shielding cross sections. Dancoff adjusted Wigner-Seitz cells were used for only inner or sides/corners in some models. Dancoff corrections were calculated using two different fuel heights in MCDancoff..... 4-26

Table 4-7: Dancoff corrections for a BWR unit cell at 40% void fraction from CASMO4e and MCDancoff. The lower energy boundary of the CASMO4e 9.88 eV group is 4 eV. MCDancoff results are for a well converged height (2000 cm).Uncertainty given is a 3σ standard deviation. .... 4-28

Table 4-8: Dancoff corrections for an altered unit cell that emphasizes the effect of water. Results from CASMO4e and MCDancoff are shown. The lower energy boundary of the CASMO4e 9.88 eV group is 4 eV. MCDancoff results are for a well converged height (2000 cm).Uncertainty given is a 3σ standard deviation..... 4-32

Table 4-9: Dancoff corrections for an altered unit cell that emphasizes the effect of Zirc2. Results from CASMO4e and MCDancoff are shown. The lower energy boundary of the CASMO4e 9.88 eV group is 4 eV. MCDancoff results are for a well converged height (2000 cm). Uncertainty given is a  $3\sigma$  standard deviation..... 4-33

## Chapter 1 - Introduction

In the world of reactor physics, there has been growing use of the Monte Carlo method for reactor analysis<sup>1,2</sup>. Monte Carlo methods are advantageous due to their ability to model arbitrary geometry, use continuous energy cross sections, and efficiently scale on various computer architectures.<sup>3</sup> However, Monte Carlo solutions converge very slowly relative to deterministic solutions, and necessary time tends to grow as the physical geometry in the model becomes larger. It has been estimated that if Moore's law holds true, that it will be 2030 before a full core calculation can be done on a single processor in less than an hour. Tens of thousands of these calculations must be completed for a single core reload of a light water reactor<sup>4</sup>. Thus it is easy to say that deterministic, multigroup calculations will be the work horse for routine reactor physics calculations for many years to come. Since any multigroup transport solver is only as accurate as its cross sections, high fidelity generation of multigroup cross sections is of utmost importance for reactor physics calculations.

The difficulty in attaining accurate multigroup cross sections lies in the fact that cross sections naturally have a very complex nature with respect to neutron energy. The neutron energy range of interest for reactor physics spans from  $10^{-5}$  eV to  $10^7$  eV while at the same time a cross section can change by two to three orders of magnitude within only a few eV change in neutron energy. Figure 1-1 shows a plot of the  $U^{238}$  absorption cross section at 293 K over just the resolved resonance energy region. The blue line in Figure 1-1 depicts the continuous energy cross section while the red line shows the values for a 238 group neutron library.

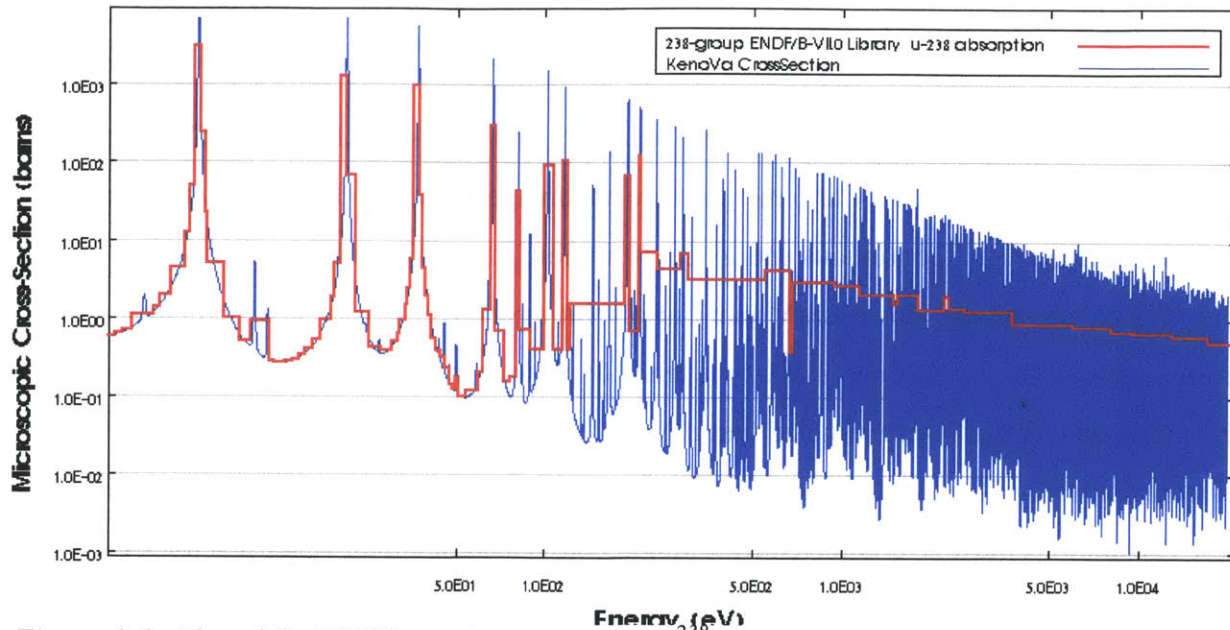
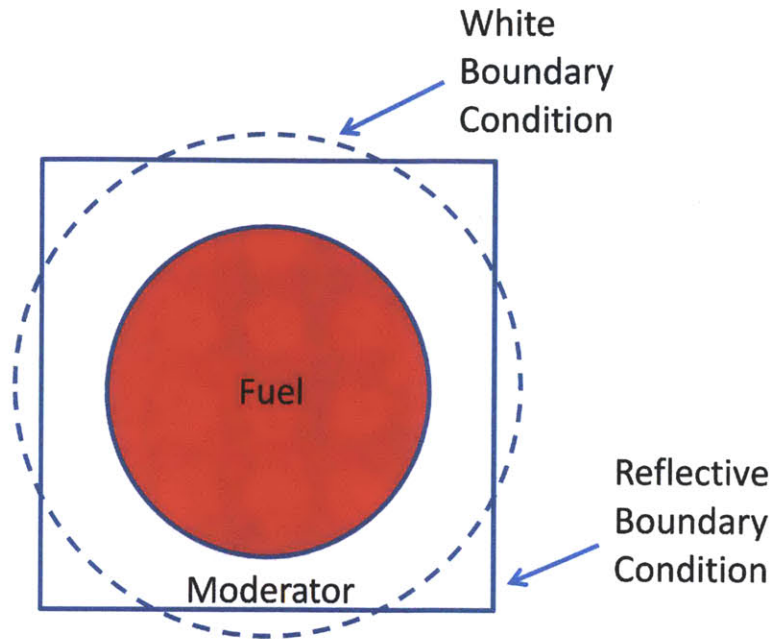


Figure 1-1: Plot of the KENO continuous energy  $U^{238}$  absorption cross section at 293 K in the resolved resonance energy region. The Scale 238 neutron group library is also shown. This plot was generated using Javapeno from the Scale6.1 package.<sup>5</sup>

From inspection of Figure 1-1 it is obvious that many resonances must be accounted for when a multigroup cross section is determined. Unfortunately calculating a simple average for the cross section over each group boundary does not preserve the physics of the system. It is the neutron reaction rate that must be conserved. Unfortunately in order to calculate reaction rates we need to know the flux, but the flux is what we are trying to solve for with the multigroup cross sections in the first place. This conundrum has led to the use of many approximations for the flux using simple zero- and one-dimensional (1-D) models. After an estimated flux has been acquired, reaction rates are calculated and preserved to create multigroup libraries that are used for two-dimensional (2-D) and three-dimensional (3-D) lattice physics codes and core simulators. Probably the most rigorous deterministic estimate for the flux, from a first principles perspective, is the class of methods called the ultrafine group method. This method is what will be used for attaining multigroup cross sections in this study.

One of the approximations that has been used for many decades is the Wigner-Seitz cell. This approximation is used to convert a unit cell of a fuel pin into a model that can be solved in 1-D only. This is done by changing the moderator region of a square unit cell into a cylindrical

shell where the moderator volume is conserved and a white (isotropic) boundary condition is used. Figure 1-2 shows a diagram of a unit cell for an infinite lattice and the equivalent Wigner-Seitz cell.



*Figure 1-2: Diagram of a unit cell for an infinite square lattice and an equivalent Wigner-Seitz cell using a white boundary condition*

When using a Wigner-Seitz cell for a model of a fuel pin there are two primary assumptions that are being made which include:

- 1) The Wigner-Seitz cell will preserve the reaction rates that exist in a square unit cell
- 2) The fuel pin being analyzed is surrounded by an infinite, regular array of similar pins

Although the Wigner-Seitz cell is a common modeling assumption that gives close results to the real geometry, it will be shown later that it underestimates  $k$ -eff for light water reactor (LWR) pins by several hundred pcm. Since this is the same model that the ultrafine method will be solving, the resulting flux will be representative of this false model. Any errors in this flux will be translated to the multigroup cross sections, and thus to the results of any downstream lattice physics calculations.

The assumption of an infinite array of similar pins will obviously begin to introduce errors into the solution when any irregularities are present. Irregularities may include things such as water holes, discrete absorbers, or even the large bypass flow channels that exist in any boiling water reactor (BWR) bundle as seen in Figure 1-3.

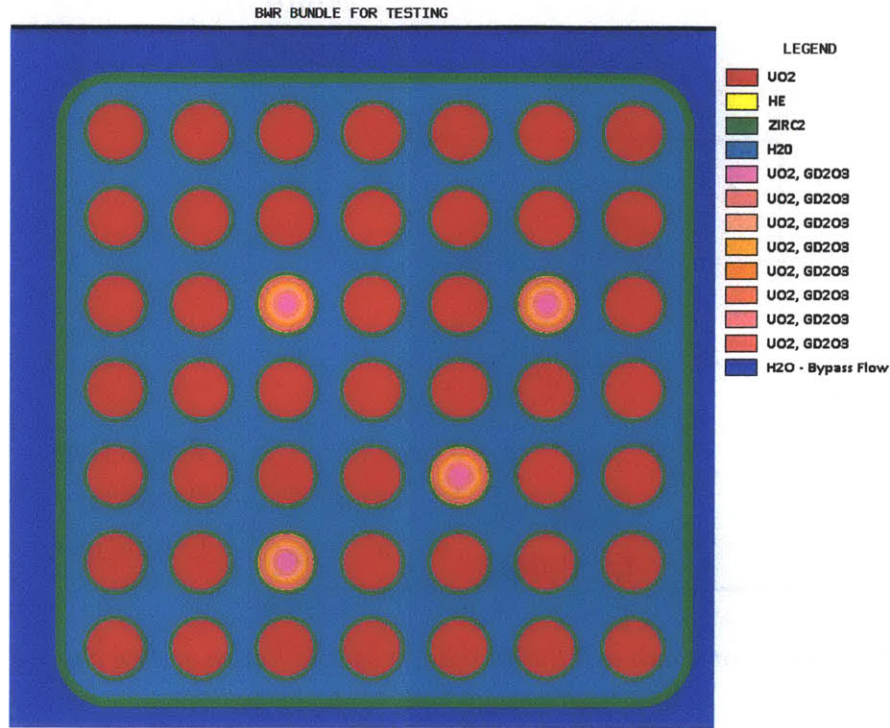


Figure 1-3: Example of common irregularities found in a BWR bundle including the bypass flow regions and the shroud.

A proposed action to partially correct both of these approximations has been optionally available for use within the Scale code package since the release of Scale6.0 in 2009.<sup>5</sup> The fix uses a Dancoff correction for each unit cell in a lattice to adjust the Wigner-Seitz cell used in the ultrafine self-shielding solution. The Dancoff correction is the probability of a neutron in the resolved resonance region, which has escaped the fuel it was born within, to interact with another fuel pin *without* having any collisions in the non-fuel materials. The Dancoff correction can approximately be used as a measure of irregularity seen by a fuel pin in a particular lattice. The Dancoff adjusted Wigner-Seitz cell (DAWSC) is the focus of this thesis.

The objective of this thesis was to qualitatively and quantitatively assess the effects of the Dancoff adjusted Wigner-Seitz cell for light water reactor conditions. The parameters which

## Chapter 1 - Introduction

were used for assessing performance were  $k$ -eff for a global measure of effects on the problem and energy dependent reaction rates for a detailed analysis of effects. A secondary goal of this thesis was to develop an automated tool for application of the DAWSC method to a pre-existing user input for the Scale code package.<sup>5</sup> Application of DAWSC to Scale inputs was being performed by hand which included many tedious steps that introduced possible user errors. Therefore the goal of the automated tool was to remove the time needed to create an altered input as well as reduce the risk for user errors.



## Chapter 2 - Background

### 2.1 - Slowing Down Theory

In the study and practice of reactor physics the energy range in which neutrons exist can be split into three regions where the physics of neutron interactions in each region are dominated by different mechanisms. The highest energy region from approximately 0.1 MeV to 20 MeV is characterized by elastic scattering which is anisotropic in the center of mass (CM) system, inelastic scattering, no upscattering, absorptions in unresolved resonances, and of course fission sources. For the energy range from about 4 eV to 0.1 MeV, the dominant neutron interactions (with respect to energy loss) can be summarized as elastic scattering which is isotropic in the CM system, no upscattering, and resolved and unresolved resonance absorptions. In the lowest energy range the neutrons have energy which is close enough to the thermal energy of the system that upscattering and chemical binding effects must be treated. Additionally, the wavelength of the neutron in this energy range is on the order of atomic spacing and therefore diffraction may need to be accounted for in some materials. Note that these energy ranges and tendencies in reaction types are specific for light water reactors and can be significantly different for other reactor types such as a fast reactor.<sup>6</sup>

In this overview we will be concerned with the middle energy range which will be referred to as the slowing down or resonance region. It is the large resolved resonances which exist primarily in  $U^{238}$  in fresh fuel which we will be concerned with since resonance absorption in  $U^{238}$  has a large impact on prediction of other reaction rates and any errors lead to further troubles when depletion of fuel is considered. Inelastic scattering will not be considered in this review, however it should be noted that accurate modeling of inelastic scattering in the fast region is necessary because the neutrons from this region are the source of neutrons for the rest of the neutron energy range. Additionally, it will be assumed that all elastic collisions in the slowing down region are isotropic in the CM frame of reference.

## Chapter 2 - Background

It is necessary to have a law for the elastic scattering between neutrons and nuclei so that the energy exchange is known. Since neutron velocities in reactor systems are non-relativistic an analysis using classical mechanics is sufficient with the assumption that the neutrons and nuclei act as perfectly elastic spheres. In the lab (L) frame of reference the nucleus is considered at rest with the neutron moving towards it. In the representative CM system the nucleus and neutron are moving towards one another with velocities such that they both have the same momentum, but in opposite directions. Due to this the total momentum with respect to the center of mass is zero before the collision, and because momentum must be conserved it will be zero after the collision as well. A solution to the energy exchange can then be easily found in the CM system and then be translated back to the L system. A further detailed description of this analysis can be found in most reactor physics books.<sup>6</sup> The resulting ratio between the neutron kinetic energy after the collision, E, and the neutron energy before the collision, E' is given by Equation 2-1.

Equation 2-1

$$\frac{E}{E'} = \frac{1}{2}(1 + \alpha) + (1 - \alpha) * \cos(\theta)$$

Equation 2-2

$$\alpha = \left( \frac{A - 1}{A + 1} \right)^2$$

where

- A: the atomic mass of the scattering nucleus
- $\theta$ : the scattering angle for the neutron in the CM system.

An important equation in slowing down problems is the transfer of neutrons from one energy to another via scattering. Equation 1 describes a relationship for energy exchange given a scattering angle in the CM system. However, what is needed is an energy exchange relationship where the scattering angle is not needed, hence we need a distribution in scattering angle to eliminate this variable. As previously mentioned, elastic scattering in the slowing down region is largely isotropic in the CM system. If an isotropic assumption is combined with Equation 1 it can be shown that the probability for scattering from energy E' to E is given by

Equation 2-3

$$P(E' \rightarrow E) = \begin{cases} \frac{1}{(1-\alpha)E'}, & \alpha E' \leq E \leq E' \\ 0, & \text{otherwise} \end{cases}$$

The quantity  $\alpha$  is a useful quantity that arises in many expressions for the slowing down of neutrons by elastic collisions. The minimum energy that a neutron can have after suffering a collision is given by  $\alpha E'$ . Additionally, the value for the maximum possible energy lost in a collision is given by  $(1-\alpha)E'$ . The same scattering law which is given in Equation 1 can be translated to units of lethargy,  $u$ , which is defined in Equation 2-4.

Equation 2-4

$$u = \ln\left(\frac{E_{ref}}{E}\right)$$

Equation 2-5

$$u - u' = \Delta u = -\ln\left\{\frac{1}{2}[1 + \alpha + (1 - \alpha)\cos(\theta)]\right\}$$

$E_{ref}$  in Equation 2-4 is a reference energy that is used to normalize the lethargy since it is a unitless quantity. It can be selected arbitrarily but is usually selected to be the highest energy that is simulated in the system. With  $E$  in the denominator the lethargy becomes increasingly positive as the neutron loses energy (becomes more lethargic). By assuming that scattering is isotropic in the CM system, Equation 2-1 and Equation 2-5 can be integrated over  $\theta$  from  $-\pi/2$  to  $\pi/2$  to find the average energy after a collision and the average logarithmic energy decrement per collision,  $\xi$ , respectively. These are shown in Equation 2-6 and Equation 2-7 respectively.

Equation 2-6

$$\overline{\Delta E} = \frac{1-\alpha}{2} E'$$

Equation 2-7

$$\overline{\Delta u} = \xi = 1 + \frac{\alpha}{1+\alpha} \ln(\alpha)$$

Lethargy and thus the average lethargy decrement will be used for a large portion of the discussion due to some conveniences they provide with regards to analyzing the slowing down problem. The parameter  $\xi$  makes it easy to calculate the average number of collisions needed for a given lethargy change or equivalently to reach a particular energy for a given scattering nucleus. An advantage of working with lethargy is that regardless of neutrons energy, a neutron must average the same number of collisions with a given material in order to result in a specified lethargy gain. With these concepts in mind we will now examine the slowing down of neutrons in an infinite medium.

## 2.2 - Slowing Down in Infinite Media

Given that fast neutrons are being produced by a fission source uniformly in space and at a constant rate in a moderator they will have collisions and lose energy until thermalized. At the same time these neutrons are being replaced by more fast neutrons which continue to be produced. A steady state distribution of neutrons will exist with some energy dependence that is referred to as the neutron spectrum. The details of the spectrum will depend on the rates at which neutrons are lost due to leakage from the system and absorptions as well as the rate of slowing down which is dependent on the mass and the scattering cross sections of the media. All of these terms will have energy dependence which contribute to the determination of the neutron spectrum.

For an infinite homogenous medium slowing down problem at steady state the space, angle and time variables can be eliminated from the general neutron balance that would normally be considered. Thus a neutron balance equation can be written based on preserving neutrons reaction rates as they change in energy only. This balance is stated in Equation 2-8 for an infinitesimal energy element  $dE$ . For this analysis we assume that we are below the energy range

## Chapter 2 - Background

where neutrons are being produced from fission or a fixed source. Thus the only source of neutrons is those that scatter down from higher energies.

Equation 2-8

$$\Sigma_s(E) \cdot \phi(E) = \int_E^{\infty} \Sigma_s(E') \cdot P(E' \rightarrow E) \cdot \phi(E') \cdot dE'$$

where

$\Sigma_s(E)$ : Macroscopic scatter cross section at energy E

$\phi(E)$ : Scalar neutron flux at energy of interest

$\phi(E')$ : Scalar neutron flux at higher energy which may contribute to the flux at E

$P(E' \rightarrow E)$ : Probability of scattering from energy E' to E

$\Sigma_s(E')$ : Macroscopic scatter cross section at energy E'

The left hand side of Equation 2-8 represents the losses from E while the right hand side is the production term. Losses from the energy of interest E, are due to collisions with the medium since any collision will change the energy such that it removes it from the infinitesimally small energy range about E. The loss term represents the neutrons at any energy, E', above energy E (E to  $\infty$ ) that may undergo a scattering reaction which drops the energy to E. If we utilize Equation 2-3 with Equation 2-8 you will get

Equation 2-9

$$\Sigma_s(E) \cdot \phi(E) = \int_E^{E/\alpha} \Sigma_s(E') \cdot \phi(E') \cdot \frac{dE'}{(1-\alpha) \cdot E'}$$

Now the slowing down equation has a energy transfer mechanism for the scattered neutrons which is based on the assumption of s-wave scattering, which results in isotropic scattering in the CM system for low mass ( $A \leq 12$ ) scattering nuclei for energies below 10 MeV.<sup>6</sup> The integral now extends from E to E/ $\alpha$  instead of to infinity. This range represents the possible energies of incoming neutron (E') that can scatter into dE about E. The upper limit of the integral could be infinity for a scattering nucleus of H<sup>1</sup> since a neutron can lose all of its energy in one collision with H<sup>1</sup>. Since nuclei with a mass greater than A=1 have a finite limit on the amount of energy they can remove from a scattering neutron, the resulting range for the integral extends to only E/ $\alpha$ . The solution to Equation 2-9 is readily found and is of the form

$$\phi(E) = \frac{C}{\Sigma_s(E) \cdot E}$$

where

C: constant that represents the source strength.

Note that Equation 2-10 infers that the neutron flux in a medium with no absorption is inversely proportional to the medium's total cross section. (the scattering cross section becomes the total cross section in the absence of absorption) and energy. We can make sense of Equation 2-10 if the physical interaction of the neutrons with the system is studied as follows.. The neutrons are being born at some constant rate C, and then are being slowed down by scattering with the nuclei in the system. The rate at which the slowing down occurs is proportional to the rate at which collisions occur, which is determined by the scattering cross section. The larger the cross section is, the more likely the neutrons will leave this energy. Thus a large scattering cross section at energy E will tend to reduce the steady state neutron population at that energy, which is consistent with the inverse relationship. The energy term in the denominator reflects the fact that an average neutron energy loss per collision is larger for neutrons at higher energies, as shown by Equation 2-6.

### 2.3 - Slowing Down in Infinite Media with a Resonate Absorber

The slowing down equation appropriate for an infinite medium with resonance absorbers, no fission and no inelastic collisions is given by:<sup>7</sup>

$$\left( \sum_k N_k \sigma_{t,k}(E) \right) \phi(E) = \sum_k \frac{1}{1 - \alpha_k} \int_E^{E/\alpha_k} N_k \sigma_{s,k}(E') \phi(E') \frac{dE'}{E'}$$

where

$N_k$  : atom density for nuclide k

$\sigma_{t,k}(E)$  : microscopic total cross section for nuclide k

$\sigma_{s,k}(E')$  : microscopic scatter cross section for nuclide k

$\phi(E)$  : total scalar flux

$$\alpha_k : \left( \frac{A-1}{A+1} \right)^2 \text{ where } A \text{ is the atomic mass in amu}$$

Unfortunately there is no analytic solution for this problem in general. In order to solve problems that are of value to a realistic system the problem must be either solved numerically or by using some approximations. The following sections review some of the common solution techniques for this problem.

### 2.3.1 - Narrow Resonance Approximation

The narrow resonance approximation is a commonly used method for estimating the perturbations in the flux that occur with the addition of resonant nuclides to a system of non-absorbers. The methods assumptions are particularly applicable to high energy resonances as will be discussed further below. Although the method can be applied to a system with more than one resonant absorber and non-absorber the equations presented will use just one of each nuclide to simplify notation. Assume that the non-resonant nuclide has no absorption so that its total cross section is equal to its potential cross section. Subscripts used for the two nuclides will be f for the resonant absorber (fuel) and m for the moderator which is a non-resonant purely scattering nuclide. Subscript p refers to the potential cross section which is of course not energy dependent. Equation 2-11 will then become:

$$\begin{aligned} (N_f \sigma_{t,f}(E) + N_m \sigma_{p,m}(E)) \phi(E) = & \frac{1}{1 - \alpha_f} \int_E^{E/\alpha_f} N_f \sigma_{s,f}(E') \phi(E') \frac{dE'}{E'} \\ & + \frac{1}{1 - \alpha_m} \int_E^{E/\alpha_m} N_m \sigma_{p,m} \phi(E') \frac{dE'}{E'} \end{aligned}$$

Equation 2-12

Equation 2-12 has several terms that will need to be approximated in order for a solution to be plausible without using numerical techniques. The flux on the right hand side is not known and will therefore need to be approximated. It is assumed the width of the resonance is narrow relative to the slowing down width. This approximation is reasonable for high energies in thermal systems since the average energy loss per collision is larger at higher energies. The neutrons at high energies are likely to have a collision with the moderator and be reduced in

## Chapter 2 - Background

energy such that the neutrons completely avoid the resonance. Another approximation to be used is that the flux can be estimated by  $1/E$ . This is obviously not true at the resonance energy and very close to it, however the resonance is so narrow that the effect on the entire integral is small. The last assumption is that the scattering cross section for the resonant nuclide outside of the resonance is considered constant. This is deemed a reasonable assumption because the potential scattering cross section for the moderator is relatively large.<sup>7</sup> Applying these assumptions Equation 2-12 will become:

$$\phi(E) = \frac{N_f \sigma_{p,f} + N_m \sigma_{p,m}}{N_f \sigma_{t,f}(E) + N_m \sigma_{p,m}} \frac{1}{E} = \frac{\sigma_{p,f} + \sigma_0}{\sigma_{t,f}(E) + \sigma_0} \frac{1}{E}$$

Equation 2-13

where

$\sigma_0$  is referred to as the background cross section and is defined by:

$$\sigma_0 = \frac{N_m \sigma_{p,m}}{N_f}$$

Equation 2-14

Note that the use of the background cross section is not limited to one non-resonant isotope, but can be applied to an infinite medium with any number of scattering nuclides. The use of the background cross section is fundamental to the use of equivalence theory which will be discussed more in the coming sections. As mentioned earlier, the assumptions behind the narrow resonance approximation make it a quick and simple solution to the slowing down equations with resonance absorption. One of the important inaccuracies of the narrow resonance approximation is its application to resonances which are not narrow relative to the energy decrement experienced by the neutron. Thus, the narrow resonance approximation should not be expected to perform well for the broad, lower energy resonances found in  $U^{238}$ . Another major drawback of the narrow resonance approximation is that it does not account for resonance overlapping. This is not a major issue for fresh fuel in a light water reactor, however as fission products and transuranic nuclides buildup in inventory with burnup resonance overlapping can be an important effect to capture.



### 2.3.2 - Wide Resonance Approximation

Equation 2-11 can be solved with some different assumptions than what was made in the previous section to come up with another analytical solution to the infinite homogeneous medium problem with resonant absorbers. In this case the resonance is considered wide relative to the average energy decrement from elastic collisions. For this solution the integral with the non-resonant nuclide is treated exactly the same as it was in the narrow resonance approximation. The major assumption that is different in this case is the resonance isotope has an infinite mass, or that  $\alpha_f$  approaches 1. This means that a neutron colliding with the resonant nuclide will not lose any energy. The resulting analytical formulation and its equivalent version using the background cross section are given in Equation 2-15.

$$\phi(E) = \frac{N_m \sigma_{p,m}}{N_f \sigma_{a,f}(E) + N_m \sigma_{p,m}} \frac{1}{E} = \frac{\sigma_0}{\sigma_{a,f}(E) + \sigma_0} \frac{1}{E}$$

Equation 2-15

It should be noted that the only difference between the flux solutions for the narrow resonance and wide resonance approximations is that in the wide resonance equations the scattering cross section for the resonant nuclide has been removed from the numerator and denominator. This is due to the assumption of the infinite mass for the resonant nuclide. This assumption removes the ability for the resonant nuclide to scatter a neutron out of its resonance.

## 2.4 - Equivalence Theory

### 2.4.1 - An Isolated Fuel Lump

The slowing down equation for a heterogeneous system whose neutron energy loss is primarily due to elastic scattering is given by:<sup>7</sup>

$$\begin{aligned} \Sigma_{t,f}(E)\phi_f(E)V_f &= P_{f \rightarrow f}(E)V_f \frac{1}{1-\alpha_f} \int_E^{E/\alpha_f} N_f \sigma_{es,f}(E')\phi_f(E') \frac{dE'}{E'} \\ &+ P_{m \rightarrow f}(E)V_m \frac{1}{1-\alpha_m} \int_E^{E/\alpha_m} N_m \sigma_{es,m}(E')\phi_m(E') \frac{dE'}{E'} \end{aligned}$$

where

$\Sigma_{t,f}(E)$ : macroscopic total cross section for the fuel

$\sigma_{es,f}(E), \sigma_{es,m}(E)$ : Elastic scattering cross sections

$\phi_f(E), \phi_m(E')$ : neutron flux in the fuel and moderator, respectively

$P_{f \rightarrow f}(E), P_{m \rightarrow f}(E)$ : fuel-to-fuel and moderator-to-fuel collision probabilities, respectively

$V_f, V_m$ : volume of the fuel and moderator

Equation 2-16 on the left hand side shows the removal term in the neutron balance equation is any neutron interaction in the fuel. The first source term on the right hand side of the equation represents the neutrons at some higher energy  $E'$  in the fuel which have an elastic scattering event and end up at energy  $E$ . The second source term, is similar to the previous except that the source neutron at energy  $E'$  are initially in the moderator and an elastic scattering results in the neutron being slowed down to energy  $E$  and in the fuel lump. If the assumptions of the narrow resonance approximation are applied to Equation 2-16 it will yield the following balance equation:

$$\Sigma_{t,f}(E)\phi_f(E)V_f = \frac{1}{E} (P_{f \rightarrow f}(E)V_f \Sigma_{p,f} + P_{m \rightarrow f}(E)V_m \Sigma_{p,m})$$

where

$\Sigma_{p,f}, \Sigma_{p,m}$ : macroscopic potential cross section for the fuel and moderator, respectively

Two important equations with regards to collision probabilities exist which will be of use for solving Equation 2-17. The first law is a simple normalization of the collision probabilities which means that the sum of the collision probabilities from some volume  $X$  to all volumes (including itself) must be equal to 1. The second law for collision probabilities is the reciprocity theorem which is given in Equation 2-18.

Equation 2-18

$$P_{f \rightarrow m}(E) V_f \Sigma_{t,f}(E) = P_{m \rightarrow f}(E) V_m \Sigma_{t,m}(E)$$

The reciprocity theorem preserves the total attenuation of neutrons in a medium, regardless of which direction they may be traveling through the medium. Using these properties of collision probabilities Equation 2-17 can finally be solved. The result for the flux is given in Equation 2-19.

Equation 2-19

$$\phi_f(E) = \frac{1}{E} \left[ (1 - P_{f \rightarrow m}(E)) \frac{\Sigma_{p,f}}{\Sigma_{t,f}(E)} + P_{f \rightarrow m}(E) \right]$$

From inspection of Equation 2-19 it is possible to calculate the energy dependent flux in the fuel if the collision probability from fuel to moderator is known. Numerical solution for this collision probability is possible however this is a time intensive process. Note that for an isolated fuel lump the fuel to moderator collision probability is equivalent to the probability of a neutron escaping ( $P_e$ ) the fuel. To provide an efficient solution to this problem Wigner's rational approximation was suggested by Weinberg and Wigner<sup>8</sup> for the estimation of the escape probability. Wigner's rational approximation, Equation 2-20, gives an accurate answer to  $P_e$  for the extreme cases of a very small fuel lump ( $P_e \sim 1$ ) and a very large fuel lump ( $P_e \sim 0$ ). Wigner's rational approximation does not hold true for intermediate sized fuel lumps and there have been a large number of suggested improvements over the decades which will not be shown here.<sup>7</sup>

Equation 2-20

$$P_e(E) = \frac{1}{\Sigma_{t,f}(E) \bar{l} + 1}$$

where

$\bar{l}$ : average chord length, which is the diameter of a fuel lump if it is cylindrical

Wigner's rational approximation can be substituted in to Equation 2-19 for a final solution to the energy dependent flux in a heterogeneous problem. After some manipulations and dividing by the resonant nuclide atom density, Equation 2-21 can be arrived at:

$$\phi(E) = \frac{\Sigma_{p,f} + \Sigma_e}{\Sigma_{t,f}(E) + \Sigma_e} \frac{1}{E} = \frac{\sigma_{p,f} + (\sigma_{0,f} + \Sigma_e/N_f)}{\sigma_{t,f}(E) + (\sigma_{0,f} + \Sigma_e/N_f)} \frac{1}{E}$$

where

$\Sigma_e = 1/l$  : macroscopic escape cross section

$N_f$  : number density of the resonant nuclide

$\sigma_{p,f}$  : potential scattering cross section for the resonant nuclide

$\sigma_{0,f}$  : background cross section for the resonant nuclide as defined previously

If Equation 21 is compared with the narrow resonance solution to a homogeneous medium with a resonant absorber in Equation 2-13 they will appear remarkably similar. The only difference is that the background cross section has an additional fictional cross section added to it, namely the escape cross section. Thus the energy dependent flux solution can be solved for a range of background cross sections and self-shielded multigroup cross sections can be tabularized based on the background cross section *regardless* of whether the system being solved is homogeneous or heterogeneous.

The background cross section and/or the escape cross section have a direct affect on the flux depression that occurs in the resonance. The background cross section represents a measure of competition that the resonant absorber must deal with in order to successfully capture a neutron. The presence of an increasingly large scattering cross section from moderating nuclei increases the probability that the neutrons will avoid the resonance, thus the depression in the flux near resonance is not as pronounced. Equivalently, as the size of a fuel lump decreases the probability for a neutron escaping the fuel increases, as does the escape cross section. A smaller fuel lump effectively has a higher probability of being moderated and avoiding the absorption resonance.

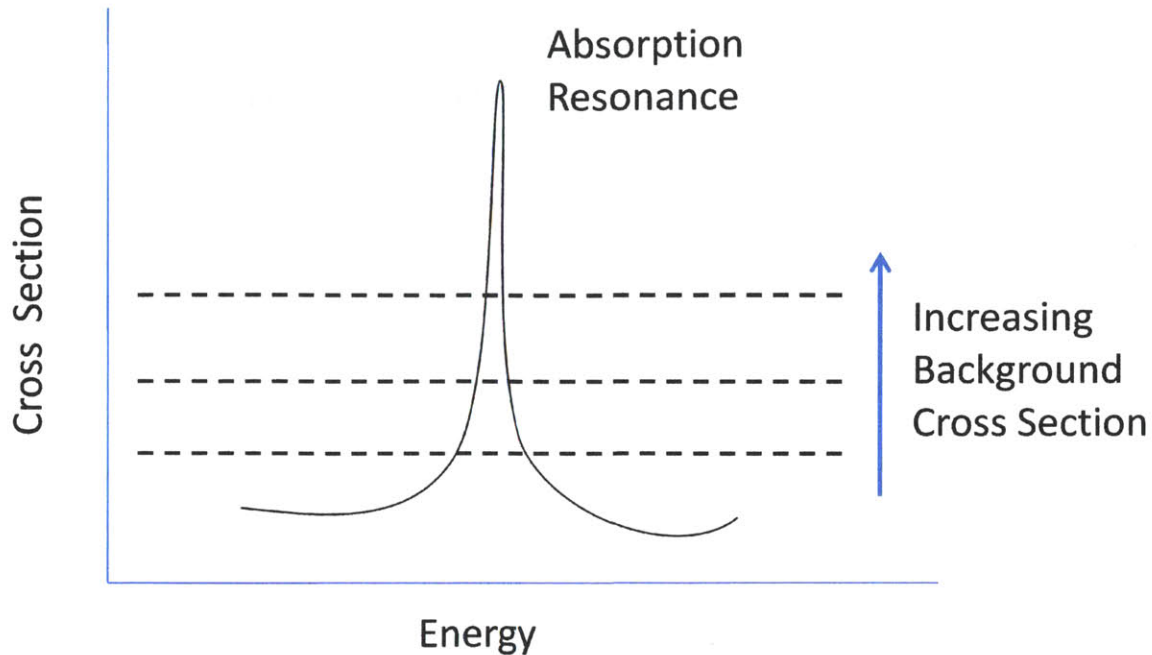


Figure 2-1: Qualitative depiction of a background cross section

### 2.4.2 - A Lattice of Fuel Lumps

One last major parameter needs to be covered in order to have a successfully implemented slowing down solution to realistic nuclear systems. Real reactors do not have isolated fuel lumps, but rather have lattices of fuel. Wigner's Rational Approximation was used to evaluate the probability of escape from the fuel. However, if other fuel lumps exist then there is a chance that a neutron escaping one fuel lump may just enter another lump. This phenomenon was studied by Dancoff in the 1940's and is referred to as the Dancoff Effect<sup>9</sup>. Thus the escape probability from the fuel is effectively reduced. In order to account for this effect the Dancoff correction (C) or the Dancoff factor ( $D = 1-C$ ) can be calculated for a lattice and incorporated into equivalence theory in order to correctly predict the neutron flux in the fuel and the resonance integrals. The Dancoff correction can be defined and calculated in multiple ways that are equivalent to one another. Stamm'ler and Abbate<sup>10</sup> state the following definition:

$$C = \frac{I_0 - I}{I_0}$$

where

$I_0$ : number of neutrons entering the fuel region in an isolated system

$I$ : number of neutrons entering the fuel region of interest in a lattice system

Thus  $C$  is a measure of how much a fuel region is shadowed by other fuel regions. For an isolated fuel region the Dancoff correction is 0, whereas for a fully shadowed fuel region the Dancoff correction is 1. Another way to describe the Dancoff correction is as the probability for a neutron leaving a lump to cross the moderator without interacting, and thus enter another fuel lump. For light water reactors the Dancoff correction,  $C$ , will generally be less than 0.5, somewhere in the range of 0.1 to 0.4. The implementation of the Dancoff correction into the background cross section is given in Equation 2-23.

$$\sigma_0 = \sigma_{0,f} + (1 - C)\Sigma_e/N_f = \sigma_{0,f} + D\Sigma_e/N_f$$

## 2.5 - Ultrafine Group Method of Self-Shielding

This topic will be analyzed in more detail in the methods section for its specific implementation in the Scale 6.1 module CENTRM. The general idea of the ultrafine group method as a method to produce self-shielded cross sections will be introduced below. The ultrafine group method solves the Boltzmann transport equation with the multigroup method however the energy variable is discretized finely enough so that self-shielding is inherently treated. Where “finely enough” is sufficiently narrower than that of the energy loss of elastic scattering by a heavy nuclide and the widths of the major resonance peaks.<sup>11</sup> Once a ultrafine group solution is attained the group structure can be used with the flux to create a collapsed, self-shielded cross-section library with practically any group structure the user would like. The major advantage of this method over others is that resonance overlapping effects are explicitly treated. The drawback of this method is that 10,000’s of energy groups are needed for the calculation and therefore the necessary computational resources can be large. Due to this the ultrafine group

## Chapter 2 - Background

method is usually applied to infinite homogeneous systems or to geometrically small problems such as a fuel pin unit cell.

## Chapter 3 - Methods

Throughout this analysis several neutron transport packages were utilized for evaluating the effects of Dancoff adjustments to the Wigner-Seitz cell. The code packages included MCNP5, Scale6.1 and CASMO4e. MCNP5 was used for the reference solution in the problems that were studied for two primary reasons. The continuous energy treatment of the energy variable in the 3-D geometry make the energy dependent reaction rates calculated by MCNP5 ideal for comparing resonance self-shielding methods\*. The second reason for the use of MCNP5 is that it scales well in parallel performance for the number of processors that were available for computation (40 to 80 processors were used). This computational performance was necessary to achieve adequate precision in a reasonable timeframe on energy dependent reaction rates needed for comparisons. Scale6.1 contains the various modules and methods that were used to perform numerous resonance self-shielding treatments as well as for multigroup transport. CASMO4e<sup>12</sup> was used for comparing Dancoff corrections with those from the Scale6.1 modules in LWR lattices. In addition to an overview of the specific modules used in the analyses, a discussion of an automated tool for the application of Dancoff corrections to Wigner-Seitz cells for self-shielding will be presented.

### 3.1 – Scale6.1

Scale6.1 is a code package with a suite of modules for simulating nuclear systems for both safety and design that is developed and maintained by Oak Ridge National Laboratory (ORNL). Scale offers a versatile set of tools for criticality safety, reactor physics, radiation shielding, radioactive source term characterization, and sensitivity and uncertainty analysis. This suite of tools can be utilized with several graphical user interfaces (GUI) for building models as well as for visualizing results.<sup>5</sup>

This overview will summarize the theory and use of the multigroup cross-section self-shielding modules and the transport solvers which were used for analysis. Each of the modules (referred to as functional modules) can be executed in a standalone mode with input and output



that is described in the Scale6.1 manual. However, *control* modules are generally used to link the output from one module to another in order to perform typical analyses. For example the TRITON control module may be used to setup the analysis of a fuel assembly. The analysis will include calling appropriate cross-section self-shielding functional modules to create problem specific cross sections followed by a transport solver at the minimum. Additional options may be included within TRITON so that other functional modules will be called upon for such actions as depletion, preparation of few group cross sections, and sensitivity and uncertainty analysis to name a few. Figure 3-1: Scale flow diagram for a typical calculation used in this study. shows a flow diagram for a typical calculation that was performed for this study. The control module CSAS6 is primarily used for criticality safety however it was also used in this study to enable the KENO-VI transport solver to be used for prediction of k-eff and reaction rates.

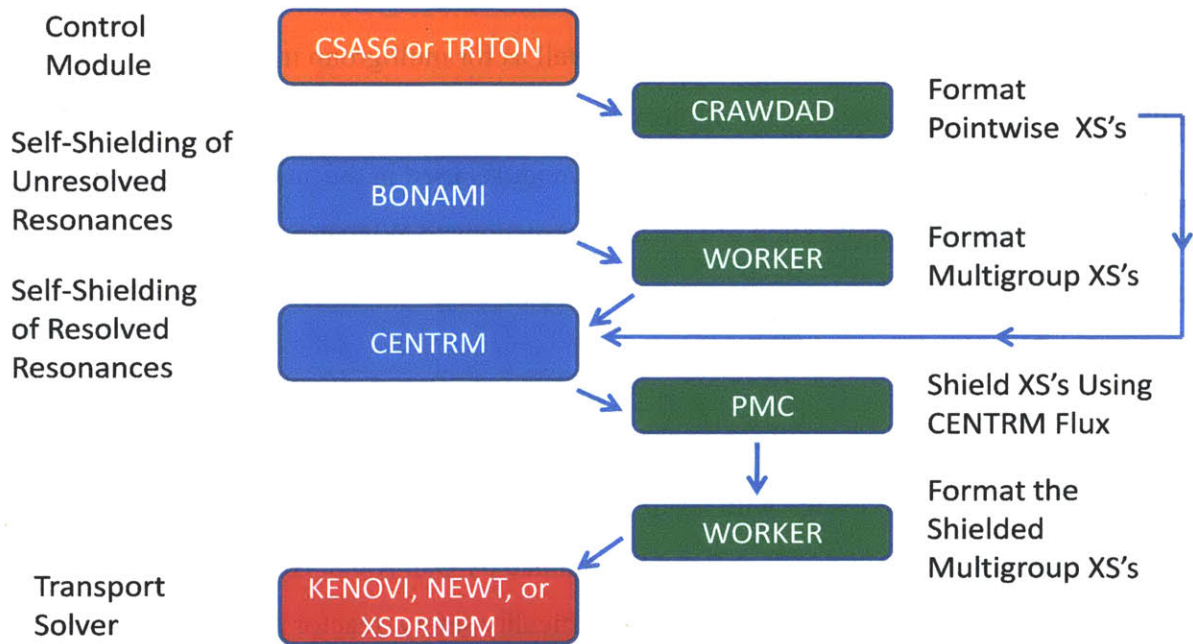


Figure 3-1: Scale flow diagram for a typical calculation used in this study.

### 3.1.1 - BONAMI

The functional module BONAMI is used for resonance self-shielding of cross sections in the unresolved resonance energy range. BONAMI uses the Bondarenko method which is a way to store and look up cross-section data in tabular form for very efficient determination of self-

shielded cross-sections. Resonance self-shielding factors, or Bondarenko factors, are stored in tables for each nuclide present in the Scale cross section library. BONAMI uses the narrow resonance approximation for determining an estimate for the flux which is then used to calculate the shielded cross sections for each energy group, while varying both the background cross section and the temperature of the nuclide independently. The energy groups used are according to the Scale 238 group neutron library. Thus, a significant amount of data is generated for any mixture and temperature that could be expected to be used in a problem. For each nuclide an infinite dilution cross section at room temperature is calculated which is used as a base cross section for the nuclide. An infinite dilution cross section is one in which a very large background cross section is present, which is usually set at an arbitrarily large number such as  $10^{10}$  barns. When a shielded cross section for a given energy, background cross section and temperature is needed it can be calculated using Equation 3-1.

Equation 3-1

$$\overline{\sigma}_g(\sigma_0, T) \equiv F_g(\sigma_0, T) \cdot \overline{\sigma}_{g,\infty}$$

where

$\overline{\sigma}_g(\sigma_0, T)$ : Resonance self-shielded cross section for group g, background cross section  $\sigma_0$  and temperature T

$F_g(\sigma_0, T)$ : Bondarenko factor for group g, background cross section  $\sigma_0$  and temperature T

$\overline{\sigma}_{g,\infty}$ : Resonance self-shielded cross section for group g at infinite dilution

BONAMI calculated Bondarenko factors for all important neutron interactions (fission, capture, elastic scattering, transport and total). Generally BONAMI stores Bondarenko factors for five or six background cross sections to cover the typical range for the nuclide as found in practice. Additionally, the Bondarenko factor is calculated at three or four different temperatures. These values may be interpolated to determine the appropriate resonance self-shielded cross section for a given problem. Note that BONAMI used a novel interpolation scheme that will not be described here but can be found in the Scale6.1 manual. BONAMI outputs its resonance self-shielded cross sections to an AMPX master library format, which is described in the section on the functional module WORKER.

It should be noted that BONAMI's solutions to the slowing down equation to obtain a flux is based on the narrow resonance approximation. As stated in the background section, the narrow resonance approximation predicts resonance absorption rates relatively well at high energies where the average energy decrement from an elastic collision is large compared to resonance widths. This assumption does not hold true in the resolved resonance range where the average energy decrement per collision is smaller and the resonances are larger in width. Thus the resulting resonance self-shielded cross section from BONAMI are only used for the unresolved resonance region, and a different Scale functional module is used to self-shield the resolved resonance region.

### **3.1.2 - WORKER**

WORKER is a functional module that reads cross-section libraries formatted as an AMPX master library or working library and ultimately creates a new working library. The AMPX master library is not structured for direct use in a multigroup transport calculation. WORKER is necessary because the AMPX master library format carries additional information that is not required for transport calculations such as Bondarenko factors and cross-section sensitivity data among many other types of data. The AMPX working library is a library containing the data necessary for a specific transport problem. One of the many important functions that WORKER performs is the appropriate scaling of scattering matrices so that the sum of group to group scatter cross sections add up to the self-shielded values.

### **3.1.3 - CENTRM**

CENTRM is the preferred functional module in Scale6.1 for resonance self-shielding in the resolved resonance energy region. CENTRM computes continuous-energy neutron spectra in zero- or one-dimensional systems. CENTRM solves the Boltzmann transport equation using a combination of pointwise and multigroup nuclear data with a discrete ordinates solution in slab, cylindrical or spherical geometry. CENTRM can also use a simplified solution techniques that includes a two region solution, zone-wise homogenized solution or an infinite media solution. CENTRM pointwise solution uses a ultrafine energy mesh of 10,000 to 70,000 energy points in

order to generate a flux which can be used to create self-shielded multigroup cross sections for other transport analyses.<sup>5</sup>

CENTRM has three energy ranges over which it performs calculations. CENTRM gets pointwise cross sections from CRAWDAD which formats KENO continuous energy cross sections for use with CENTRM. Multigroup cross sections are provided by BONAMI and WORKER so that the unresolved resonance region cross sections have been self-shielded before CENTRM begins any calculations. A pointwise solution is performed in the resolved resonance region, with multigroup treatment above and below this pointwise region. The energies over which the pointwise solution is calculated are at the user's discretion; however the defaults are from 20 KeV (where the resolved resonance region begins for U<sup>238</sup>) down to the lowest energy resonance of any nuclide in the problem. Both the low energy multigroup region (LMR) and the pointwise region have support for upscattering and  $S(\alpha, \beta)$  treatment for energy groups where data is applicable.

The energy structure in the LMR and the upper multigroup region (UMR) are based on the Scale 238 group neutron library. The energy structure in the pointwise region is based on the resonances of the nuclides in the problem and the pre-determined minimum degree of accuracy for cross section interpolation. By default the continuous energy cross sections from KENO libraries are thinned so that energy points can be interpolated between without causing more than 0.1% error in the cross section. This tolerance is adjustable. In all three solution regions the discrete ordinates solution can use an arbitrary quadrature order, and use Legendre expansions up to P<sub>5</sub> to represent the scattering source. There are no restrictions on the number of spatial regions and spatially dependent temperatures that can be specified for appropriate Doppler broadening. The pointwise region supports elastic scattering as well as discrete level inelastic scattering. Continuum elastic scattering is approximated for the higher energies with an analytical evaporation spectrum.

The rigorous solution provided by CENTRM gives results comparable to continuous energy Monte Carlo algorithms. The largest source of error from the CENTRM calculation is the fact that is a one-dimensional model. In order for CENTRM to produce resonance self-shielded cross sections for a fuel pin the square unit cell must be approximated by a Wigner-Seitz cell

with a white boundary condition. This approximation and its effects are at the center of this study and will be discussed further.

### 3.1.4 - PMC

PMC (Produce Multigroup Cross sections) is a functional module which is used to create shielded multigroup libraries from the pointwise neutron flux file given by CENTRM, a pre-existing AMPX multigroup library, and a pointwise library file. PMC uses the CENTRM pointwise flux and cross sections to produce a self-shielded multigroup library by using the flux as a weighting function. However, this is done only for the section where the pointwise solution was calculated. The multigroup cross sections in the energy region above the pointwise solution (unresolved resonance region) have previously been processed by BONAMI and therefore are not changed. Any thermal groups which were below the energy boundary for pointwise solutions are also not processed by PMC.

Since each multigroup partial cross section (absorption, elastic scatter, etc) is created independently, there is no guarantee that the sum of these partial cross sections will add up exactly to the total cross section if it is also calculated from the pointwise data. Any small imbalances may cause errors in criticality calculations, thus to avoid this total group cross sections are redefined as the sum of the partial cross sections.

The other main task that PMC must accomplish is proper scaling of 2-D scattering matrices. The default choice for this is to scale all group to group cross sections, as well as higher order moments by the ratio of the new 1-D scatter cross section (from CENTRM pointwise data) to the original 1-D scatter cross section. The scaling of the  $P_0$  moments will ensure the total of all group to group cross sections will sum to the total scattering cross section. By scaling the higher order moments this way, the group to group scattering rates do not change relative to one another, only the total scatter rate is scaled. This is always how the discrete and continuum inelastic cross sections are processed. However, this is not always a valid treatment for the higher order moments of elastic scattering moments. PMC has two other available options for restructuring the elastic scatter matrix which will not be discussed here but can be found in the Scale6.1 manual. Due to the complex nature of thermal scattering law, these scattering matrices are all scaled equally to match the total scattering rate of the group.

### **3.1.5 - NEWT**

NEWT is a multigroup discrete-ordinates radiation transport solver that with flexible meshing capabilities that allow two-dimensional neutron transport calculations using complex models. NEWT uses a unique differencing scheme called Extended Step Characteristics (ESC) which allows a computational mesh based on arbitrary polygons. This feature allows curvilinear geometry such a fuel rod to be modeled which is usually difficult to accomplish in most discrete ordinates codes. Geometrical shapes such as a cylinder are specified in the geometry and NEWT automatically creates a polygon with an arbitrary number of sides while conserving the volume of each region according to the real curvilinear dimensions. NEWT can be used for eigenvalue, critical-buckling correction, source calculations, and preparation of weighted, collapsed cross sections in AMPX working library format. NEWT is incorporated into the TRITON control sequence, which can be used to prepare cross sections for a NEWT transport calculation and automatically execute NEWT.<sup>5</sup>

### **3.1.6 - KENO-VI**

KENO-VI is three-dimensional Monte Carlo criticality program which can model any volume that can be constructed using quadratic equations. KENO-VI uses the SCALE Generalized Geometry Package (SGGP) and has several predefined geometry volumes which makes the geometry definitions nearly identical to the definitions used in an equivalent NEWT model. KENO-VI includes support for square, hexagonal and dodecahedral arrays to make the creation of complex, repeated geometries easy such as light water reactor fuel or pebble bed reactors. Although the primary purpose of KENO-VI is to determine k-eff, it can calculate other useful quantities such as energy-dependent leakages, energy- and region-dependent absorptions, fissions, flux densities and fission densities. KENO-VI can perform calculations using either continuous energy cross sections or multigroup cross sections.

### **3.1.7 - MCDancoff**

MCDancoff (Monte Carlo Dancoff) is a slightly altered version of KENO-VI which is specialized for the calculation of Dancoff corrections in a three-dimensional model. MCDancoff uses a one-group neutron library in order to calculate the Dancoff correction for a fuel containing

volume. The computation proceeds by starting neutrons on the outer surface of the fuel volume, sampling uniformly over the surface and with a cosine distribution for the neutron direction. The neutron is transported through the model until either it crosses the surface of a fuel containing volume or until it has a collision in a non-fuel bearing mixture (the moderator, clad, or structural materials). One definition of the Dancoff correction is the probability of a neutron isotropically leaving the surface of a fuel lump and having its first collision with a fuel lump. Since MCDancoff is calculating a black Dancoff correction, any neutron reaching a volume containing fuel counts as a collision.

One feature that a user of MCDancoff must be familiar with is that the calculated Dancoff correction will vary with the height of the fuel used in the model, even though a reflective boundary condition may be used in the dimension of the length of the fuel. This is due to the fact that MCDancoff emits neutrons off the surface of a fuel element, including the top and bottom circular cross sectional areas of a cylindrical fuel pin. Any neutrons that are started on the top or bottom faces of the cylinder will immediately be reflected back into the fuel volume they were just emitted from and thus captured. This will cause the Dancoff correction to be overestimated. Using a large fuel height will reduce this effect to a negligible change. This effect on the results of  $k$ -eff and reaction rates is investigated in this study.

The exact same geometry and materials definitions are used between MCDancoff and KENO-VI. The major change needed to be performed to a KENO-VI input to make a MCDancoff input is in the start data block. This is where MCDancoff must be told which volumes containing fuel should have a Dancoff correction calculated. MCDancoff has a prescribed syntax for identifying particular fuel regions since they may be within a fuel pin that is inside a lattice or hole, or even a nested combination of these. This syntax is described and examples are given in the Scale6.1 manual. A separate entry must be given for each fuel lump that the user wishes to have a Dancoff correction calculated.

### **3.2 - MCNP5**

MCNP5 (Monte Carlo N-Particle) is a general purpose radiation transport code which can handle neutrons, photons, electrons or coupled neutron/photon/electron transport. Although

MCNP was first designed to be a shielding code and therefore has a plethora of variance reduction techniques, it also has the capability to calculate the eigenvalue of critical systems. MCNP treats an arbitrary three-dimensional configuration of materials in geometric cells bounded by first- and second-degree surfaces and fourth-degree elliptical tori. Both continuous energy and multigroup cross sections can be used with MCNP. There are also very flexible and powerful tallying possibilities.<sup>3</sup>

### 3.3 - STEDFAST

The Dancoff altered Wigner-Seitz cell (DAWSC) treatment has been in use for at least a couple years in the Scale package. Its use was advertised and recommended in the Summer/Fall 2010 Scale newsletter for users to take advantage of when analyzing high void fraction BWR lattices. High void fraction BWR lattices were particularly emphasized because these conditions do not bode well with the assumptions made by the Wigner-Seitz cell. The Wigner-Seitz cell assumes that the fuel pin is surrounded by an infinite lattice of similar pins. However, irregularities in the lattice are more visible to a pin as the moderator density decreases. Although the use of DAWSC was recommended, at the time its application was a cumbersome process that posed several chances for users to commit errors which had no obvious error checking other than a keen eye. The code STEDFAST (Self-shielding Tool for Equivalent Dancoff Factor Addjusted Wigner-Seitz Treatment) was developed to automate the application of DAWSC to lattices. This includes the conversion of the input from NEWT to MCDancoff, calculation of Dancoff corrections, interpretation of Dancoff corrections for similar fuel pins, creation of new materials and geometry for fuel pins identified with unique Dancoff corrections, creation of necessary CENTRM inputs for all fuel pins, and final compilation of the new NEWT input. STEDFAST consists of 36 modules written in Python. A large majority of these modules can be run standalone to assist with error checking. A flow diagram showing the major functions of the code is shown in Figure 3-2



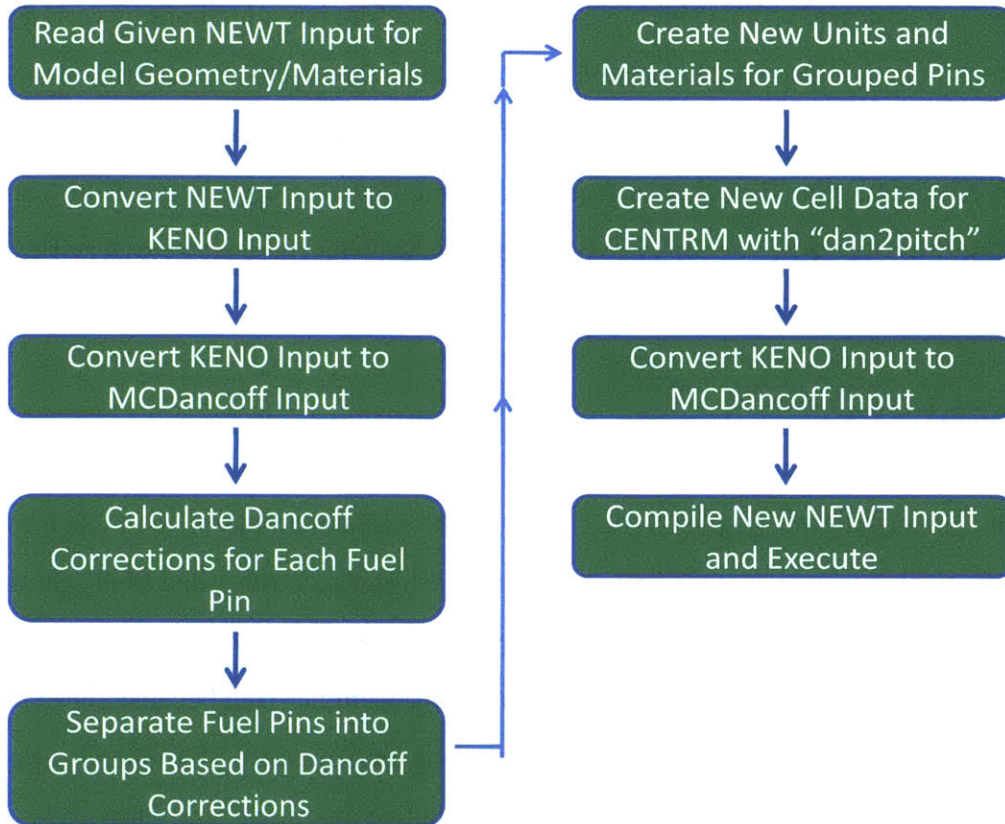


Figure 3-2: A simplified flow diagram for the code STEDFAST

The first steps taken by STEDFAST are to read the NEWT input and gather information regarding the geometry and materials. The next steps included making necessary changes to the NEWT input to convert it to a KENO input. Since MCDancoff is a slightly altered version of KENO, MCDancoff inputs are extremely similar. A significant effort was made to automate the conversion of a NEWT input to the MCDancoff input and because of this some of the differences between the two formats will be highlighted. There are small, obvious differences which must be changed such as needing to add a z-dimension to all of the geometric cells, removing the grid specifications from the boundary of each unit, removing any NEWT specific syntax such as “sides=” or the pin power option for arrays, etc. In addition, the commonly used FIDO input shortcuts of “r” and “p” had to be supported.

One of the major differences between NEWT and KENO is that NEWT sequences can include depletion data for use in TRITON. With depletion data comes the possibility of using assigned mixtures. Assigned mixtures are used to assign several mixtures to a “parent” mixture.

## Chapter 3 - Methods

This parent mixture is used in the resonance self-shielding calculations for each burnup step during the depletion in place of performing a separate resonance self-shielding calculation for each of the assigned mixtures. This is commonly applied to fuel pins that start out with the same fuel mixture, but exist in different positions in the lattice. Each assigned mixture uses independent atom densities for the two-dimensional calculations, however for the resonance self-shielding calculations use an average value for the number densities of nuclides in each assigned mixture. What this means in practice is that the parent mixtures are defined in the composition data, *but* the mixtures used inside the geometry description are the assigned mixtures. The end result is that if a NEWT input with assigned mixtures is converted to KENO, none of the mixtures used in the problem are defined in the composition data! Thus, a significant amount of bookkeeping was necessary to create new mixtures for the KENO input. This was increased when it was necessary to add new mixtures and units to the new NEWT input because the mixtures assignments within the depletion block had to be changed.

Another key difference between NEWT and KENO inputs that users should be aware of is how an array can/must be placed into the model. It turns out that NEWT is somewhat more flexible in the way it can place an array into the model. In NEWT an array can be defined and then placed into a unit on top of an already existing mixture. In fact, a mixture *must* be filled into the region that the array goes into, even if it is just void. KENO on the other hand must have cell defined that array fits into, with no mixtures pre-existing in that cell. Additionally, the cell size cannot be larger the dimensions of the array. Thus, when converting an array from NEWT to KENO it is possible to be placing a KENO array into an incorrectly sized cell that is unacceptably pre-filled with mixture. In order to remedy this situation STEDFAST calculates the dimensions of the array in NEWT, and if this is not the size of the cell a new cell is made in order to properly fit the array. Media descriptions are then appropriately updated for the new cell relationships.

After the KENO input is created this is converted to MCDancoff. A few minor changes include the computational sequence, the cross sections, and the parameters block. The main change that must be made is the addition of a Start Data block that specifies the regions for which Dancoff corrections will be calculated. MCDancoff uses a syntax that allows a fuel region

to be selected regardless of how deeply it may be buried inside nested holes or arrays. A key point for the proper setup of the Start Data is ensuring that the correct region is selected from the unit with fuel. If multiple rings of fuel bearing mixtures exist in a fuel pin, the outermost fuel region must be selected. The Dancoff correction for an inner fuel ring will be 1.0 since the fuel is black to neutrons in MCDancoff. This is accomplished in STEDFAST by identifying which cells in a fuel pin contain fuel, and then selecting the one with the largest radius. MCDancoff is then executed by STEDFAST.

After MCDancoff has finished running, STEDFAST collects all the Dancoff corrections for fuel pins while keeping track of any skipped array locations due to water holes. Another notable difference between NEWT and KENO is the order in which array units are read. NEWT reads array units from left to right, and bottom to top (similar to MCNP). KENO on the other hand reads array units from left to right, and from top to bottom (so the array definition is oriented the way you would expect it to be in real life). Next, the Dancoff corrections are analyzed so that fuel pins sharing the same fuel mixture but that have significantly different Dancoff corrections are segregated into groups of similar Dancoff corrections. The actual number that determines significance among Dancoff corrections is adjustable by the user; however a 2% tolerance has yielded reasonable results in the cases tested. This segregation of fuel pins is accomplished by taking a list of all fuel pins using the same fuel mixture and sorting their Dancoff corrections from least to greatest. Next the list is stepped through, one Dancoff correction at a time and the average Dancoff correction is calculated for all previous Dancoff corrections in the list. If the Dancoff correction being analyzed is not within the Dancoff tolerance (2%) of the average then the Dancoff correction list is split at this point into two separate lists. The list with the lower Dancoff corrections are now considered their own unique group of fuel pins. This calculation is continued for the other part of the split list to see if additional groups of pins have significantly different Dancoff corrections.

After decisions regarding the Dancoff corrections have been made, new mixtures and units are created. The array map of units must also be updated with the new units. CENTRM inputs are then created in the Cell Data block with the appropriate  $\text{dan2pitch}(\text{fuel\_mix\_id}) =$  Dancoff correction. The geometry for the CENTRM inputs is determined based on the geometry

## Chapter 3 - Methods

and materials data that was read from the input in the first step. For a fuel pin that has multiple fuel rings, the multiregion CENTRM treatment is necessary. Unfortunately this sequence is not setup to work with the dan2pitch keyword which is used to adjust the pitch in the Wigner-Seitz cell in CENTRM. This is overcome in STEDFAST by creating a CSAS1 input with the “parm=check” option and a unit cell description that uses *just one* fuel region and the dan2pitch option. When this is executed the desired pitch for the given Dancoff correction is printed in the output. STEDFAST uses this value in order to apply DAWSC treatment to a multiregion unit cell.

At this point a new NEWT input has been created with new mixtures and units have been created. CENTRM input with the “dan2pitch” keyword has been implemented and the input is ready to execute. Note that the use of STEDFAST in order to create just the CENTRM input is a worthwhile function in my opinion because it removes chances for the user to make mistakes in the self-shielding model.

## Chapter 4 – Results and Discussion

### 4.1 - Analysis of the Wigner-Seitz Cell Approximation

The Wigner-Seitz cell approximation is a very old idea and has been analyzed many times, however it is a significant modeling assumption because it changes the fundamental geometry and its effects must not be overlooked. For historical purposes an equivalent cylindrical cell with a reflective boundary condition was also analyzed for comparison. MCNP5 version 1.51 with ENDF/B-VII.0 continuous energy cross sections was used to analyze the unit cells. The unit cells analyzed were for a 2.93 wt. % U-235 enriched  $\text{UO}_2$  pin with a pitch-to-diameter ratio of 1.547 and radius of 0.60579 cm. The pin geometry and materials are given in Table 4-1. Satisfactory statistics were obtained by running 100 inactive cycles followed by 500 active cycles of  $5\text{E}+05$  histories per cycle. F4 tallies were performed while using the 238 group neutron library structure used in Scale. Further details can be found in the input which is provided in Appendix A. Results are shown and discussed below.

*Table 4-1: Model parameters for a  $\text{UO}_2$  pin cell modeled in MCNP5*

Parameter	Value
Fuel Radius	0.60579 [cm]
Gap Outer Radius	0.6210 [cm]
Clad Outer Radius	0.7150 [cm]
Pitch	1.8745 [cm]
Moderator Density	0.4349 [ $\text{g cm}^{-3}$ ]
$\text{UO}_2$ Density	10.32 [ $\text{g cm}^{-3}$ ]

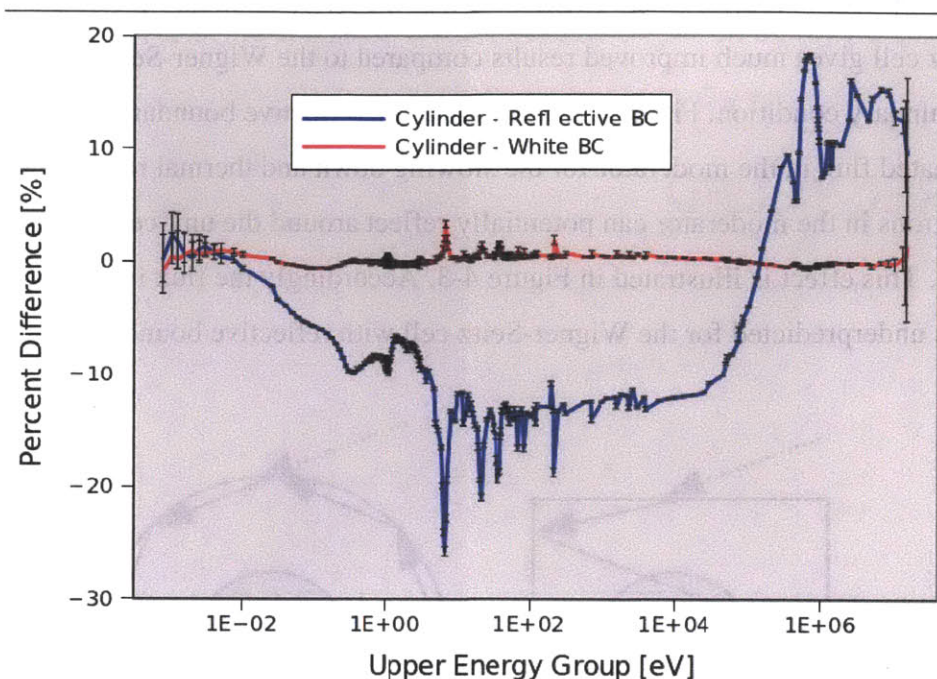


Figure 4-1: Percent Difference in Flux in the Fuel for Equivalent Cylindrical Unit Cells Using Reflective and White Boundary Conditions Relative to a Square Unit Cell. All error bars depicted represent a 99% confidence interval.

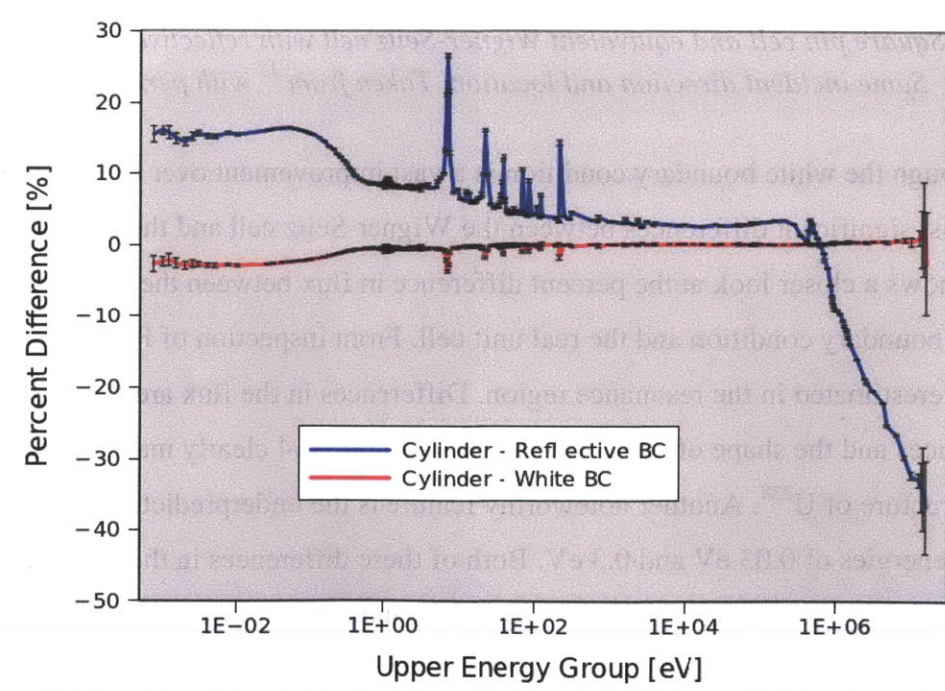
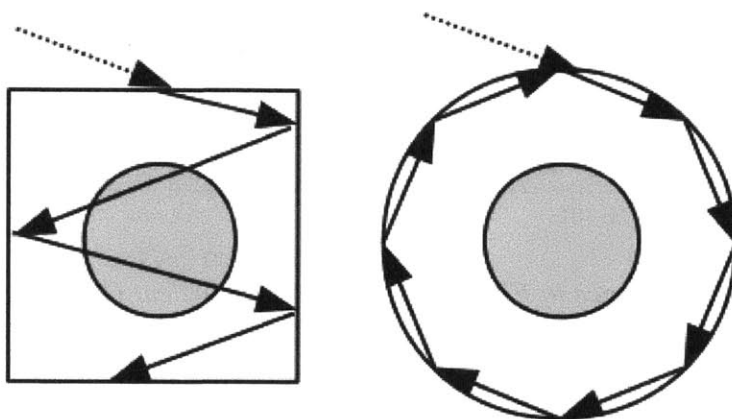


Figure 4-2: Percent Difference in Flux in the Moderator for Equivalent Cylindrical Unit Cells Using Reflective and White Boundary Conditions Relative to a Square Unit Cell. All error bars depicted represent a 99% confidence interval.

It is clear from Figure 4-1 and Figure 4-2 that the white boundary condition applied to the Wigner-Seitz cell gives much improved results compared to the Wigner-Seitz cell with a reflective boundary condition. Figure 4-2 shows that the reflective boundary condition leads to an overestimated flux in the moderator for the slowing down and thermal regions. This is because neutrons in the moderator can potentially reflect around the unit cell without intersection with the fuel. This effect is illustrated in Figure 4-3. Accordingly the flux in the fuel seen in Figure 4-1 is underpredicted for the Wigner-Seitz cell with reflective boundary condition.



*Figure 4-3: Square pin cell and equivalent Wigner-Seitz cell with reflective boundary condition. Same incident direction and location. Taken from <sup>13</sup> with permission.*

Although the white boundary condition is a vast improvement over the reflective case, there still exist significant differences between the Wigner-Seitz cell and the actual unit cell. Figure 4-4 shows a closer look at the percent difference in flux between the Wigner-Seitz cell with a white boundary condition and the real unit cell. From inspection of Figure 4-4 the flux in the fuel is overestimated in the resonance region. Differences in the flux are most notable near large resonances and the shape of these differences in Figure 4-4 clearly map out the well known resonance structure of  $U^{238}$ . Another noteworthy feature is the underpredicted flux in the fuel between the energies of 0.03 eV and 0.3 eV. Both of these differences in the flux will reduce k-eff relative to the actual unit cell. K-eff for each of the unit cell representations is reported in Table 4-2.

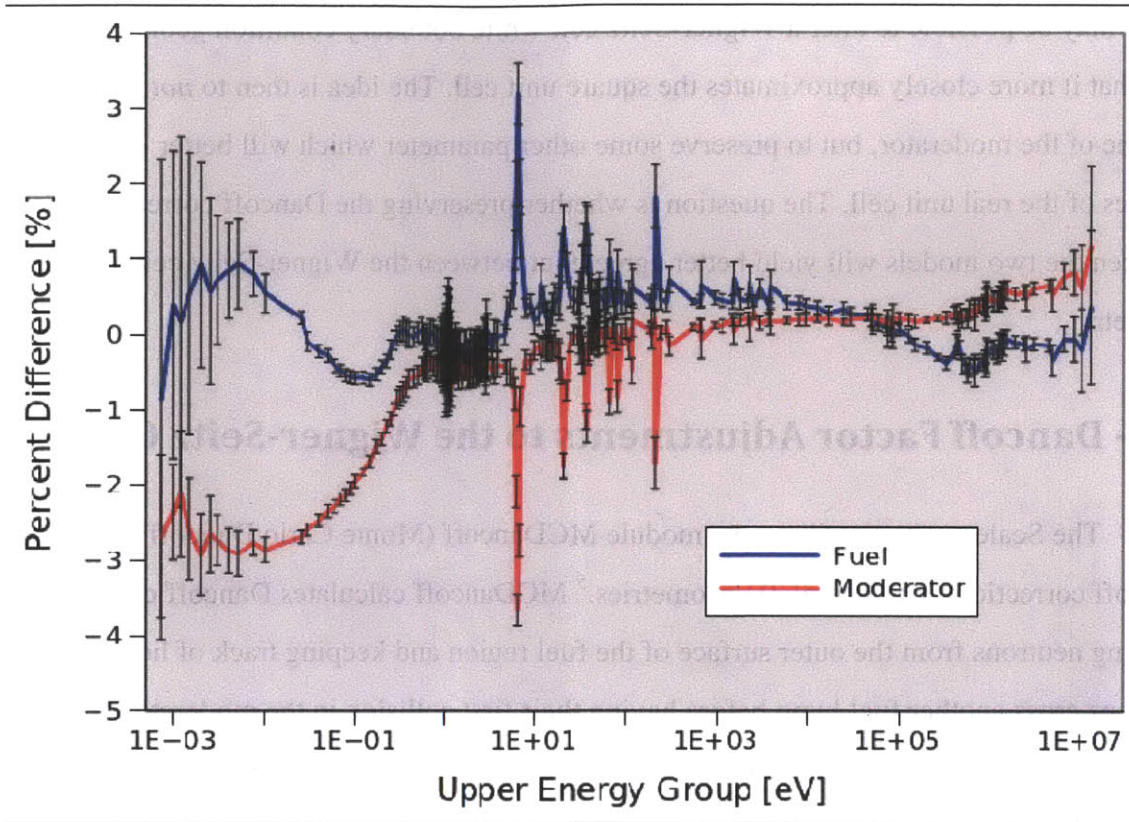


Figure 4-4: Percent difference in flux in the moderator and fuel for a Wigner-Seitz cell using a white boundary condition relative to a square unit cell. All error bars depicted represent a 99% confidence interval.

Table 4-2:  $K_{eff}$  for the unit cell for the real geometry compared to Wigner-Seitz approximations with white and reflective boundary conditions.

	k-eff	$3\sigma$ Uncertainty (pcm)	Difference (pcm)
Square	1.22818	12	-
Wigner-Seitz - White	1.22510	12	$-308 \pm 17$
Wigner-Seitz - Reflective	1.28109	12	$5291 \pm 17$

$K_{eff}$  for the Wigner-Seitz cell with a white boundary condition is approximately 308 pcm less than  $k_{eff}$  of the real geometry, which is consistent with the qualitative analysis of the flux in the fuel. For typical light water reactor unit cells, the white boundary condition produces a harder spectrum than the square unit cell. These differences in neutron spectra between a square unit cell and an equivalent Wigner-Seitz cell have an effect on the collapsed cross sections used in higher dimensional transport simulations. One conjecture that will be tested is



that it may be possible to alter a Wigner-Seitz cell white boundary condition geometry in such a way that it more closely approximates the square unit cell. The idea is then to *not* preserve the volume of the moderator, but to preserve some other parameter which will better match the physics of the real unit cell. The question is whether preserving the Dancoff correction/factor between the two models will yield better agreement between the Wigner-Seitz cell and the actual geometry.

## 4.2 - Dancoff Factor Adjustments to the Wigner-Seitz Cell

The Scale package utilizes the module MCDancoff (Monte Carlo Dancoff) to calculate Dancoff corrections for general 3D geometries.<sup>5</sup> MCDancoff calculates Dancoff corrections by emitting neutrons from the outer surface of the fuel region and keeping track of how many neutrons cross another fuel lump before having their first collision in the moderator or structural material. Due to the way the code is implemented, the neutrons which are emitted from the surface of the fuel are also emitted from the top and bottom of a cylindrical fuel element. A Neutron emitted from one of these surfaces will be reflected due to the boundary conditions imposed and captured into the fuel element, thus impacting the calculated value of the Dancoff correction in a way inconsistent with definition of a Dancoff correction. Making the fuel element long relative diameter of pin will reduce this effect and make the Dancoff correction converge to a particular value. From experience it has been observed that the Dancoff correction will not converge until the length of the fuel region is well over 100 cm. However, it has also been observed that many users of MCDancoff use values of 10 cm to 40 cm. Several adjusted Wigner-Seitz cells were evaluated using MCNP5. The unit cells differ due to changes in the moderator thickness which is altered to match the Dancoff correction as calculated by MCDancoff. Table 4-3 shows k-eff for each of these cases compared to the real geometry and the unaltered Wigner-Seitz cell that conserves moderator volume. The resulting changes in flux and reaction rates for these models are analogous to the changes in a CENTRM model using a Dancoff adjustment. Figure 4-5 shows the geometry of the square unit cell, the Wigner-Seitz cell that conserves moderator volume, as well as the Dancoff factor adjusted Wigner-Seitz cells.

Table 4-3: *K*-eff for the unit cell with the real geometry compared to cells using the Wigner-Seitz approximations with white boundary conditions. Several different Dancoff corrections were used to examine tendencies. Outer radius of moderator is determined by the Dancoff correction.

Unit Cell Type	Fuel Length for Dancoff Calculation (cm)	Dancoff Correction	Outer Radius of Moderator (cm)	k-eff	3 $\sigma$ Uncertainty (pcm)	Difference (pcm)
Square	-	-	-	1.22818	12	-
Wigner-Seitz - Volume Conserved	-	-	1.05758	1.22510	12	-308 $\pm$ 17
Wigner-Seitz - Dancoff Conserved	160	0.3540	1.05402	1.22186	12	-632 $\pm$ 17
Wigner-Seitz - Dancoff Conserved	40	0.3616	1.04584	1.21457	12	-1361 $\pm$ 17
Wigner-Seitz - Dancoff Conserved	30	0.3649	1.04234	1.21139	12	-1679 $\pm$ 17
Wigner-Seitz - Dancoff Conserved	20	0.3709	1.03596	1.20532	12	-2286 $\pm$ 17
Wigner-Seitz - Dancoff Conserved	10	0.3890	1.01757	1.18714	12	-4104 $\pm$ 17

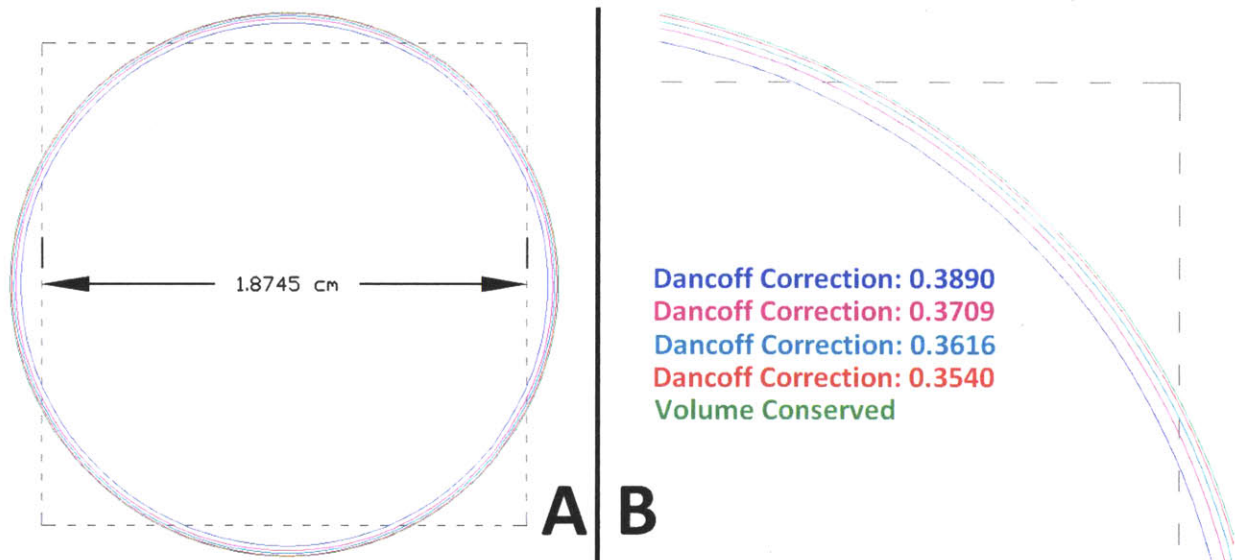


Figure 4-5: Unit cell geometry for a square lattice element, an equivalent Wigner-Seitz cell and several Dancoff correction adjusted Wigner-Seitz cells with dimensions listed in Table 4-3. Side A depicts the all of the unit cells while Side B shows a close up of the unit cell boundaries.

Table 4-3 shows that there is a significant variation in k-eff for the unit cell depending on the height of the fuel used to calculate the Dancoff correction in MCDancoff. All of the Wigner-Seitz cells underpredict k-eff including the cell that conserves moderator volume which underestimated k-eff by 308 pcm. The converged value for the Dancoff correction (length of 160cm) leads to a 632 pcm underestimation in k-eff. All of the Dancoff factor adjusted cells had less moderator than the true moderator volume. Values of 40 cm, 30 cm, 20 cm and 10 cm for the length of the fuel element in MCDancoff were also analyzed since this is what has been used

in practice. Decreasing the fuel height in MCDancoff increases the Dancoff correction (decreases the Dancoff factor) for the cell and leads to a decrease in moderator radius. Removing moderator from an already undermoderated system of course leads to further lower values for k-eff.

Figure 4-6 shows the relative difference for the flux in the fuel for the different Wigner-Seitz cells compared to the square unit cell. The smallest reduction in moderator is given by the 160 cm fuel height flux results. The reduction in moderation leads to an increased estimate for the flux above thermal energies and a decreased flux in the thermal energy range. Further reduction in moderation seen in the 40 cm fuel height simulation gives similar perturbations to the flux just to a larger degree. The 10 cm fuel height simulation is a much more extreme case of reducing moderator and the same general reduction/increase in thermal/fast fluxes is observed just at an even larger magnitude than for the other cases. A key difference for the 10 cm fuel height case is that the flux near resonances is depressed relative to the flux just outside the resonances.

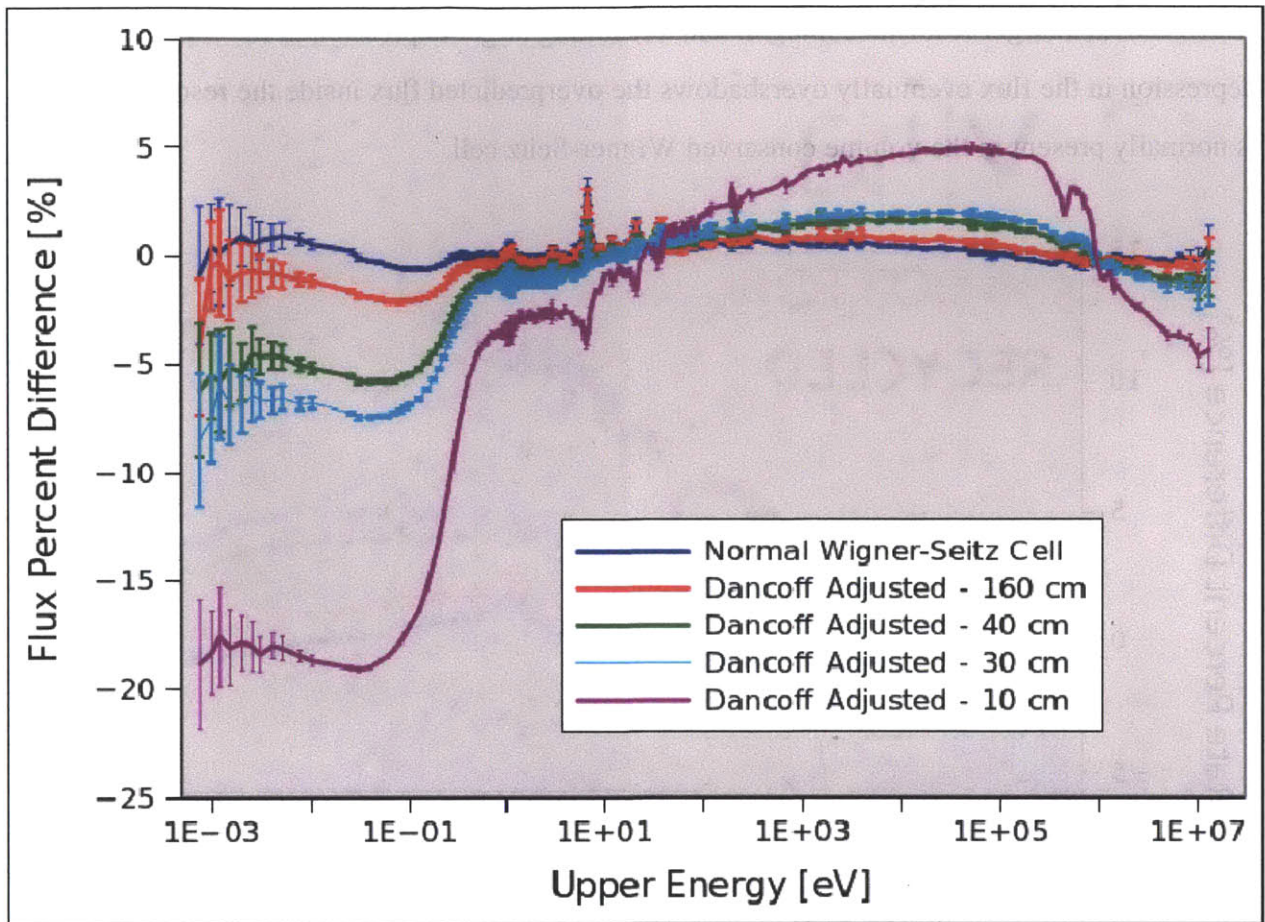


Figure 4-6: Percent difference in flux in the fuel for a normal Wigner-Seitz cell where the volume of moderator is conserved as well as for three different Dancoff adjusted Wigner-Seitz cells. Percent difference is relative to the actual square unit cell. All error bars depicted represent a 99% confidence interval

Figure 4-7 and Figure 4-8 show percent differences in  $U^{238}$  absorption reaction rates and  $U^{235}$  fission reaction rates, respectively, between the standard Wigner-Seitz cell and the 160 cm, 40 cm, 30 cm and 10 cm Dancoff adjusted Wigner-Seitz cells relative to the square unit cell. As it would be expected, the trends in the reaction rates are the same as for the flux. Reducing moderator volume tends to increase reaction rates in the slowing down energy region and decrease reaction rates in the thermal energy range. Note that even though the reaction rates are increased in the resonance energy range, for the 10 cm fuel height case there are obviously differences because the sign of the error flips inside the resonance. For the normal Wigner-Seitz cell the flux is clearly overpredicted inside the resonances. In terms of equivalence theory, as moderator is removed from the system, the background cross section for the unit cell is reduced,

which causes a larger resonance integral and a resulting larger depression in the flux. This larger depression in the flux eventually overshadows the overpredicted flux inside the resonances that is normally present in the volume conserved Wigner-Seitz cell.

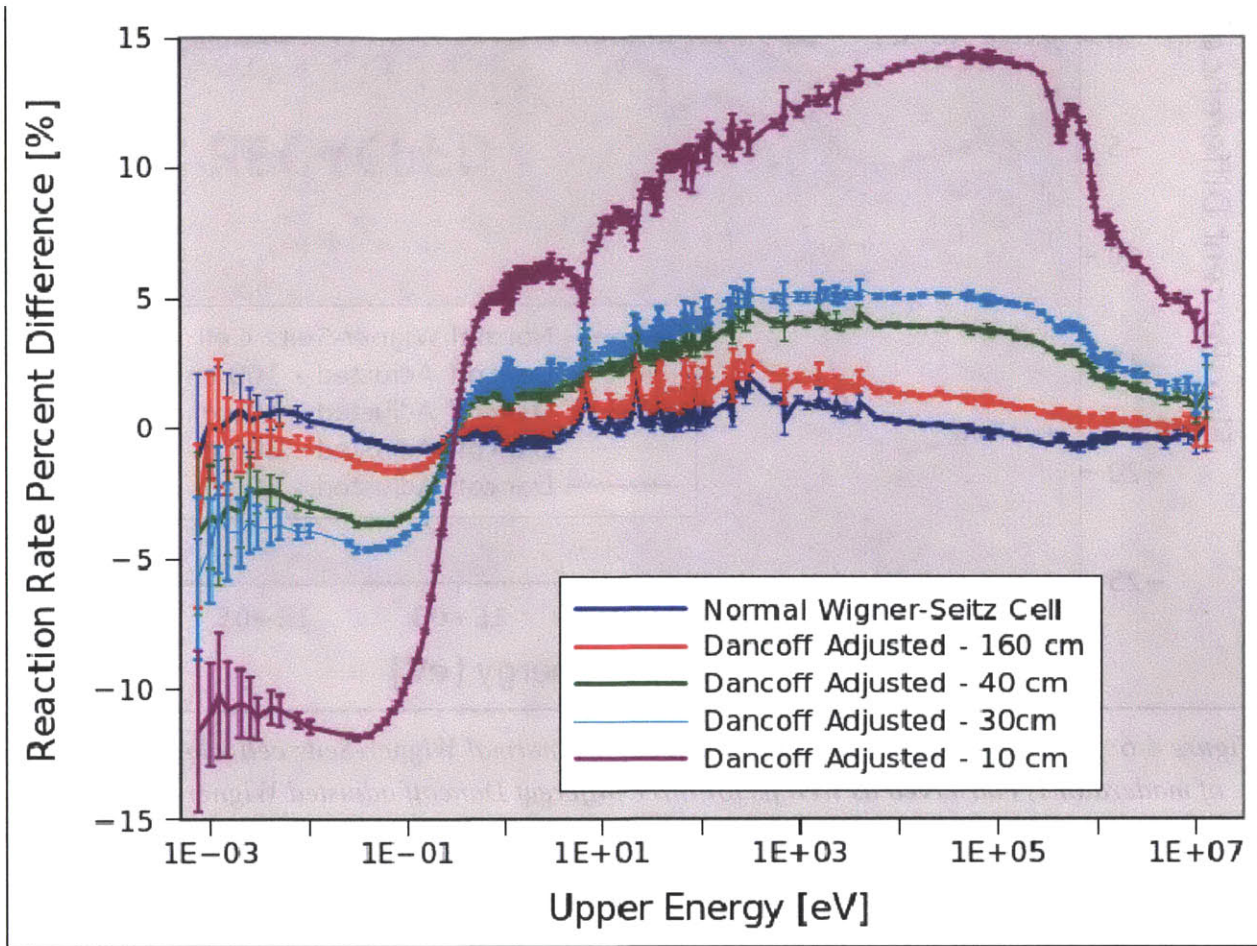


Figure 4-7:  $U^{238}$  absorption reaction rates for a normal Wigner-Seitz cell where the volume of moderator is conserved as well as for three different Dancoff adjusted Wigner-Seitz cells. Percent difference is relative to the actual square unit cell. All error bars represent 99% confidence intervals.

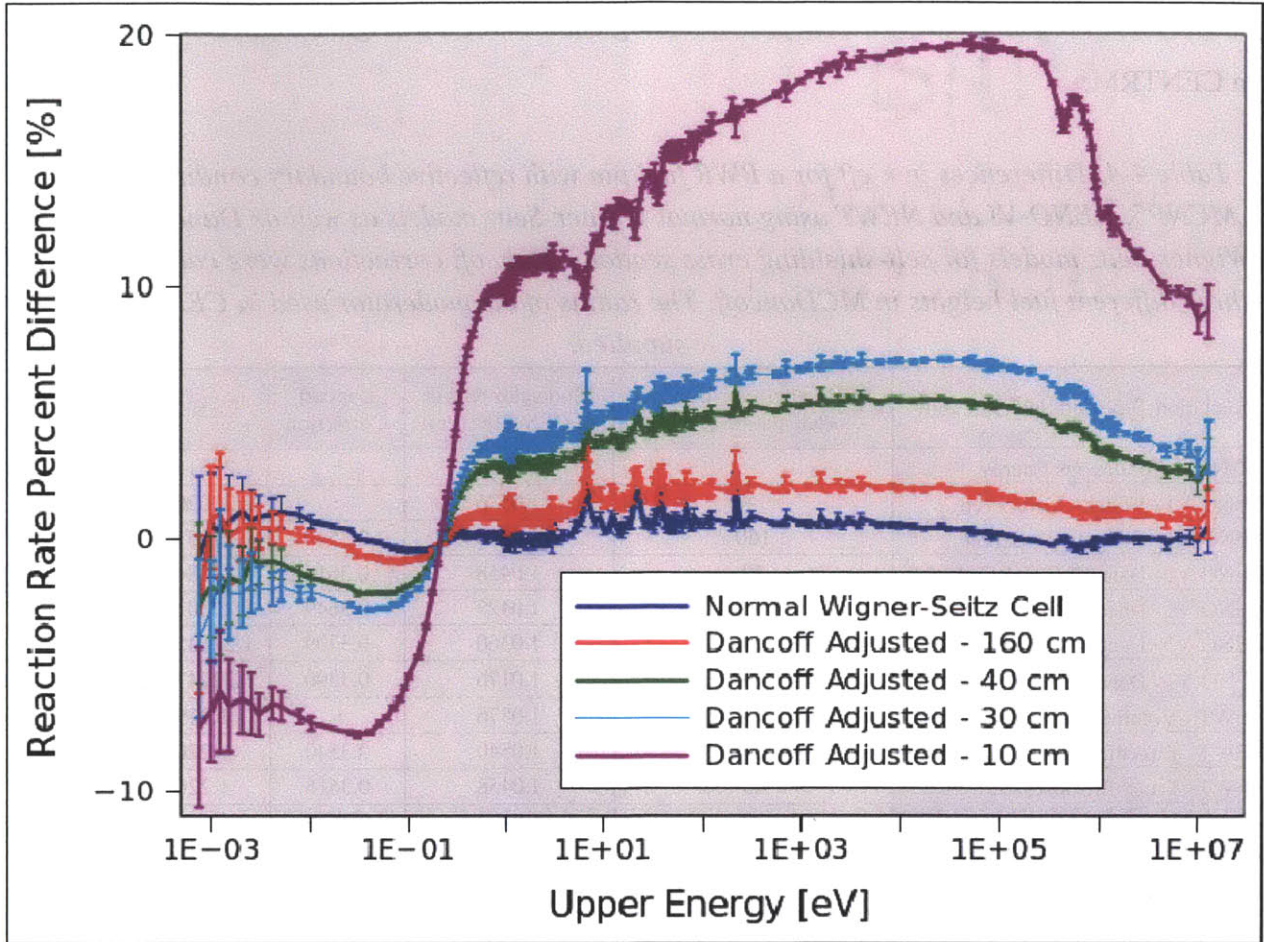


Figure 4-8:  $U^{235}$  fission reaction rates for a normal Wigner-Seitz cell where the volume of moderator is conserved as well as for three different Dancoff correction adjusted Wigner-Seitz cells. Percent difference is relative to the actual square unit cell. All error bars represent 99% confidence intervals.

### 4.3 - Effects of Dancoff Factor Adjustments on Infinite Lattices

The previous section examined the effects of using a Dancoff correction to alter the moderator geometry of a unit cell. The effects shown so far on the flux and reaction rates *are within the self-shielding model*. This section will examine the effects on the 2-D or 3-D model that makes use of the cross sections which were previously self-shielded. A fuel pin with reflective boundary conditions was modeled using MCNP5 in continuous energy mode and was used as the reference solution. KENO-VI and NEWT were both used as multigroup transport solvers to compare results of different self-shielding choices for cross sections. Table 4-4 shows

results for k-eff using four different self-shielding choices for the Wigner-Seitz cell that was used in CENTRM.

*Table 4-4: Differences in k-eff for a BWR fuel pin with reflective boundary conditions among MCNP5, KENO-VI and NEWT using normal Wigner-Seitz models as well as Dancoff adjusted Wigner-Seitz models for self-shielding cross sections. Dancoff corrections were calculated using three different fuel heights in MCDancoff. The radius of the moderator used in CENTRM is also supplied.*

Simulation Type and Self-Shielding	Fuel Length for Dancoff Calculation (cm)	Moderator Radius in CENTRM (cm)	Dancoff Correction	k-eff ± 3σ	Difference (pcm)
MCNP5 - Continuous Energy	-	-	-	1.22818 ± 12	-
KENO-VI - Volume Conserved	-	1.0576	-	1.22020 ± 22	-798 ± 25
KENO-VI - Dancoff Conserved	160	1.0540	0.3540	1.22051 ± 21	-767 ± 24
KENO-VI - Dancoff Conserved	40	1.0458	0.3616	1.22084 ± 20	-734 ± 24
KENO-VI - Dancoff Conserved	30	1.0423	0.3649	1.22103 ± 21	715 ± 24
KENO-VI - Dancoff Conserved	20	1.0360	0.3709	1.22142 ± 21	-676 ± 24
KENO-VI - Dancoff Conserved	10	1.0176	0.3890	1.22247 ± 21	-571 ± 24
NEWT - Volume Conserved	-	1.0576	-	1.21995	-823 ± 12
NEWT - Dancoff Conserved	160	1.0540	0.3540	1.22014	-804 ± 12
NEWT - Dancoff Conserved	40	1.0458	0.3616	1.22058	-760 ± 12
NEWT - Dancoff Conserved	30	1.0423	0.3649	1.22077	-741 ± 12
NEWT - Dancoff Conserved	20	1.0360	0.3709	1.22113	-705 ± 12
NEWT - Dancoff Conserved	10	1.0176	0.3890	1.22220	-598 ± 12

K-eff is underpredicted in all multigroup simulations however the Dancoff factor adjusted self-shielding improved results in k-eff by 19 pcm, 63 pcm, 82 pcm, 118 pcm and 206 pcm for the 160 cm, 40 cm, 30cm, 20 cm and 10 cm cases, respectively. The radius of the moderator used in the CENTRM Wigner-Seitz model is also given in Table 4-4 and decreases with decreasing height used in the MCDancoff model as expected. In all Dancoff factor adjusted models the moderator radius is smaller than the moderator radius used in the normal Wigner-Seitz model which conserves moderator volume. Improvement in prediction of k-eff increases as the moderator radius in CENTRM decreases for the cases simulated.

The microscopic cross sections for U<sup>238</sup> absorption that were used by KENO-VI and NEWT for different MCDancoff fuel heights were compared to the effective microscopic cross sections from MCNP5. Multigroup MCNP5 cross sections were calculated using the neutron flux and U<sup>238</sup> absorption reaction rate data which were both tallied using the Scale 238 neutron group library structure. Results are shown in Figure 4-9 for the resolved resonance range, which is

where the significant differences occur. The results show that the less converged Dancoff corrections yielded better results than the converged Dancoff correction cases. Also, there were much larger changes in the cross sections for the higher energy resolved resonances than the changes seen in the lower energy resonances (the three lowest energy large resonances). This difference is likely because the flux perturbation in the fuel is larger at high energies than in the 10's of eV as shown in previous data such as Figure 4-6.

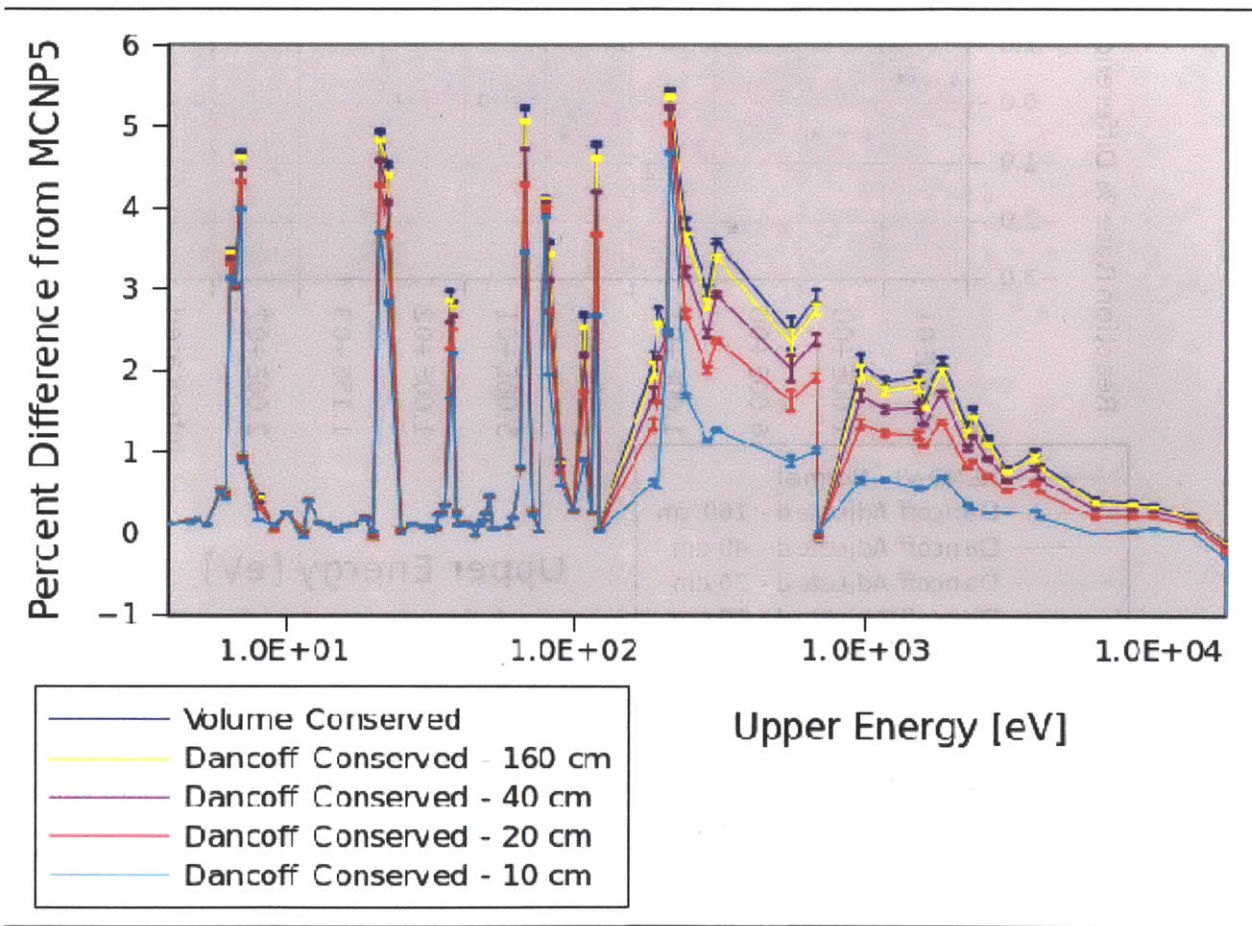


Figure 4-9: Percent difference relative to MCNP5 in  $U^{238}$  absorption microscopic cross sections from CENTRM using several Dancoff adjusted Wigner-Seitz cell.

Figure 4-10 and Figure 4-11 compare the  $U^{235}$  fission reaction rates and the  $U^{238}$  absorption reaction rates, respectively, among the different cross-section self-shielding choices. All reaction rates were normalized to the same power. Due to this normalization the integrated fission reaction rates were all equal; however there was very little variation in  $U^{235}$  fission



reaction rates in the 9 energy group structure. The only statistically significant differences were found in the highest energy group. Figure 4-11 shows statistically significant differences for the  $U^{238}$  reaction rates among all of the Dancoff factor adjusted simulations. The shorter the fuel height used in the MCDancoff simulation (the smaller the moderator radius) the more that  $U^{238}$  reaction rates approached the MCNP5 solution.

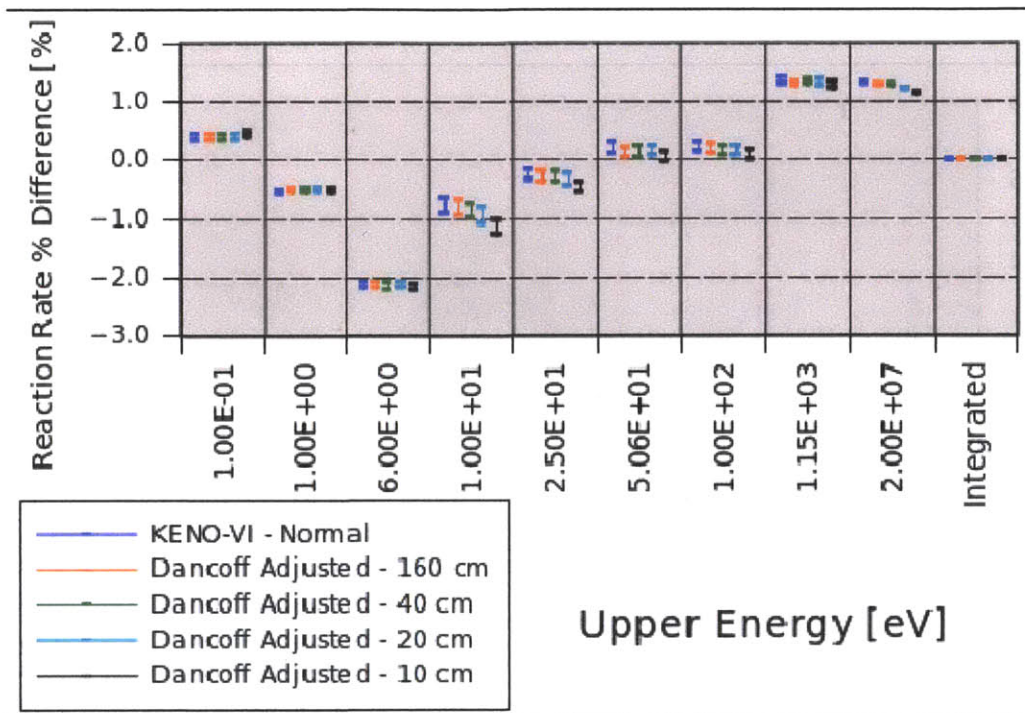


Figure 4-10: 99% confidence intervals for the percent difference in  $U^{235}$  fission reaction rates for a BWR fuel pin with reflective boundary conditions. Four different self-shielded cross section sets are compared and used with KENO-VI. Percent differences are relative to the actual square unit cell which was modeled with MCNP5.

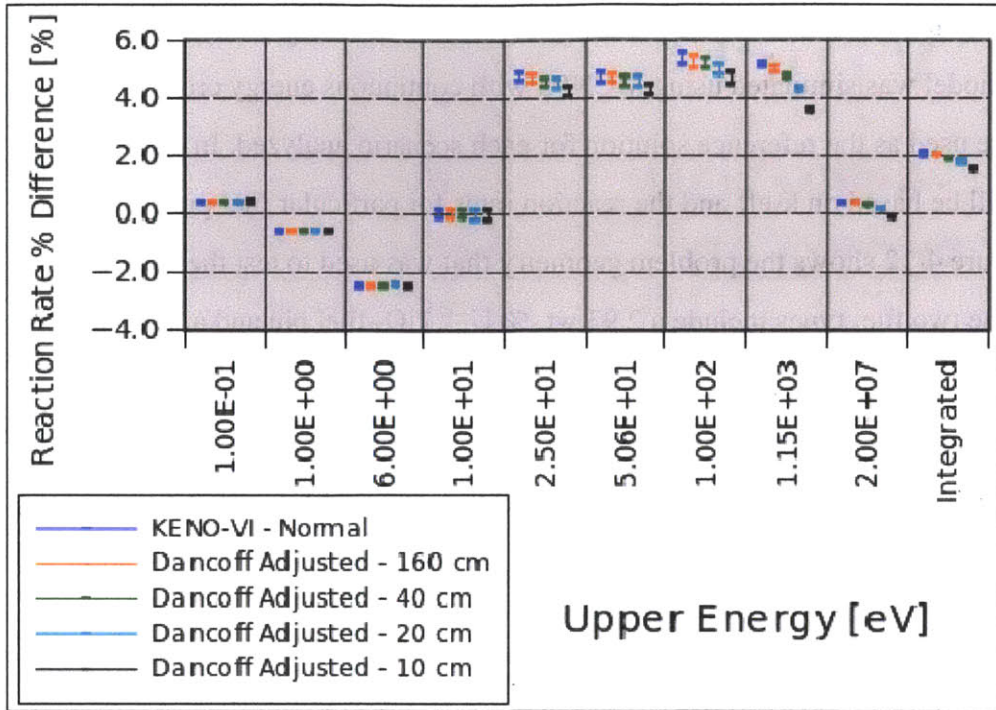


Figure 4-11: 99% confidence intervals for the percent difference in  $U^{238}$  absorption reaction rates for a BWR fuel pin with reflective boundary conditions. Four different self-shielded cross section sets are compared and used with KENO-VI. Percent differences are relative to the actual square unit cell which was modeled with MCNP5.

### 4.4 - Effects of Dancoff Factor Adjustments on Irregular Lattices

In the following simulations Dancoff corrections from the 3-D bundle geometry were used to adjust unit cells modeled in the cross-section self-shielding module CENTRM. For each scenario that was analyzed, an accompanying simulation where traditional Wigner-Seitz unit cells were used in CENTRM was run for comparison. These simulations were done using KENO-VI and NEWT with the ENDF/B-VII.0 238 group neutron library in Scale 6.1. Although KENO-VI was the originally preferred transport solver for this application, due to irreconcilable differences in pin powers predicted by KENO-IV it was decided to use NEWT instead. In order to ensure that the NEWT simulations were well converged spatially a 32 by 32 mesh was used on each unit cell. In addition to this an angular quadrature of S12 was used to ensure that the angular variable was treated with sufficient fidelity as too low of quadrature can cause errors with the fast flux. These settings were used to make sure that any differences in results among

simulations could be attributed to the differences in self-shielding of the cross sections. A duplicate model was simulated using MCNP5 with continuous energy cross sections and the results were used as the reference solution for each scenario analyzed. In each scenario the analysis will be based on k-eff and the reaction rates for particular fuel pins.

Figure 4-12 shows the problem geometry that was used to test the Dancoff correction method. The two fuel types include a 2.93 wt. %  $U^{235}$   $UO_2$  fuel pin and a 2.93 wt. %  $U^{235}$   $UO_2$  with 3 wt. % gadolina fuel pin. The moderator density inside the bundle may vary depending on the void fraction modeled and will be specified for each analysis. Void fractions of 0 %, 40 %, and 80 % were analyzed to represent BWR conditions that commonly exist in practice. The moderator density in the bypass flow channel is always at saturated liquid conditions for 1100 psi. Detailed inputs can be found in Appendix C.

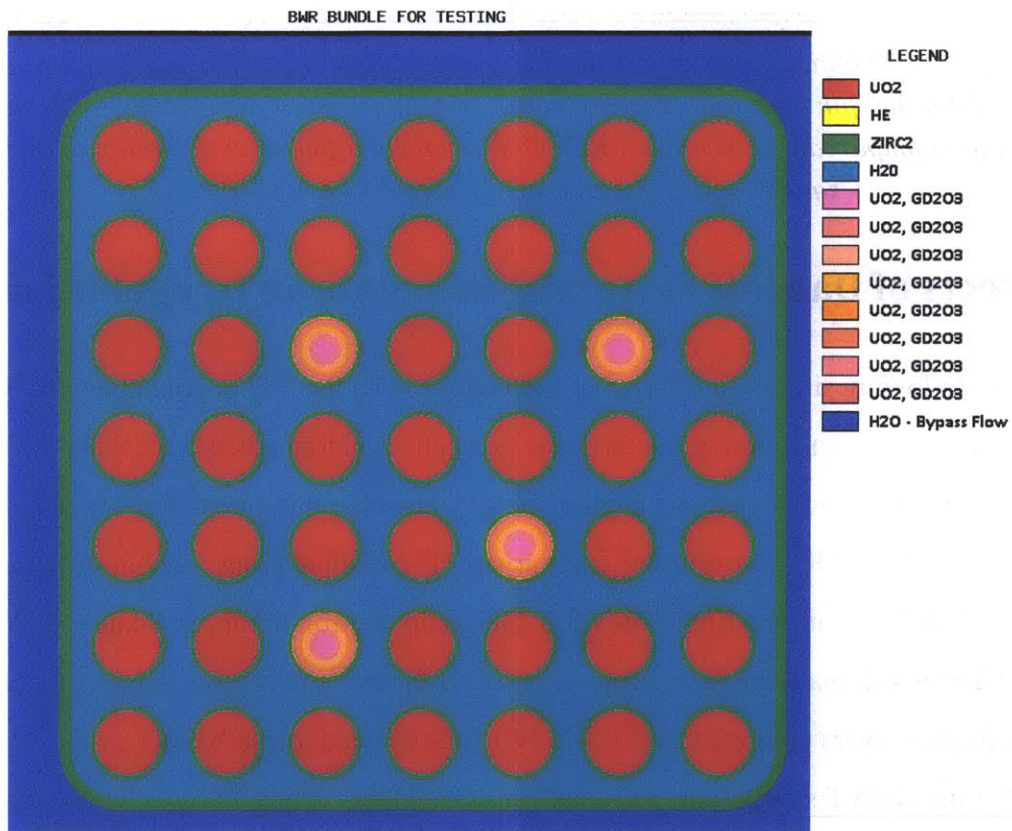


Figure 4-12: The problem geometry used in all simulations. A typical BWR bundle geometry using two fuel pin types with the wide bundle gap on the top and left side of the shroud. This figure was produced using Scale 6.1.<sup>5</sup>

## Chapter 4 – Results and Discussion

The BWR geometry with a void fraction of 40 % for the moderator was analyzed using the Python scripts described in the methods section and summarized within this paragraph. MCDancoff was used to calculate a Dancoff correction for every fuel element in the bundle. Fuel pins were separated into groups with similar Dancoff corrections and new materials and unit/universes were created for each group of similar pins. Each unit/universe had an independent set of cross sections that used an adjusted moderator thickness in the Wigner-Seitz cell within CENTRM according to the average Dancoff correction for that group of fuel pins. Fuel pin groups were determined such that for a particular pin to be assigned to a group, its Dancoff correction must be within 2 % of the average Dancoff correction for that group of pins.

As discussed in the previous section, the Dancoff correction that is calculated is dependent on the height of the fuel used in the MCDancoff model. Although theoretically a long fuel element should be used to correctly predict the Dancoff correction, fuel lengths of 10 cm and 40 cm were also analyzed since lengths in this range have been used in practice. Figure 4-13 shows the initial unit/universe map for the lattice, Dancoff correction maps for each of three fuel lengths used in MCDancoff, and the new unit/universe map for the lattice after fuel pins have been grouped by Dancoff correction.

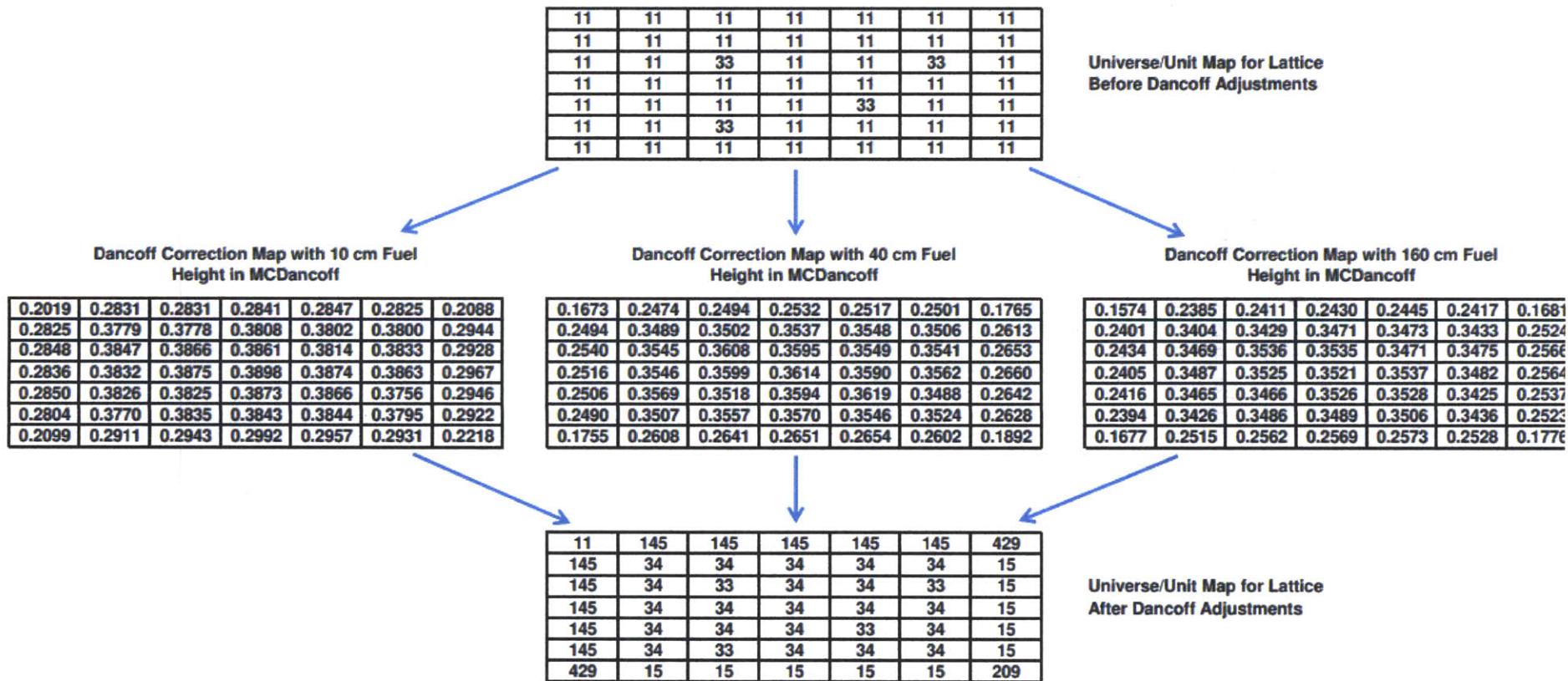


Figure 4-13: Unit/universe maps for the lattice before and after pins are grouped by Dancoff correction for a BWR bundle with a void fraction of 40 % for the moderator. Dancoff correction maps using fuel heights of 10 cm, 40 cm, and 160 cm in MCDancoff are shown. All Dancoff correction relative uncertainties are less than 0.15

Figure 4-13 shows that the Dancoff correction for the north west and south east corner fuel pins were unique and thus required unique unit/universe definitions (11 and 209 respectively). The remaining two corner pins shared the fact that they had the wide gap on one side and the thin gap on the other side and thus had similar Dancoff corrections. Other fuel pins along the side of the bundle were separated based on whether they were beside the wide gap (unit 145) or the narrow gap (unit 15). All the interior pins which did not have gadolinia had similar Dancoff corrections and thus were grouped together into unit 34. For this bundle, the fuel height used in MCDancoff did not affect the grouping of fuel pins however it had a significant effect on the actual value of the Dancoff corrections. For example the Dancoff correction for the fuel pin in unit 209 increased by 24.9 % when 10 cm was used instead of 160 cm for the fuel height.

*Table 4-5: Differences in k-eff for a BWR bundle with a void fraction of 40 % from MCNP5, KENO-VI and NEWT using normal Wigner-Seitz models for self-shielding cross sections, and KENO-VI and NEWT using Dancoff adjusted Wigner-Seitz models for self-shielding cross sections. Dancoff corrections were calculated using four different fuel heights in MCDancoff.*

Method Used	Fuel Length for Dancoff Calculation (cm)	k-eff	k-eff 3 $\sigma$ Uncertainty (pcm)	Difference (pcm)	Difference 3 $\sigma$ Uncertainty (pcm)
MCNP5 - Continuous Energy	-	1.15051	9.0	-	-
KENO-VI - No Adjustment	-	1.14487	15.3	-564	17.8
KENO-VI - Dancoff Adjusted	10	1.14425	14.9	-626	17.4
KENO-VI - Dancoff Adjusted	30	1.14336	15.0	-715	17.5
KENO-VI - Dancoff Adjusted	40	1.14329	15.2	-722	17.6
KENO-VI - Dancoff Adjusted	160	1.14304	16.1	-747	18.5
NEWT – No Adjustment	-	1.14751	-	-300	9.0
NEWT – Dancoff Adjusted	10	1.14681	-	-370	9.0
NEWT – Dancoff Adjusted	30	1.14601	-	-450	9.0
NEWT – Dancoff Adjusted	40	1.14588	-	-463	9.0
NEWT – Dancoff Adjusted	160	1.14562	-	-489	9.0

Table 4-5 shows differences in k-eff between MCNP5 using continuous energy cross sections and KENO-VI and NEWT using multigroup cross sections. The only difference in the KENO-VI and NEWT models is the way in which the self-shielded cross sections were generated. All cross sections were self-shielded using CENTRM with varying thicknesses of moderator by either conserving moderator volume or conserving the Dancoff correction for the

fuel pin. All KENO-VI models underpredicted k-eff for the bundle by more than 500 pcm while NEWT underpredicted k-eff by 300 or more pcm for all models. Although the results for k-eff are not the same for corresponding KENO-VI and NEWT simulations, the changes in k-eff among KENO-VI simulations are consistent with the changes in k-eff among respective NEWT simulations. For example the difference between NEWT k-eff values for the unadjusted self-shielding case and the 10 cm fuel height Dancoff adjusted case was  $70 \pm 13$  pcm. The difference in k-eff values from KENO-VI for respective self-shielding models was  $62 \pm 25$  pcm. The use of the Dancoff corrections to adjust the cross-section self shielding increased the already negative bias on k-eff for both KENO-VI and NEWT in statistically equivalent amounts.

MCNP Pin Powers						
1.8030	1.4775	1.3254	1.2667	1.2697	1.3334	1.5109
1.4770	1.1436	0.9696	0.9379	0.9384	0.9771	1.1774
1.3258	0.9702	0.2966	0.7509	0.7487	0.2971	0.9977
1.2677	0.9376	0.7498	0.7078	0.6892	0.7560	0.9716
1.2703	0.9391	0.7481	0.6887	0.2822	0.7968	1.0062
1.3327	0.9785	0.2973	0.7558	0.7965	0.9062	1.0931
1.5112	1.1802	0.9988	0.9724	1.0063	1.0948	1.2705

NEWT Percent Difference						
-0.90%	-0.07%	0.17%	0.33%	0.21%	-0.10%	-0.64%
-0.04%	0.09%	0.25%	0.23%	0.29%	0.14%	0.13%
0.14%	0.18%	0.34%	-0.11%	-0.05%	0.26%	0.31%
0.25%	0.25%	0.03%	0.22%	0.02%	0.17%	0.41%
0.16%	0.21%	0.02%	0.08%	0.13%	-0.06%	0.15%
-0.05%	-0.01%	0.21%	0.20%	-0.03%	-0.11%	-0.10%
-0.65%	-0.11%	0.20%	0.32%	0.14%	-0.25%	-0.73%

All Relative Errors are less than 0.15%

Figure 4-14: Pin power from MCNP5 and the percent difference from NEWT.

Figure 4-14 shows the pin power distribution from MCNP5 and the associated percent difference from NEWT calculations (all of them). Note that the pin power distribution was relatively insensitive to the self-shielding method. The maximum difference in any pin power from various NEWT calculations was less than 0.02%. All reaction rates that will follow were normalized to the entire assembly fission reaction rate so that each assembly was evaluated at the same power level. Since the pin powers from NEWT are all within 1% of the MCNP5 pin

## Chapter 4 – Results and Discussion

powers it can be expected that the differences in fission reaction rates integrated over all energies will also be within this range.

The following figures will show differences in reaction rates for  $U^{238}$  captures among each of the self-shielding models compared to MCNP5 continuous energy results.  $U^{235}$  fission rates remained relatively unchanged among models. Reaction rate differences are analyzed for each unique fuel pin group which is shown in the unit/universe map in Figure 4-13. Reaction rates for a given unit are summed for all similar units and thus represent the average value for a particular group of pins. Units 11 and 209 both contain just one fuel pin in their group, the wide gap corner pin and the narrow gap corner pin, respectively. Unit 429 values are an average of the other two corner pins. Values for units 145 and 15 given are averages of their respective ten edge pins they represent. Values for unit 34 are an average of the 21 interior fuel pins which do not contain gadolinia. Values for unit 33 are an average for the four fuel pins which contain gadolinia in the bundle.



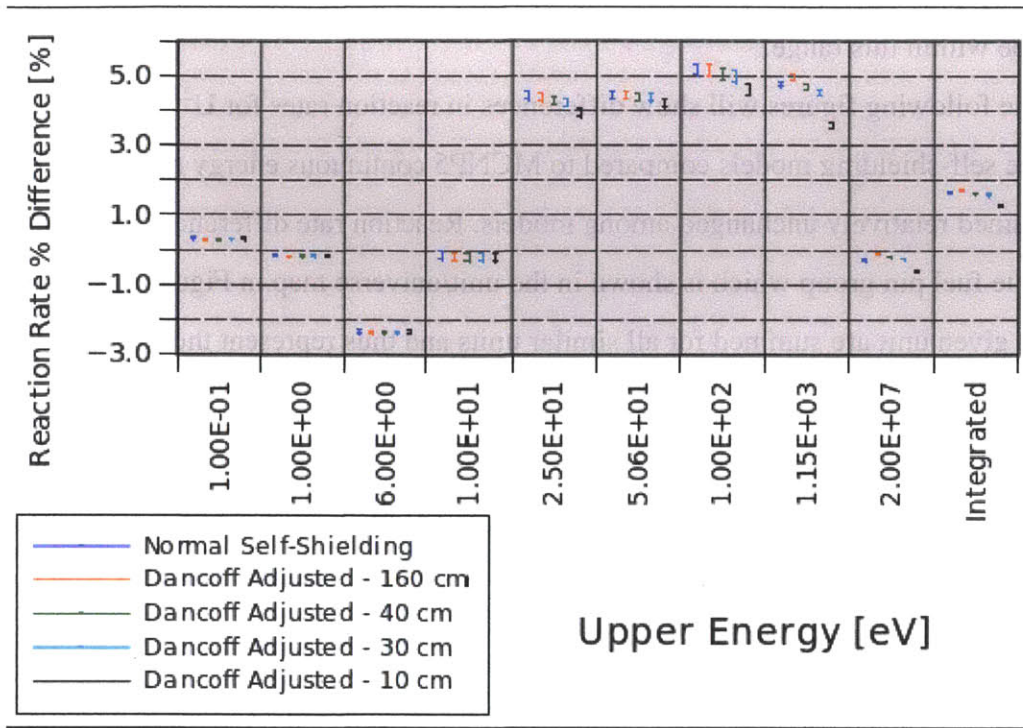


Figure 4-15: Unit 34 (Inner Fuel Pin)  $U^{238}$  reaction rate percent differences among self-shielding models relative to MCNP5 continuous energy results.

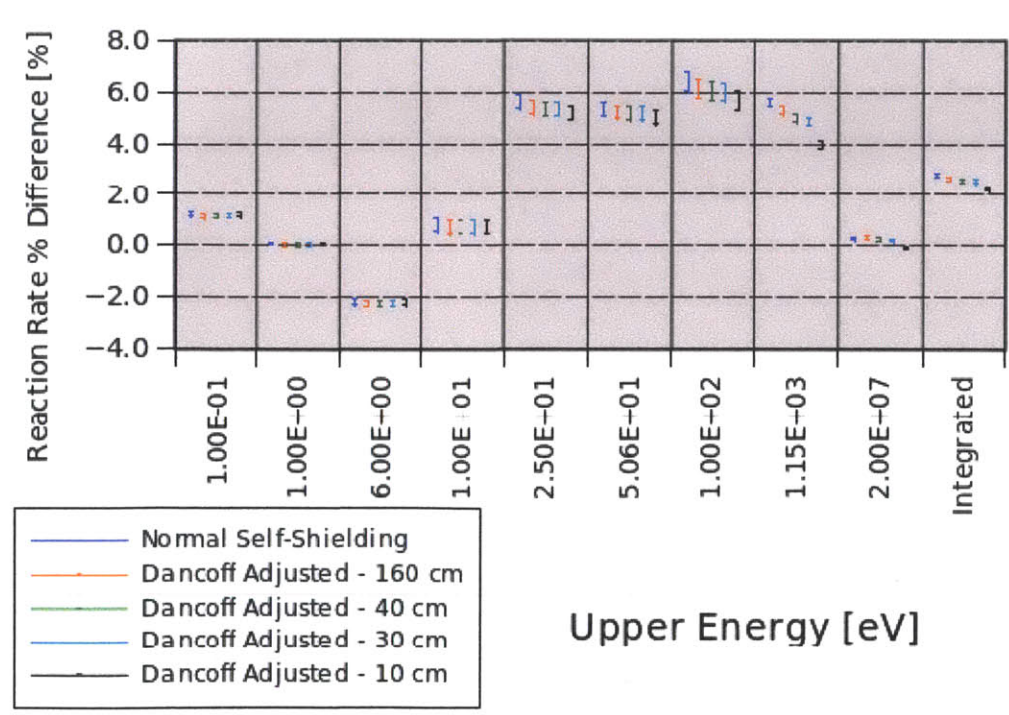


Figure 4-16: Unit 33 (Inner Fuel Pin with gadolinia)  $U^{238}$  reaction rate percent differences among self-shielding models relative to MCNP5 continuous energy results.

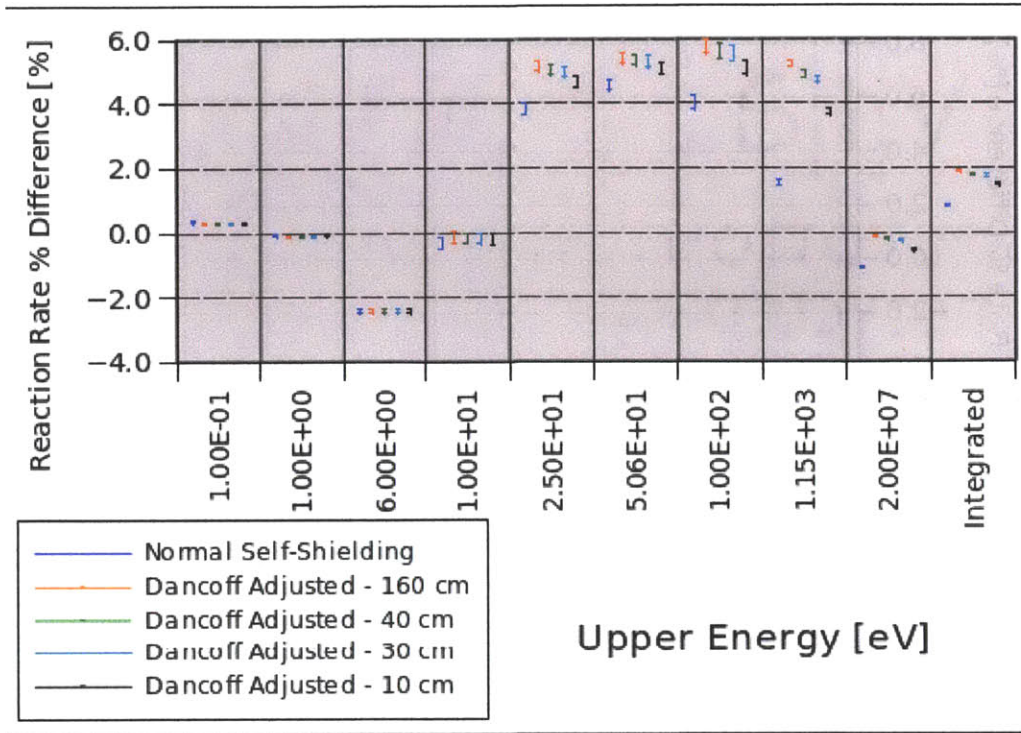


Figure 4-17: Unit 15 (Side Pins on Narrow Gap)  $U^{238}$  reaction rate percent differences among self-shielding models relative to MCNP5 continuous energy results.

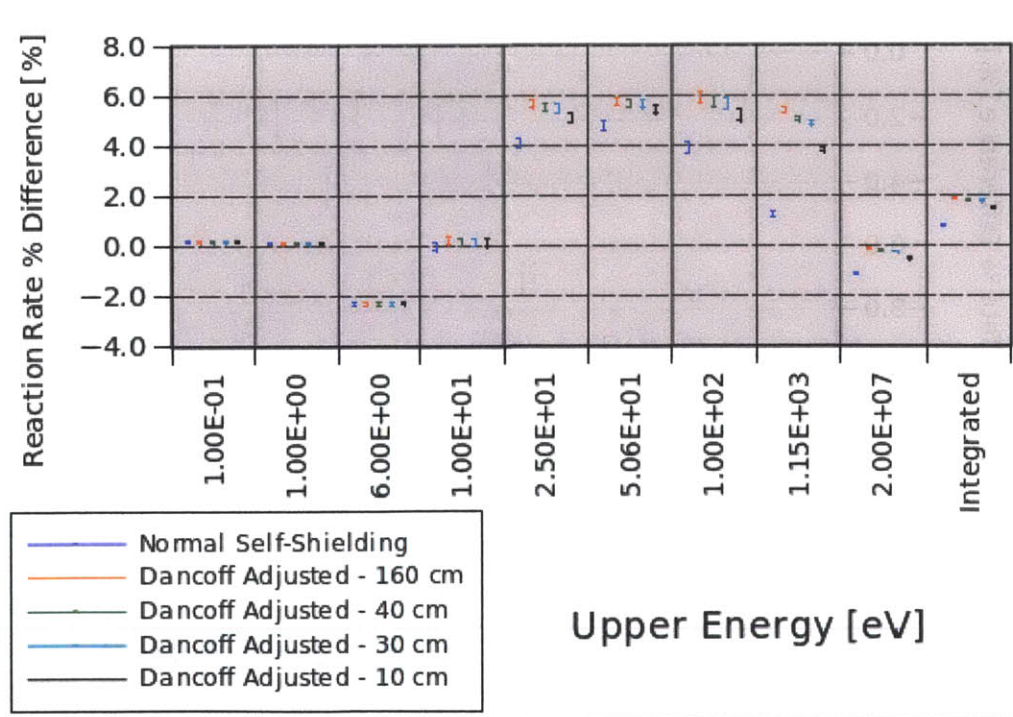


Figure 4-18: Unit 145 (Side Pins on Wide Gap)  $U^{238}$  reaction rate percent differences among self-shielding models relative to MCNP5 continuous energy results.

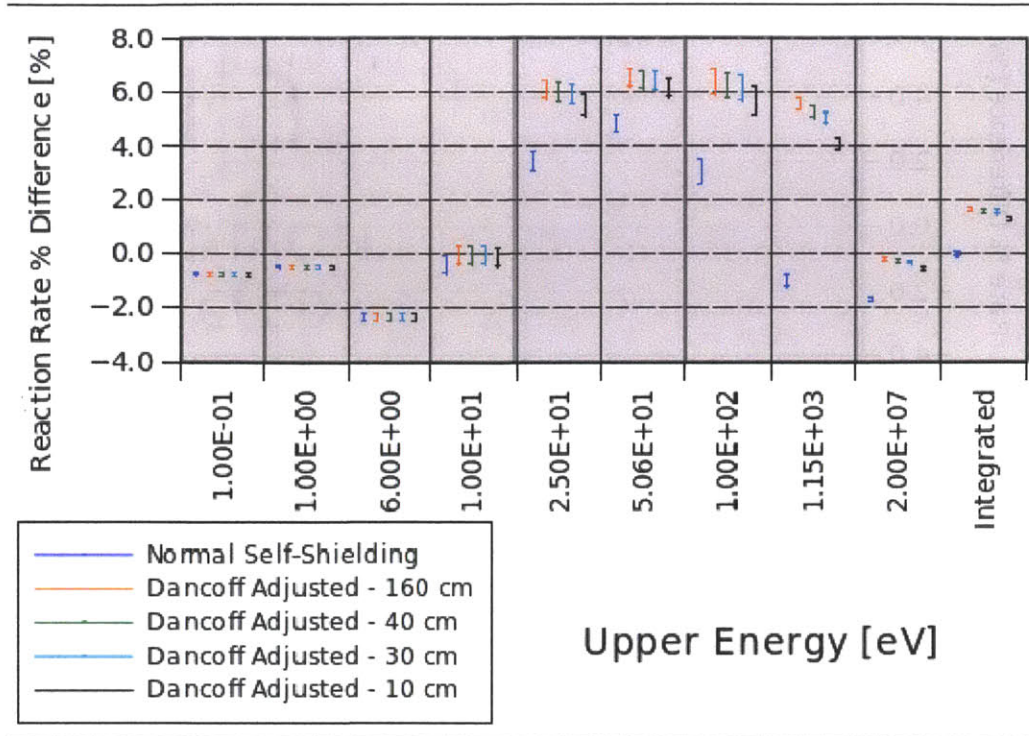


Figure 4-19: Unit 429 (Corner Pins between Wide and Narrow )  $U^{238}$  reaction rate percent differences among self-shielding models relative to MCNP5 continuous energy results.

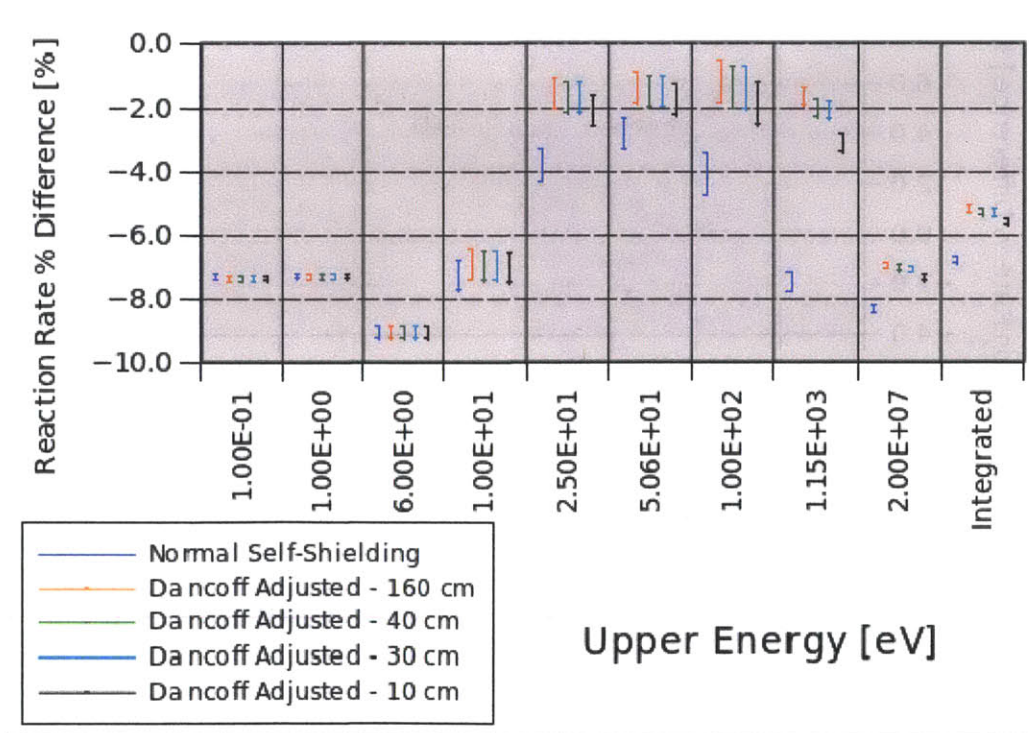


Figure 4-20: Unit 209 (Corner Pin between Narrow Gaps)  $U^{238}$  reaction rate percent differences among self-shielding models relative to MCNP5 continuous energy results.

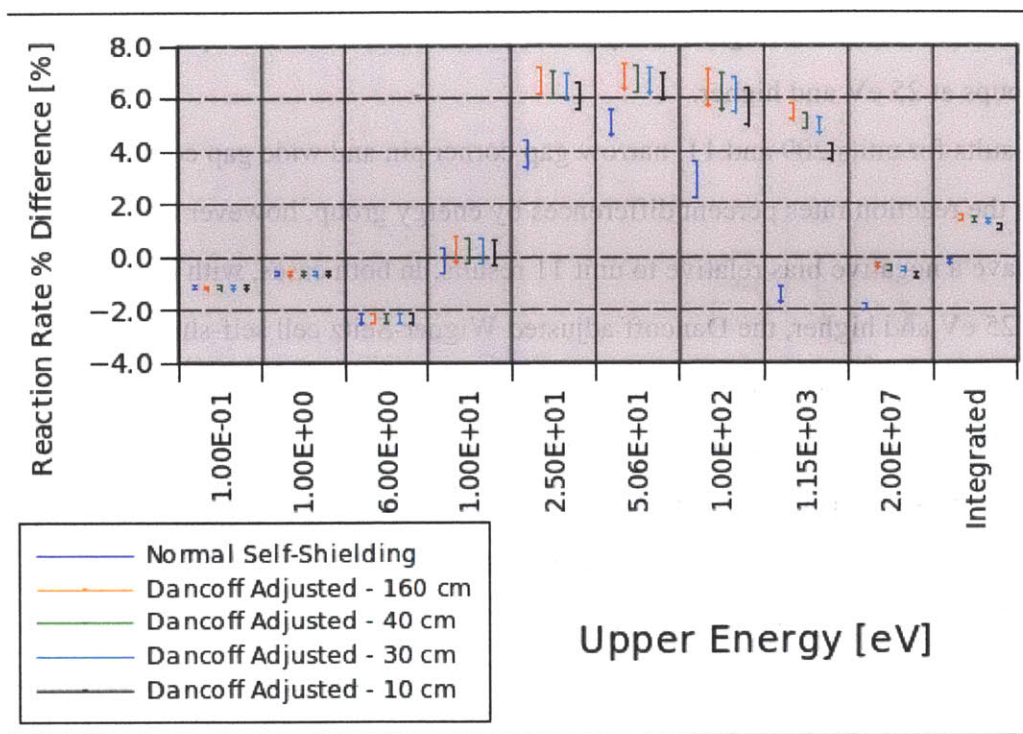


Figure 4-21: Unit 11 (Corner Pin between Wide Gaps)  $U^{238}$  reaction rate percent differences among self-shielding models relative to MCNP5 continuous energy results.

In general the same shape is seen in all the percent difference figures, namely that the percent error in reaction rates in the slowing down region are larger (more positive) than the percent error in reaction rates in the thermal region. This is consistent with the flux and reaction rate profiles that are present in the Wigner-Seitz cells that were studied. The interior pins, units 33 and 34, both showed improvements in reaction rate predictions in the high energy groups. Improvements in the reaction rates, including the total integrated reaction rates tended to increase as the height used in MCDancoff decreased.

Results for units 15 and 145, the narrow and wide gap side pins, were closer to MCNP5 results for the volume conserved Wigner-Seitz cell self-shielded case than any of the Dancoff adjusted Wigner-Seitz cell treatments. Relatively little variation was seen among the self-shielding choices in the thermal range, however for the group at 25 eV and all higher energy groups the normal Wigner-Seitz cell results were better. Unit 429, (corner pin between narrow and wide gaps) had similar tendencies to the side pins. The normal Wigner-Seitz cell treatment

showed the best results, with significantly better prediction of  $U^{238}$  absorption reaction rates for energy groups at 25 eV and higher.

Results for units 209 and 11, narrow gap corner pin and wide gap corner pin, had similar shapes for the reaction rates percent differences by energy group, however all of the results for unit 209 have a negative bias relative to unit 11 results. In both cases, with regards to energy groups of 25 eV and higher, the Dancoff adjusted Wigner-Seitz cell self-shielding treatment causes larger reaction rates when compared to the normal Wigner-Seitz cell results. For unit 11, the normal Wigner-Seitz cell self-shielding treatment gives better reaction rate results at high energies and for the energy integrated result. However, due to the negative bias in unit 209 results, the Dancoff adjusted Wigner-Seitz cell results were closer to MCNP5 predicted reactions rates than the normal Wigner-Seitz cell results.

Assessment of the reaction rates for the interior fuel pins (units 33 and 34) showed that the Dancoff adjusted Wigner-Seitz cells improved results. The same cannot be said for the edge and corner pins, which are the one that have a high degree of irregularity relative to the infinite lattice assumption the self-shielding model uses. The results for k-eff were worse for all models that used Dancoff adjusted Wigner-Seitz cells, even though the interior pins showed improvement in reaction rates. To see if improvements in k-eff could be attained, Dancoff adjusted Wigner-Seitz cells were applied to **only** the interior pins or **only** the edge/corner pins. This analysis was performed while using Dancoff corrections from 10 cm and 160 cm fuel height MCDancoff calculations. The results for k-eff are summarized in Table 4-6. Some previous results where all the fuel pins used the Dancoff adjusted Wigner-Seitz cell were included for comparison.

Table 4-6: Differences in k-eff for a BWR bundle with a void fraction of 40 % from MCNP5 and NEWT using normal Wigner-Seitz models for self-shielding cross sections, and NEWT using Dancoff adjusted Wigner-Seitz models for self-shielding cross sections. Dancoff adjusted Wigner-Seitz cells were used for only inner or sides/corners in some models. Dancoff corrections were calculated using two different fuel heights in MCDancoff.

Method Used	Fuel Length for Dancoff Calculation (cm)	k-eff	k-eff 3 $\sigma$ Uncertainty (pcm)	Difference (pcm)	Difference 3 $\sigma$ Uncertainty (pcm)
MCNP5 - CE	-	1.15051	9	-	-
NEWT - None Adjusted	-	1.14751	-	-300	9
NEWT - All Pins Adjusted	160	1.14562	-	-488	9
NEWT - Inner Adjusted	160	1.14630	-	-421	9
NEWT - Sides/Corners Adjusted	160	1.14560	-	-491	9
NEWT - All Pins Adjusted	10	1.14681	-	-370	9
NEWT - Inner Adjusted	10	1.14804	-	-247	9
NEWT - Sides/Corners Adjusted	10	1.14630	-	-421	9

Table 4-6 shows that the use of a Dancoff adjusted Wigner-Seitz cell on the sides and corners only of the BWR bundle result in a worse prediction for k-eff relative to using Dancoff adjusted Wigner-Seitz cells on all fuel pins. However, the use Dancoff adjusted Wigner-Seitz cells on only the inner fuel pins showed improved prediction of k-eff compared to the corresponding model with all fuel pins being adjusted. The 10 cm MCDancoff fuel height case actually showed the best results, with an improvement of 53 pcm in the prediction of k-eff relative to the bundle using no adjustments.

### Summary

The use of Dancoff adjusted Wigner-Seitz cells showed improvements in predicted  $U^{238}$  absorption rates for interior pins of a BWR bundle where little irregularity in the lattice was present. However, the  $U^{238}$  reaction rates in corner and side fuel pins did not show any consistent improvement. The use of Dancoff adjusted Wigner-Seitz cells on all fuel pins resulted in worse prediction of k-eff. If Dancoff adjusted Wigner-Seitz cells were only used for inner fuel pins, the prediction of k-eff was better compared to a corresponding model where all fuel pins were adjusted. *The results from  $U^{238}$  reaction rates and k-eff prediction both demonstrate that Dancoff adjusted Wigner-Seitz cells does not help account for lattice irregularities when using the Dancoff corrections as currently predicted by MCDancoff.*

## 4.5 - Analysis of Dancoff Corrections

It is clear from the previous results that prediction of the Dancoff corrections needed for adjusting the Wigner-Seitz cell is highly sensitive to the height used in the MCDancoff model. In order to examine the prediction of Dancoff corrections a BWR unit cell was modeled with CASMO4e and MCDancoff with various heights for the fuel. CASMO4e does an independent calculation of the Dancoff correction at each energy group within the  $U^{238}$  resolved resonance range. This allows CASMO to correct for the escape probability from the fuel in each energy group. Since the version of CASMO that was used had ENDF/B-VI cross sections the resolved resonance range for  $U^{238}$  reached 10 KeV. Table 4-7 shows the energy dependence of the Dancoff correction from CASMO4e along with the MCDancoff value for the same BWR unit cell. The results show that the Dancoff correction calculated by MCDancoff is underestimated relative to all of the CASMO4e Dancoff corrections, regardless of energy group. The MCDancoff was close to (-0.34 % difference) the lowest energy group Dancoff correction from CASMO4e.

*Table 4-7: Dancoff corrections for a BWR unit cell at 40% void fraction from CASMO4e and MCDancoff. The lower energy boundary of the CASMO4e 9.88 eV group is 4 eV. MCDancoff results are for a well converged height (2000 cm). Uncertainty given is a 3σ standard deviation.*

Upper Energy (eV)	CASMO4e Dancoff Correction	MCDancoff Dancoff Correction
9118.00	0.3661	-
5530.00	0.3620	-
3519.10	0.3602	-
2239.45	0.3585	-
1425.10	0.3569	-
906.90	0.3560	-
367.26	0.3554	-
148.73	0.3550	-
75.50	0.3549	-
48.05	0.3548	-
27.70	0.3548	-
15.97	0.3547	-
9.88	0.3544	-
1-Group	-	0.3532 ± 0.0007

In order to further examine the Dancoff correction prediction, the BWR bundle at 40% void fraction which was modeled in previous sections was modeled with CASMO4e. MCDancoff results for many fuel heights are compared to the 9.88 eV group results from CASMO4e since these closest matched MCDancoff results for the BWR pin results. Results are displayed in Figure 4-22.



Chapter 4 – Results and Discussion

**CASMO4e Dancoff Corrections**  
9.877 eV to 4 eV

0.147	0.234	0.234	0.234	0.234	0.234	0.156
0.234	0.355	0.355	0.355	0.355	0.355	0.244
0.234	0.355	0.355	0.355	0.355	0.355	0.244
0.234	0.355	0.355	0.355	0.355	0.355	0.244
0.234	0.355	0.355	0.355	0.355	0.355	0.244
0.234	0.355	0.355	0.355	0.355	0.355	0.244
0.156	0.244	0.244	0.244	0.244	0.244	0.166

All standard deviations from MCDancoff are < 0.001

**MCDancoff Dancoff Corrections - 10 cm**

0.202	0.280	0.284	0.285	0.284	0.284	0.211
0.282	0.376	0.379	0.384	0.383	0.379	0.292
0.284	0.383	0.388	0.388	0.382	0.385	0.296
0.284	0.383	0.389	0.389	0.387	0.383	0.298
0.285	0.383	0.385	0.390	0.390	0.378	0.296
0.281	0.378	0.385	0.386	0.386	0.378	0.291
0.211	0.294	0.297	0.297	0.298	0.295	0.223

**10 cm - Percent Difference**

36.9	19.9	21.5	21.9	21.6	21.5	35.2
20.8	6.2	6.8	8.3	8.0	6.9	19.4
21.5	8.0	9.5	9.3	7.7	8.6	21.4
21.8	8.1	9.7	9.5	9.1	8.0	22.1
22.2	7.9	8.4	9.9	9.9	6.7	21.1
20.2	6.7	8.6	8.9	8.9	6.7	19.2
35.4	20.3	21.8	21.6	22.1	20.8	33.8

**MCDancoff Dancoff Corrections - 20 cm**

0.180	0.260	0.263	0.263	0.264	0.261	0.190
0.260	0.358	0.359	0.365	0.366	0.360	0.272
0.263	0.366	0.371	0.370	0.366	0.365	0.276
0.263	0.366	0.370	0.371	0.371	0.366	0.276
0.263	0.367	0.365	0.371	0.371	0.360	0.276
0.260	0.360	0.366	0.368	0.368	0.360	0.273
0.189	0.272	0.277	0.277	0.278	0.273	0.199

**20 cm - Percent Difference**

22.1	11.2	12.8	12.4	13.1	11.6	21.8
11.5	0.9	1.2	2.9	3.2	1.5	11.5
12.7	3.1	4.5	4.3	3.1	3.0	13.2
12.7	3.3	4.5	4.7	4.5	3.1	13.1
12.7	3.5	2.9	4.7	4.5	1.6	12.8
11.3	1.4	3.2	3.6	3.7	1.4	11.8
21.1	11.3	13.3	13.4	13.7	11.9	19.5

**MCDancoff Dancoff Corrections - 30 cm**

0.172	0.252	0.255	0.254	0.258	0.253	0.182
0.253	0.353	0.354	0.358	0.358	0.356	0.265
0.257	0.360	0.363	0.363	0.359	0.360	0.269
0.256	0.360	0.364	0.365	0.364	0.359	0.269
0.257	0.359	0.358	0.364	0.365	0.354	0.268
0.253	0.354	0.361	0.361	0.361	0.355	0.267
0.182	0.266	0.271	0.269	0.270	0.265	0.191

**30 cm - Percent Difference**

16.7	8.0	9.2	8.8	10.4	8.5	17.0
8.3	-0.5	-0.3	1.1	1.1	0.3	8.4
10.1	1.4	2.5	2.3	1.3	1.4	10.1
9.5	1.5	2.7	2.8	2.5	1.3	10.3
10.0	1.2	0.9	2.8	2.8	-0.3	9.7
8.3	-0.3	1.7	1.8	1.8	0.0	9.2
16.5	9.0	10.9	10.2	10.5	8.3	14.7

**MCDancoff Dancoff Corrections - 40 cm**

0.168	0.249	0.252	0.252	0.253	0.249	0.178
0.249	0.351	0.348	0.356	0.356	0.352	0.262
0.255	0.355	0.361	0.360	0.355	0.357	0.266
0.252	0.356	0.361	0.363	0.361	0.356	0.266
0.253	0.356	0.355	0.361	0.362	0.352	0.263
0.250	0.351	0.357	0.357	0.358	0.352	0.262
0.177	0.262	0.265	0.266	0.266	0.262	0.188

**40 cm - Percent Difference**

13.9	6.4	8.1	8.0	8.3	6.8	14.1
6.8	-1.2	-1.9	0.3	0.3	-0.8	7.3
9.1	0.2	1.7	1.6	0.1	0.7	8.8
8.0	0.3	1.9	2.3	1.7	0.4	8.9
8.3	0.3	0.2	1.9	1.9	-0.9	7.7
7.1	-1.1	0.6	0.8	1.0	-0.9	7.2
13.5	7.3	8.7	8.9	8.8	7.1	12.6

MCDancoff Dancoff Corrections - 60 cm

0.163	0.246	0.248	0.248	0.249	0.246	0.173
0.246	0.346	0.344	0.352	0.353	0.348	0.259
0.250	0.353	0.359	0.357	0.353	0.353	0.262
0.248	0.352	0.358	0.358	0.358	0.352	0.262
0.249	0.353	0.352	0.358	0.360	0.347	0.260
0.247	0.347	0.353	0.354	0.355	0.347	0.258
0.173	0.260	0.263	0.262	0.263	0.258	0.183

60 cm - Percent Difference

10.9	5.5	6.2	6.3	6.7	5.1	10.9
5.4	-2.5	-2.9	-0.7	-0.5	-2.0	5.9
7.1	-0.4	1.2	0.7	-0.5	-0.5	7.4
6.4	-0.7	0.9	1.0	1.1	-0.7	7.3
6.5	-0.5	-0.8	1.0	1.5	-2.3	6.7
5.6	-2.3	-0.6	-0.2	0.0	-2.0	5.7
10.9	6.4	7.7	7.4	7.6	5.5	10.0

MCDancoff Dancoff Corrections - 160 cm

0.158	0.241	0.243	0.242	0.243	0.241	0.168
0.242	0.343	0.342	0.347	0.349	0.344	0.253
0.245	0.347	0.354	0.354	0.349	0.349	0.258
0.243	0.350	0.354	0.355	0.353	0.348	0.257
0.244	0.348	0.348	0.354	0.354	0.344	0.257
0.242	0.342	0.349	0.351	0.350	0.344	0.254
0.168	0.254	0.257	0.258	0.259	0.253	0.177

160 cm - Percent Difference

7.3	3.4	4.2	3.8	4.2	3.2	7.8
3.7	-3.3	-3.6	-2.1	-1.5	-3.1	3.8
4.8	-2.0	-0.2	-0.3	-1.6	-1.5	5.6
4.2	-1.4	0.0	0.2	-0.4	-2.0	5.4
4.6	-1.8	-2.0	-0.2	-0.2	-3.1	5.0
3.8	-3.6	-1.6	-1.1	-1.4	-2.9	4.0
7.6	3.8	5.3	5.6	6.1	3.8	6.5

MCDancoff Dancoff Corrections - 400 cm

0.157	0.239	0.242	0.242	0.243	0.241	0.166
0.239	0.340	0.341	0.346	0.348	0.342	0.252
0.241	0.347	0.351	0.353	0.346	0.347	0.257
0.243	0.347	0.353	0.353	0.351	0.348	0.255
0.242	0.348	0.347	0.353	0.353	0.342	0.255
0.240	0.340	0.347	0.350	0.348	0.343	0.252
0.166	0.251	0.256	0.256	0.257	0.251	0.176

400 cm - Percent Difference

6.5	2.2	3.6	3.5	3.9	3.0	6.6
2.5	-4.1	-3.8	-2.6	-2.0	-3.5	3.0
3.3	-2.2	-1.0	-0.5	-2.5	-2.2	5.0
3.8	-2.2	-0.5	-0.4	-1.1	-2.0	4.6
3.8	-1.8	-2.1	-0.5	-0.5	-3.6	4.6
2.8	-4.1	-2.0	-1.4	-1.8	-3.3	3.4
6.6	2.9	4.9	5.0	5.2	2.6	5.6

MCDancoff Dancoff Corrections - 2000 cm

0.155	0.238	0.240	0.241	0.241	0.240	0.165
0.240	0.339	0.339	0.346	0.346	0.343	0.251
0.242	0.347	0.351	0.353	0.345	0.347	0.255
0.241	0.347	0.353	0.353	0.350	0.346	0.255
0.242	0.347	0.346	0.352	0.353	0.342	0.255
0.239	0.342	0.348	0.348	0.348	0.342	0.252
0.165	0.250	0.255	0.255	0.257	0.251	0.175

2000 cm - Percent Difference

5.3	1.7	2.8	3.2	3.2	2.8	6.1
2.6	-4.3	-4.5	-2.5	-2.4	-3.3	2.8
3.7	-2.1	-1.1	-0.6	-2.7	-2.3	4.5
3.4	-2.1	-0.5	-0.4	-1.2	-2.3	4.4
3.6	-2.2	-2.5	-0.6	-0.6	-3.5	4.4
2.4	-3.7	-1.9	-2.0	-1.7	-3.5	3.1
5.7	2.4	4.2	4.5	5.1	2.9	5.2

Figure 4-22: Dancoff correction predictions for a BWR bundle at 40% void fraction using CASMO4e and MCDancoff with several different fuel heights used in the model.

Results in Figure 4-22 show a large variation in values for Dancoff corrections from MCDancoff at varying heights. This variability is especially present in the side and corner pins. It should be emphasized that there is no energy group of CASMO4e Dancoff corrections which are necessarily the appropriate one to compare MCDancoff results to. The lowest energy group was selected to be the comparison because it was the best match for the reflected unit cell results, which should correlate well with the innermost pins of the BWR bundle. There is no particular

fuel height for MCDancoff that gives results close to CASMO4e for all pins. For 400 cm and 2000 cm the innermost 9 fuel pins give similar results with what was seen in the infinite lattice case in Table 4-7: Dancoff corrections for a BWR unit cell at 40% void fraction from CASMO4e and MCDancoff. The lower energy boundary of the CASMO4e 9.88 eV group is 4 eV. MCDancoff results are for a well converged height (2000 cm). Uncertainty given is a  $3\sigma$  standard deviation.. This is expected since the innermost pins do not see any irregularities in the lattice. The fuel pins that are one position removed from the edge show an additional negative bias when compared to the CASMO4e results. The fuel pins which are on the edges and corners show a positive bias which largest in the corner pins.

Except for the innermost 9 pins, the results of the Dancoff corrections from MCDancoff compared to CASMO4e values seem almost erratic. Two reflected pin cells were modeled to attempt to elucidate some of this behavior. The effects of water and the cladding on the Dancoff correction were isolated by creating two test problems which were simulated in MCDancoff and CASMO4e. The water model was made by reducing the thickness of the cladding from 0.094 cm to  $7E-05$  cm and the cell pitch was increased from 1.8745 cm to 2.5 cm. The zirconium model was made by reducing the water density from  $0.4572 \text{ g cm}^{-3}$  to  $0.001 \text{ g cm}^{-3}$ , increasing the cell pitch to 2.5 cm, and increasing the cladding outer radius from 0.715 cm to 1.24 cm. All other parameters were left the same as the previously modeled unit cell. Diagrams of the two altered models are shown in Figure 4-23. The results of the water model and the Zirc2 model are given in Table 4-8 and Table 4-9, respectively.

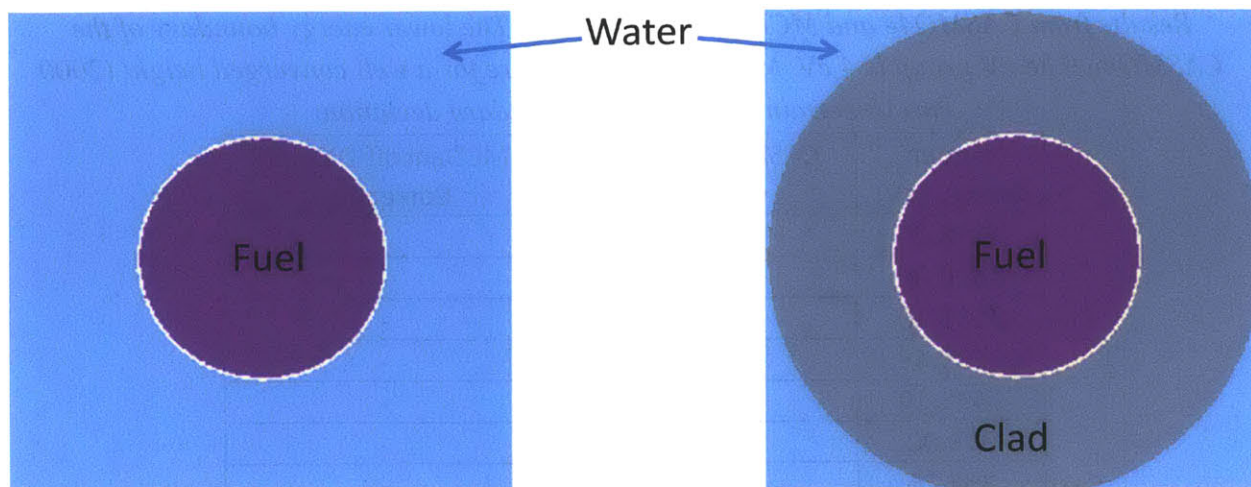


Figure 4-23: Altered reflected unit cells to emphasize the effect of water (left) and Zirc2 (right) on the Dancoff corrections predicted by MCDancoff and CASMO4e.

Table 4-8: Dancoff corrections for an altered unit cell that emphasizes the effect of water.

Results from CASMO4e and MCDancoff are shown. The lower energy boundary of the CASMO4e 9.88 eV group is 4 eV. MCDancoff results are for a well converged height (2000 cm). Uncertainty given is a 3σ standard deviation.

Upper Energy (eV)	CASMO4e Dancoff Correction	MCDancoff Dancoff Correction
9118.00	0.1413	-
5530.00	0.1382	-
3519.10	0.1369	-
2239.45	0.1356	-
1425.10	0.1344	-
906.90	0.1338	-
367.26	0.1334	-
148.73	0.1330	-
75.50	0.1330	-
48.05	0.1329	-
27.70	0.1329	-
15.97	0.1328	-
9.88	0.1326	-
1-Group	-	0.1332 ± 0.0004

*Table 4-9: Dancoff corrections for an altered unit cell that emphasizes the effect of Zirc2. Results from CASMO4e and MCDancoff are shown. The lower energy boundary of the CASMO4e 9.88 eV group is 4 eV. MCDancoff results are for a well converged height (2000 cm). Uncertainty given is a 3σ standard deviation.*

Upper Energy (eV)	CASMO4e Dancoff Correction	MCDancoff Dancoff Correction
9118.00	0.42813	-
5530.00	0.42812	-
3519.10	0.42812	-
2239.45	0.42811	-
1425.10	0.42811	-
906.90	0.42810	-
367.26	0.42810	-
148.73	0.42810	-
75.50	0.42810	-
48.05	0.42810	-
27.70	0.42810	-
15.97	0.42810	-
9.88	0.42810	-
1-Group	-	0.4445 ± 0.0004

The water model results show that the Dancoff correction from CASMO4e have significant energy dependence in the higher energy resonance groups. The MCDancoff predicted Dancoff correction agrees with Dancoff corrections from energy groups between 367.26 eV and 15.97 eV within a 99% confidence interval. The MCDancoff one-group total cross section for H<sup>1</sup> as well as the corresponding 238 neutron group values are plotted for the resolved resonance region in Figure 4-24.

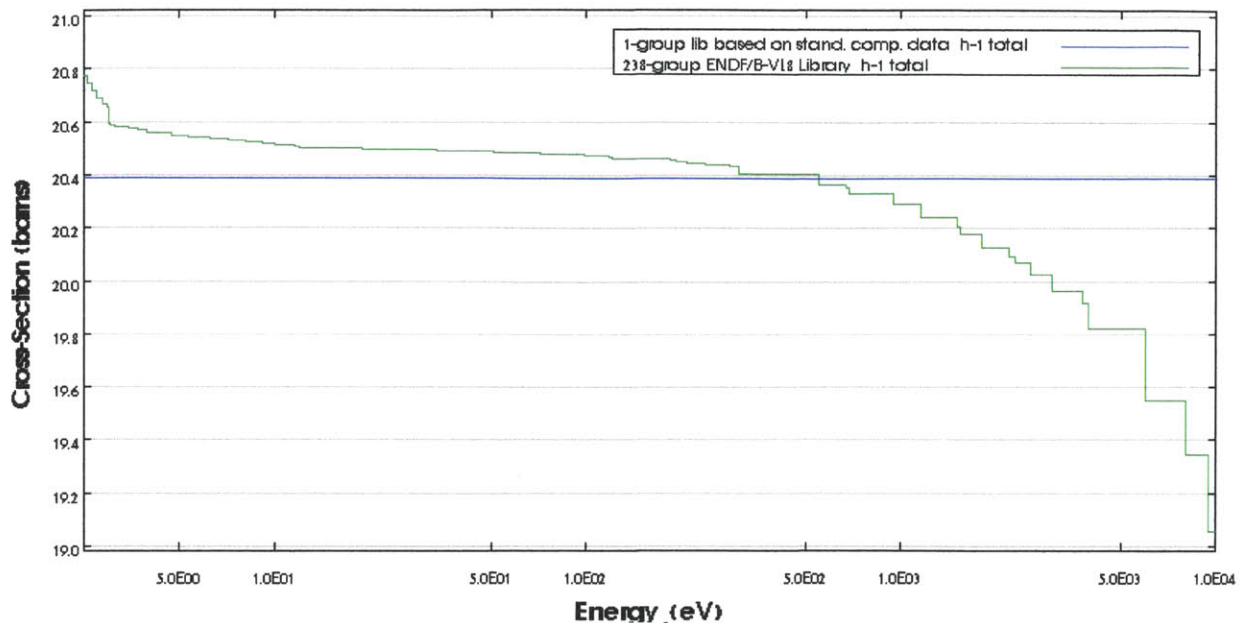


Figure 4-24: Plot of the total cross section for  $H^1$  in the resolved resonance region. The one group cross section used by MCDancoff and the 238 group ENDF/B-VI.8 cross sections are shown. This plot was generated using Javapeno from the Scale6.1 package.<sup>5</sup>

The Zirc2 model results show that the cross sections used in the CASMO4e model for Zirc2 had very little effect on the Dancoff corrections with respect to energy group. The MCDancoff Dancoff correction was approximately 3.8% larger than any of the CASMO4e results. The MCDancoff one-group total cross section for Zr as well as the corresponding 238 neutron group values are plotted for the resolved resonance region in Figure 4-25. From the fact that the values for the Dancoff corrections from CASMO4e were smaller than the MCDancoff it can be inferred that the cross section used for Zr in CASMO4e is larger than the corresponding cross section in MCDancoff. By inspection of Figure 4-25, a large cross section probably means that a larger emphasis was placed on the higher energy groups where resonances exist.

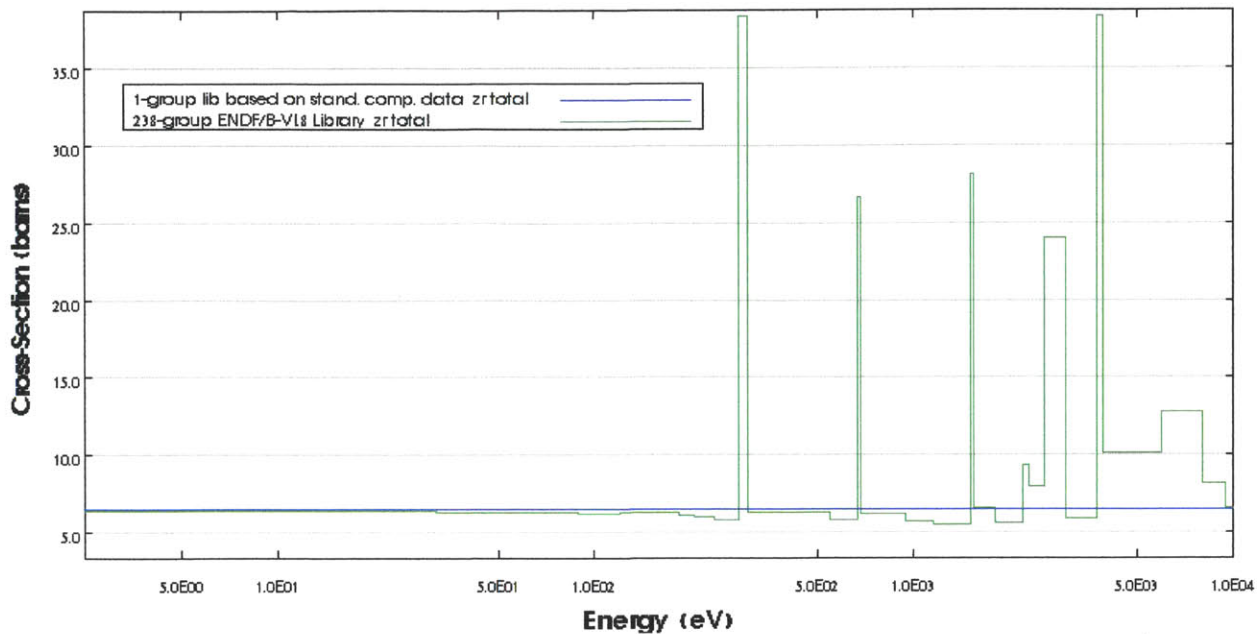


Figure 4-25: Plot of the total cross section for Zr in the resolved resonance region. The one group cross section used by MCDancoff and the 238 group ENDF/B-VI.8 cross sections are shown. This plot was generated using Javapeno from the Scale6.1 package.<sup>5</sup>

The isolation of the  $H^1$  effects on Dancoff corrections did not yield any particular conclusion on the cross sections used between the two codes. The analysis of Zr's effect on Dancoff corrections did show that MCDancoff overestimated the resulting Dancoff correction by approximately 3.8% compared to CASMO4e. If indeed the cross section used for Zr in MCDancoff tends to overpredict the Dancoff correction this could partially explain why the positive bias exhibited by all edge and corner pins since they are surrounded by a Zr shroud.

It should be noted that although the MCDancoff calculated Dancoff correction may agree well with a particular range of energy dependent Dancoff corrections, *there is no reason to consider that this is the correct or best Dancoff correction to be used for adjusting the Wigner-Seitz cell*. An effective, single Dancoff correction for the use of adjusting the Wigner-Seitz cell may exist, but the current implementation of MCDancoff and its cross sections do not appear to be calculating it.

## Chapter 5 - Conclusions

The objective of this thesis was to assess the effects of using a Dancoff correction to adjust the Wigner-Seitz cell approximation for an ultrafine group model of a light water reactor fuel pin. The use of the Wigner-Seitz cell approximation is necessary for a one-dimensional model of a unit cell that uses cylindrical fuel pins. Due to the computational effort required for an ultrafine group solution these solvers are usually limited to infinite-homogeneous media or one-dimensional calculations. The effects of using the approximation on the neutron spectra, reaction rates and k-eff are analyzed in section 4.1.

The use of the Dancoff Adjusted Wigner-Seitz Cell (DAWSC) relies on the accurate prediction of Dancoff corrections so that the size of the moderator can be adjusted accordingly. The module, MCDancoff, is used in the Scale6.1 code package to calculate Dancoff corrections using a three-dimensional model of the lattice geometry. Unfortunately, due to the way MCDancoff was implemented many users of the module have mistakenly been using Dancoff corrections which have not converged to the correct answer, yet improved results have been reported. Thus the focus of this research focused largely on the effects of using the converged Dancoff correction as well as a range of unconverged Dancoff corrections which have been used in practice.

There are two main flaws with the Wigner-Seitz cell approximation which DAWSC has been utilized to alleviate. The first is that the Wigner-Seitz cell approximation does not preserve the flux, and therefore reaction rates for a fuel pin in an infinite lattice. An analysis in section 4.3 showed that DAWSC resulted in improvements in both  $U^{238}$  absorption rates and k-eff when using continuous energy Monte Carlo as the reference solution. Unfortunately the improvement in results was relatively small when using converged Dancoff corrections relative to improvements in results when using unconverged Dancoff corrections. The improvement in results consistently grew as Dancoff corrections further from the converged value were used. The error in k-eff for a reflected pin was reduced by only 2.3% when the converged Dancoff



correction was used while the error was reduced by 27.3% for the least converged Dancoff correction.

The second main flaw in using the Wigner-Seitz cell approximation is that it assumes the fuel pin is surrounded by an infinite lattice of similar fuel pins. Thus any irregularities that exist in a fuel bundle such as water holes or bypass flow channels will cause the Wigner-Seitz cell approximation to be less accurate. The DAWSC has been used to help account for irregularities that exist in nuclear reactors. Section 4.4 analyses the use of DAWSC for a BWR bundle with a void fraction of 40%. A BWR naturally has a large deviation from an infinite lattice due to the bypass flow channel that is a different density than the moderator inside the shroud. Using DAWSC on all of the fuel pins in the bundle resulted in increased error for  $k$ -eff for all sets of Dancoff corrections used; however using unconverged Dancoff corrections increased the error less significantly. A closer look at the results showed that the  $U^{238}$  reaction rates predictions actually improved for interior fuel pins (fuel pins at least one position removed from the shroud). The results of  $U^{238}$  reaction rates for the interior pins showed that reaction rates improved as the Dancoff correction was farther from the converged Dancoff correction. This is the same trend that was found in section 4.3 for infinite lattices. This should hold true since from an interior pins perspective it is roughly in an infinite lattice. Analysis of the reaction rates for the side and corner fuel pins gave mixed results and many fuel pins had reaction rates with increased error when DAWSC was implemented. Thus from these results, using the Dancoff corrections from MCDancoff the ability for DAWSC to account for lattice irregularities seems doubtful. However, it is not clear that the Dancoff corrections being calculated by MCDancoff are necessarily the correct ones.

Due to the high sensitivity of results to the values for the Dancoff corrections an assessment of MCDancoff was performed in section 4.5. CASMO4e was used to compare Dancoff corrections for both the infinite lattice case and for a BWR bundle. A significant difference between the two codes was that CASMO4e calculated a Dancoff correction for every energy group in the resolved resonance range of  $U^{238}$ . The use of these Dancoff corrections is for the original application of adjusting the fuel escape probability for equivalence theory calculations. For an infinite lattice MCDancoff was within 0.34% of the lowest energy group

## Chapter 5 – Conclusions

Dancoff correction from CASMO4e. When Dancoff corrections for a BWR bundle were assessed, only the nine most-interior fuel pins agreed well with CASMO4e Dancoff corrections from the lowest energy group. The side and corner fuel pins from MCDancoff were overestimated relative to CASMO4e by an average of 3.8 %, while the fuel pins one position closer to the center were underestimated by an average of -2.8%. On a closer look into materials the cross section for water in MCDancoff appeared to agree with roughly 6 out of the 13 energy groups in CASMO4e, whereas none of the energy groups matched MCDancoff for Zirc2.

From the analysis that was performed there is no reason to say why one energy group is the “correct” one over another. It is clear that the unconverged Dancoff corrections resulted in superior prediction of k-eff and reaction rates for infinite lattices. Due to these potential improvements that are present for unconverged Dancoff corrections it is the authors opinion that development of new cross sections for MCDancoff should be sought after. Unlike in equivalence theory where a Dancoff correction adjusts the fuel escape probability for only one energy group, the single Dancoff correction used in DAWSC affects the fuel escape probability for all groups. A multigroup approach could be taken with MCDancoff, however only one Dancoff correction can be used to adjust the moderator size within the Wigner-Seitz cell. The question would then be what weighting function should be used to produce a single, effective Dancoff correction that is ideal for the DAWSC approach. An ideal Dancoff correction would of course be one that makes the reaction rates for a Wigner-Seitz cell match the reaction rates of the square unit cell that it approximates. Since the unconverged Dancoff corrections yielded better improvements in the reaction rates than the converged Dancoff corrections, a first step may be to try to reproduce the unconverged Dancoff corrections with a converged solution. More precisely, determine what cross sections need to be used to reproduce the unconverged Dancoff corrections while using a converged model. After cross sections have been determined, look up what energy groups these cross sections may correspond to. Hopefully, trends will arise that will lead to a better understanding for what the *best* Dancoff correction is for the Dancoff adjusted Wigner-Seitz cell.

## References

1. Team MD. 2008. MCNPX User's Manual.
2. Fridman E, Leppänen J. 2011. On the Use of the Serpent Monte Carlo Code for Few-group Cross Section Generation. *Ann. Nucl. Energy* 38:1399-405
3. Team X-MC. 2003. MCNP - A General Monte Carlo N-Particle Transport Code.
4. Smith K. 2003. "Kord Smith Challenge". Math&Comp Invited Lecture
5. June 2011. Scale: A Comprehensive Modeling and Simulation Suite for Nuclear Safety Analysis and Design. ORNL/TM-2005/39: Available from Radiation Safety Information Computational Center at Oak Ridge National Laboratory as CCC-785.
6. Duderstadt J, Hamilton L. 1976. Nuclear Reactor Analysis. John Wiley & Sons
7. Cacuci D. 2010. *Handbook of Nuclear Engineering*. pp 918-1239. New York: Spring Science+Business Media. 3580 pp.
8. AM W, EP W. 1958. The physical theory of neutron chain reactors. Chicago: University of Chicago Press
9. Dresner L. 1960. *Resonance Absorption in Nuclear Reactors*. New York, Oxford, London, Paris: Pergamon Press
10. Stamm'ler RJJ, MJ A. 1983. *Methods of steady state reactor physics in nuclear design*. London: Academic
11. Y I. 1974. PEACO-II: a code for calculation of effective cross sections in heterogeneous systems. *JAERI-M:5527*
12. J. R, M. E. CASMO-4E Extended Capability CASMO-4 User's Manual.
13. Forget B. 2011. 22.106 - Transport Notes. ed. J Roberts

## Appendix A

### MCNP5 Input for a Square Cell

Square Cell

C Universe 11

140 11 6.90667e-02 -30 -5 6 tmp=8.1728e-08 imp:n=1 vol=23.05813 \$ uo2

141 121 3.34283e-05 -31 30 -5 6 tmp=6.128e-08 imp:n=1 \$ he

142 101 4.32414e-02 -32 31 -5 6 tmp=4.9867e-08 imp:n=1 \$ zirc2

C 143 111 4.62655e-02 -33 32 -5 6 tmp=4.8079e-08 imp:n=1 \$ h2o zirc4 inconel

C 144 111 4.62655e-02 33 -5 6 tmp=4.8079e-08 imp:n=1 \$ h2o zirc4 inconel

144 111 4.62655e-02 32 40 -41 42 -43 -5 6 tmp=4.8079e-08 imp:n=1 vol=38.1544 \$ h2o zirc4  
inconel

C

999 0 -40:43:41:-42:5:-6 imp:n=0

C

C !!!

\*5 pz 10.0

\*6 pz -10.0

30 cz 0.60579

31 cz 0.62103

32 cz 0.71501

33 cz 0.78501

C

C 163 rpp -0.93726 0.93726 -0.93726 0.93726 -10.0 10.0

\*40 px -0.93726

\*41 px 0.93726

\*42 py -0.93726

\*43 py 0.93726

C

mode n

kcode 500000 1.1 100 600

ksrc 0.0 0.0 0.0

c

m11 8016.72c 0.0460444

92234.72c 6.10942e-06

92235.72c 0.000682921

92236.72c 3.13321e-06

92238.72c 0.0223301

## Appendix A

C

C Dummies for m11

m1105 92235.72c 0.000682921

m1108 92238.72c 0.0223301

C

m101 40090.71c 0.021891

40091.71c 0.00477389

40092.71c 0.007297

28058.71c 2.52016e-05

40094.71c 0.00739486

40096.71c 0.00119135

26054.71c 5.58197e-06

28060.71c 9.70762e-06

72178.71c 6.03806e-07

28061.71c 4.21983e-07

26056.71c 8.7625e-05

28062.71c 1.34547e-06

72180.71c 7.76449e-07

26058.71c 2.6931e-07

50112.71c 4.68066e-06

28064.71c 3.42651e-07

50114.71c 3.18478e-06

50115.71c 1.64064e-06

50116.71c 7.01616e-05

50117.71c 3.70592e-05

50118.71c 0.000116872

50119.71c 4.14504e-05

50120.71c 0.000157212

26057.71c 2.02364e-06

50122.71c 2.23417e-05

50124.71c 2.79392e-05

72174.71c 3.54138e-09

72176.71c 1.16423e-07

72177.71c 4.11686e-07

24050.71c 3.30121e-06

72179.71c 3.0146e-07

24052.71c 6.36606e-05

24053.71c 7.2186e-06

24054.71c 1.79686e-06

C

m111 40090.71c 0.000155101

40091.71c 3.38237e-05

40092.71c 5.17003e-05

28058.71c 4.5376e-05

40094.71c 5.23936e-05

22047.71c 2.07635e-07

Appendix A

40096.71c 8.44086e-06  
22049.71c 1.50982e-07  
22050.71c 1.44563e-07  
14028.71c 4.3865e-06  
26054.71c 4.56715e-07  
28060.71c 1.73475e-05  
72178.71c 4.27892e-09  
28061.71c 7.51059e-07  
26056.71c 7.10934e-06  
28062.71c 2.38611e-06  
72180.71c 5.50237e-09  
22046.71c 2.3024e-07  
26058.71c 2.17231e-08  
50112.71c 3.31699e-08  
28064.71c 6.04836e-07  
50114.71c 2.25692e-08  
50115.71c 1.16266e-08  
50116.71c 4.97206e-07  
50117.71c 2.62623e-07  
50118.71c 8.28221e-07  
50119.71c 2.93742e-07  
50120.71c 1.1141e-06  
26057.71c 1.62966e-07  
50122.71c 1.58326e-07  
50124.71c 1.97993e-07  
14029.71c 2.22838e-07  
14030.71c 1.47068e-07  
8016.71c 0.0152876  
1001.71c 0.0305753  
72174.71c 2.50963e-11  
72176.71c 8.25042e-10  
72177.71c 2.91745e-09  
24050.71c 6.93173e-07  
72179.71c 2.13632e-09  
24052.71c 1.33673e-05  
24053.71c 1.51557e-06  
24054.71c 3.77297e-07  
22048.71c 2.05737e-06

mt111 lwtr.15t \$ h2o S(a,b) scattering kernel at 550K

C

m121 2004.71c 3.34283e-05

C

C Scale 238 group neutron library energy structure

e0 1.000E-10 5.000E-10 7.500E-10 1.000E-09 1.200E-09 1.500E-09  
2.000E-09 2.500E-09 3.000E-09 4.000E-09 5.000E-09 7.500E-09 1.000E-08  
2.530E-08 3.000E-08 4.000E-08 5.000E-08 6.000E-08 7.000E-08 8.000E-08

Appendix A

9.000E-08 1.000E-07 1.250E-07 1.500E-07 1.750E-07 2.000E-07 2.250E-07  
2.500E-07 2.750E-07 3.000E-07 3.250E-07 3.500E-07 3.750E-07 4.000E-07  
4.500E-07 5.000E-07 5.500E-07 6.000E-07 6.250E-07 6.500E-07 7.000E-07  
7.500E-07 8.000E-07 8.500E-07 9.000E-07 9.250E-07 9.500E-07 9.750E-07  
1.000E-06 1.010E-06 1.020E-06 1.030E-06 1.040E-06 1.050E-06 1.060E-06  
1.070E-06 1.080E-06 1.090E-06 1.100E-06 1.110E-06 1.120E-06 1.130E-06  
1.140E-06 1.150E-06 1.175E-06 1.200E-06 1.225E-06 1.250E-06 1.300E-06  
1.350E-06 1.400E-06 1.450E-06 1.500E-06 1.590E-06 1.680E-06 1.770E-06  
1.860E-06 1.940E-06 2.000E-06 2.120E-06 2.210E-06 2.300E-06 2.380E-06  
2.470E-06 2.570E-06 2.670E-06 2.770E-06 2.870E-06 2.970E-06 3.000E-06  
3.050E-06 3.150E-06 3.500E-06 3.730E-06 4.000E-06 4.750E-06 5.000E-06  
5.400E-06 6.000E-06 6.250E-06 6.500E-06 6.750E-06 7.000E-06 7.150E-06  
8.100E-06 9.100E-06 1.000E-05 1.150E-05 1.190E-05 1.290E-05 1.375E-05  
1.440E-05 1.510E-05 1.600E-05 1.700E-05 1.850E-05 1.900E-05 2.000E-05  
2.100E-05 2.250E-05 2.500E-05 2.750E-05 3.000E-05 3.125E-05 3.175E-05  
3.325E-05 3.375E-05 3.460E-05 3.550E-05 3.700E-05 3.800E-05 3.910E-05  
3.960E-05 4.100E-05 4.240E-05 4.400E-05 4.520E-05 4.700E-05 4.830E-05  
4.920E-05 5.060E-05 5.200E-05 5.340E-05 5.900E-05 6.100E-05 6.500E-05  
6.750E-05 7.200E-05 7.600E-05 8.000E-05 8.200E-05 9.000E-05 1.000E-04  
1.080E-04 1.150E-04 1.190E-04 1.220E-04 1.860E-04 1.925E-04 2.075E-04  
2.100E-04 2.400E-04 2.850E-04 3.050E-04 5.500E-04 6.700E-04 6.830E-04  
9.500E-04 1.150E-03 1.500E-03 1.550E-03 1.800E-03 2.200E-03 2.290E-03  
2.580E-03 3.000E-03 3.740E-03 3.900E-03 6.000E-03 8.030E-03 9.500E-03  
1.300E-02 1.700E-02 2.500E-02 3.000E-02 4.500E-02 5.000E-02 5.200E-02  
6.000E-02 7.300E-02 7.500E-02 8.200E-02 8.500E-02 1.000E-01 1.283E-01  
1.500E-01 2.000E-01 2.700E-01 3.300E-01 4.000E-01 4.200E-01 4.400E-01  
4.700E-01 4.995E-01 5.500E-01 5.730E-01 6.000E-01 6.700E-01 6.790E-01  
7.500E-01 8.200E-01 8.611E-01 8.750E-01 9.000E-01 9.200E-01 1.010E+00  
1.100E+00 1.200E+00 1.250E+00 1.317E+00 1.356E+00 1.400E+00 1.500E+00  
1.850E+00 2.354E+00 2.479E+00 3.000E+00 4.304E+00 4.800E+00 6.434E+00  
8.187E+00 1.000E+01 1.284E+01 1.384E+01 1.455E+01 1.568E+01 1.733E+01  
2.000E+01

phys:n 20.0 1.0e-11

C

C Tallies

C FM4 num\_dens dum\_mat\_num RX\_num, -6(18) for fission, -2(101)for abs

C

FC4 Tally 2 is for universe 11, U-235 Absorption

F4:N 140

FM4 0.000682921 1105 -2

C

FC14 Tally 12 is for universe 11, U-235 Fission

F14:N 140

FM14 0.000682921 1105 -6

C

FC24 Tally 22 is for universe 11, U-238 Absorption

## Appendix A

F24:N 140

FM24 0.0223301 1108 -2

C

FC34 Tally 32 is for universe 11, U-238 Fission

F34:N 140

FM34 0.0223301 1108 -6

C

FC44 Tally 44 - Flux in Fuel

F44:N 140

C

FC54 Tally 54 - Flux in Mod

F54:N 144

C

FC64 Tally 64 - Flux in Fuel - Coarse Group

F64:N 140

E64 1.0E-7 1.0E-6 6.0E-6 1.0E-5 2.5E-5 50.6E-6 1.0E-4 1.15E-3 20.0

C

FC74 Tally 74 - Flux in Mod - Course Group

F74:N 144

E74 1.0E-7 1.0E-6 6.0E-6 1.0E-5 2.5E-5 50.6E-6 1.0E-4 1.15E-3 20.0

C

FC84 Tally 84 is for universe 11, U-235 Fission - Coarse Group

F84:N 140

FM84 0.000682921 1105 -6

E84 1.0E-7 1.0E-6 6.0E-6 1.0E-5 2.5E-5 50.6E-6 1.0E-4 1.15E-3 20.0

C

FC94 Tally 94 is for universe 11, U-238 Absorption - Course Group

F94:N 140

FM94 0.0223301 1108 -2

E94 1.0E-7 1.0E-6 6.0E-6 1.0E-5 2.5E-5 50.6E-6 1.0E-4 1.15E-3 20.0



## Appendix B

### NEWT Input for a Square Cell Using Dan2pitch

```
'batch_args \-m
=t-newt
in lattice for bwr pin
v7-238
read composition
uo2      1 den=10.32 1 948.45
          92234 0.0261
          92235 2.93
          92236 0.0135
          92238 97.0304 end
he       2 den=0.00022218 1 711.15 end
zirc2    3 den=6.56 1 578.71 end
h2o      4 den=0.457211 1 557.96 end
zirc4    4 den=0.046488 1 557.96 end
inconel  4 den=0.008873 1 557.96 end
end composition
read celldata
  latticecell squarepitch fuelr=0.60579 1 gapr=0.62103 2 cladr=0.71501 3 hpitch=0.93726 4 end
  centrm data dan2pitch(1)=0.388963 isn=8 isct=3 iup=25 iscti=3 end centrm
end celldata
read model
read parameter
drawit=yes
echo=yes
cmfd=yes
prtbalnc=yes
epseigen=1e-05
outers=9999
sn=12
timed=yes
prtxsec=1d
end parameter
read materials
  mix=1 pn=2 com='uo2' end
  mix=2 pn=2 com='he for uo2' end
  mix=3 pn=2 com='zirc for uo2 pin' end
  mix=4 pn=2 com='h2o for uo2 pin' end
end materials
```

## Appendix B

```
read geometry
unit 10
com="uo2 pin"
cylinder 1 0.60579 sides=24
cylinder 2 0.62103 sides=24
cylinder 3 0.71501 sides=24
cylinder 4 0.78501 sides=24
cuboid 5 0.93726 -0.93726 0.93726 -0.93726
media 1 1 1
media 2 1 2 -1
media 3 1 3 -2
media 4 1 4 -3
media 4 1 5 -4
boundary 5 32 32
global unit 1
com="unit the array fits into"
cuboid 1 0.93726 -0.93726 0.93726 -0.93726
hole 10
media 0 1 1
boundary 1 1 1
end geometry
read bnds
  all=mirror
end bnds
end model
end
```

## KENO-VI Input for a Square Cell Using Dan2pitch

```
'batch_args \-m
=csas6
in lattice for bwr pin
v7-238
read composition
uo2      1 den=10.32 1 948.45
          92234 0.0261
          92235 2.93
          92236 0.0135
          92238 97.0304 end
he       2 den=0.00022218 1 711.15 end
zirc2    3 den=6.56 1 578.71 end
h2o      4 den=0.457211 1 557.96 end
zirc4    4 den=0.046488 1 557.96 end
```

## Appendix B

```
inconel 4 den=0.008873 1 557.96 end
end composition
read celldata
  latticecell squarepitch fuelr=0.60579 1 gapr=0.62103 2 cladr=0.71501 3 hpitch=0.93726 4 end
  centrm data dan2pitch(1)=0.388963 isn=8 isct=3 iup=25 iscti=3 end centrm
end celldata
read parameter
  htm=no
  gen=6000
  npg=20000
  nsk=150
  wrs=35
  far=yes
  fdn=yes
  flx=yes
  res=6000
  mfp=yes
end parameter
read geometry
global unit 10
com="uo2 pin"
cylinder 1 0.60579 10 -10
cylinder 2 0.62103 10 -10
cylinder 3 0.71501 10 -10
cuboid 5 0.93726 -0.93726 0.93726 -0.93726 10 -10
media 1 1 1 vol=23.05813
media 2 1 2 -1 vol=1.174751
media 3 1 3 -2 vol=7.889233
media 4 1 5 -3 vol=38.15439
boundary 5

end geometry
read bnds
  all=mirror
end bnds
end data
end
=shell
cp ft04f001 $RTNDIR/ft04f001_pin_void40_20cm
cp restart.keno_calculated $RTNDIR/restart.keno_calculated_pin_void40_20cm
cp restart.keno_input $RTNDIR/restart.keno_input_pin_void40_20cm
end
```

## Appendix C

### NEWT Input for a BWR Bundle Using Dan2pitch

```
'batch_args \-m
=t-newt
bwr with cr replaced by water
v7-238
read composition
uo2      11 den=10.32 1 948.45
          92234 0.0261
          92235 2.93
          92236 0.0135
          92238 97.0304 end
uo2      33 den=10.19 0.97 948.45
          92234 0.0261
          92235 2.93
          92236 0.0135
          92238 97.0304 end
gd2o3    33 den=10.19 0.03 948.45 end
zirc2    101 den=6.56 1 578.71 end
h2o      111 den=0.457211 1 557.96 end
zirc4    111 den=0.046488 1 557.96 end
inconel  111 den=0.008873 1 557.96 end
he       121 den=0.00022218 1 711.15 end
zirc2    301 den=6.56 1 578.71 end
h2o      311 den=0.457211 1 557.96 end
zirc4    311 den=0.046488 1 557.96 end
inconel  311 den=0.008873 1 557.96 end
h2o      314 den=0.457211 1 557.96 end
zirc4    314 den=0.046488 1 557.96 end
inconel  314 den=0.008873 1 557.96 end
uo2      331 den=10.19 0.97 948.45
          92234 0.0261
          92235 2.93
          92236 0.0135
          92238 97.0304 end
gd2o3    331 den=10.19 0.03 948.45 end
uo2      332 den=10.19 0.97 948.45
          92234 0.0261
          92235 2.93
          92236 0.0135
```

Appendix C

92238 97.0304 end  
gd2o3 332 den=10.19 0.03 948.45 end  
uo2 333 den=10.19 0.97 948.45  
92234 0.0261  
92235 2.93  
92236 0.0135  
92238 97.0304 end  
gd2o3 333 den=10.19 0.03 948.45 end  
uo2 334 den=10.19 0.97 948.45  
92234 0.0261  
92235 2.93  
92236 0.0135  
92238 97.0304 end  
gd2o3 334 den=10.19 0.03 948.45 end  
uo2 335 den=10.19 0.97 948.45  
92234 0.0261  
92235 2.93  
92236 0.0135  
92238 97.0304 end  
gd2o3 335 den=10.19 0.03 948.45 end  
uo2 336 den=10.19 0.97 948.45  
92234 0.0261  
92235 2.93  
92236 0.0135  
92238 97.0304 end  
gd2o3 336 den=10.19 0.03 948.45 end  
uo2 337 den=10.19 0.97 948.45  
92234 0.0261  
92235 2.93  
92236 0.0135  
92238 97.0304 end  
gd2o3 337 den=10.19 0.03 948.45 end  
h2o 620 den=0.738079 1 557.96 end  
zirc4 630 den=6.56 1 557.96 end  
h2o 655 den=0.738079 1 557.96 end  
h2o 656 den=0.738079 1 557.96 end  
uo2 112 den=10.32 1 948.45 92234 0.0261 92235 2.93 92236 0.0135 92238 97.0304 end  
he 221 den=0.00022218 1 711.15 end  
zirc2 201 den=6.56 1 578.71 end  
h2o 211 den=0.457211 1 557.96 end  
zirc4 211 den=0.046488 1 557.96 end  
inconel 211 den=0.008873 1 557.96 end  
uo2 113 den=10.32 1 948.45 92234 0.0261 92235 2.93 92236 0.0135 92238 97.0304 end  
he 222 den=0.00022218 1 711.15 end  
zirc2 202 den=6.56 1 578.71 end  
h2o 212 den=0.457211 1 557.96 end

## Appendix C

```
zirc4 212 den=0.046488 1 557.96 end
inconel 212 den=0.008873 1 557.96 end
uo2 114 den=10.32 1 948.45 92234 0.0261 92235 2.93 92236 0.0135 92238 97.0304 end
he 223 den=0.00022218 1 711.15 end
zirc2 203 den=6.56 1 578.71 end
h2o 213 den=0.457211 1 557.96 end
zirc4 213 den=0.046488 1 557.96 end
inconel 213 den=0.008873 1 557.96 end
uo2 115 den=10.32 1 948.45 92234 0.0261 92235 2.93 92236 0.0135 92238 97.0304 end
he 224 den=0.00022218 1 711.15 end
zirc2 204 den=6.56 1 578.71 end
h2o 214 den=0.457211 1 557.96 end
zirc4 214 den=0.046488 1 557.96 end
inconel 214 den=0.008873 1 557.96 end
uo2 116 den=10.32 1 948.45 92234 0.0261 92235 2.93 92236 0.0135 92238 97.0304 end
he 225 den=0.00022218 1 711.15 end
zirc2 205 den=6.56 1 578.71 end
h2o 215 den=0.457211 1 557.96 end
zirc4 215 den=0.046488 1 557.96 end
inconel 215 den=0.008873 1 557.96 end
end composition
```

'----- CELL DATA -----'

read celldata

'The following celldata entry is for unit 33

multiregion cylindrical left\_bdy=reflected right\_bdy=white end

33 0.21418

331 0.3029

332 0.37097

333 0.42836

334 0.47892

335 0.52463

336 0.56666

337 0.60579

314 0.62103

301 0.71501

311 1.01063280159 end zone

centrmdata isn=8 isct=3 iup=25 iscti=3 end centrmdata

'The following celldata entry is for unit 209

latticecell squarep hpitch=0.93726 211 fuelr=0.60579 112 gapr=0.62103 221 cladr=0.71501  
201 end

centrmdata dan2pitch(112)=0.221833 alump=0.3 isn=8 isct=3 iup=25 iscti=3 end  
centrmdata

'The following celldata entry is for unit 34

latticecell squarep hpitch=0.93726 212 fuelr=0.60579 113 gapr=0.62103 222 cladr=0.71501  
202 end

## Appendix C

```
centrmdata dan2pitch(113)=0.382682428571 alump=0.3 isn=8 isct=3 iup=25 iscti=3 end
centrmdata
'The following celldata entry is for unit 15
latticecell squarep hpitch=0.93726 213 fuelr=0.60579 114 gapr=0.62103 223 cladr=0.71501
203 end
centrmdata dan2pitch(114)=0.2944181 alump=0.3 isn=8 isct=3 iup=25 iscti=3 end
centrmdata
'The following celldata entry is for unit 429
latticecell squarep hpitch=0.93726 214 fuelr=0.60579 115 gapr=0.62103 224 cladr=0.71501
204 end
centrmdata dan2pitch(115)=0.209372 alump=0.3 isn=8 isct=3 iup=25 iscti=3 end
centrmdata
'The following celldata entry is for unit 145
latticecell squarep hpitch=0.93726 215 fuelr=0.60579 116 gapr=0.62103 225 cladr=0.71501
205 end
centrmdata dan2pitch(116)=0.2833769 alump=0.3 isn=8 isct=3 iup=25 iscti=3 end
centrmdata
'The following celldata entry is for unit 11
latticecell squarep hpitch=0.93726 111 fuelr=0.60579 11 gapr=0.62103 121 cladr=0.71501
101 end
centrmdata dan2pitch(11)=0.201909 alump=0.3 isn=8 isct=3 iup=25 iscti=3 end centrmdata
end celldata

read model
read parameter
cmfd=yes
xycmfd=2
drawit=yes
echo=yes
epseigen=1e-05
sn=12
timed=yes
converge=mix
prtbalnc=yes
prtmxsec=1d
end parameter
read materials
mix=11 pn=2 com='fuel' end
'Mixture 116 is a copy of mixture 11
mix=116 pn=2 com='fuel' end
'Mixture 114 is a copy of mixture 11
mix=114 pn=2 com='fuel' end
'Mixture 113 is a copy of mixture 11
mix=113 pn=2 com='fuel' end
'Mixture 112 is a copy of mixture 11
mix=112 pn=2 com='fuel' end
```

## Appendix C

'Mixture 115 is a copy of mixture 11  
mix=115 pn=2 com='fuel' end  
mix=33 pn=2 com='fuel with gd' end  
mix=101 pn=2 com='clad' end  
'Mixture 205 is a copy of mixture 101  
mix=205 pn=2 com='clad' end  
'Mixture 204 is a copy of mixture 101  
mix=204 pn=2 com='clad' end  
'Mixture 203 is a copy of mixture 101  
mix=203 pn=2 com='clad' end  
'Mixture 202 is a copy of mixture 101  
mix=202 pn=2 com='clad' end  
'Mixture 201 is a copy of mixture 101  
mix=201 pn=2 com='clad' end  
mix=111 pn=2 com='moderator for normal pin' end  
'Mixture 215 is a copy of mixture 111  
mix=215 pn=2 com='moderator for normal pin' end  
'Mixture 214 is a copy of mixture 111  
mix=214 pn=2 com='moderator for normal pin' end  
'Mixture 213 is a copy of mixture 111  
mix=213 pn=2 com='moderator for normal pin' end  
'Mixture 212 is a copy of mixture 111  
mix=212 pn=2 com='moderator for normal pin' end  
'Mixture 211 is a copy of mixture 111  
mix=211 pn=2 com='moderator for normal pin' end  
mix=121 pn=2 com='gap he' end  
'Mixture 223 is a copy of mixture 121  
mix=223 pn=2 com='gap he' end  
'Mixture 222 is a copy of mixture 121  
mix=222 pn=2 com='gap he' end  
'Mixture 221 is a copy of mixture 121  
mix=221 pn=2 com='gap he' end  
'Mixture 225 is a copy of mixture 121  
mix=225 pn=2 com='gap he' end  
'Mixture 224 is a copy of mixture 121  
mix=224 pn=2 com='gap he' end  
mix=301 pn=2 com='clad for gd pin' end  
mix=311 pn=2 com='moderator for gd pin' end  
mix=314 pn=2 com='moderator for gd pin' end  
mix=331 pn=2 com='fuel and gd' end  
mix=332 pn=2 com='fuel and gd' end  
mix=333 pn=2 com='fuel and gd' end  
mix=334 pn=2 com='fuel and gd' end  
mix=335 pn=2 com='fuel and gd' end  
mix=336 pn=2 com='fuel and gd' end  
mix=337 pn=2 com='fuel and gd' end



## Appendix C

```
mix=620 pn=2 end
mix=630 pn=2 end
mix=655 pn=2 end
mix=656 pn=2 end
end materials
read geometry
unit 11
com="Unit 11"
cylinder 1 0.60579
cylinder 2 0.62103
cylinder 3 0.71501
cylinder 4 0.78501
cuboid 5 0.93726 -0.93726 0.93726 -0.93726
media 11 1 1
media 121 1 2 -1
media 101 1 3 -2
media 111 1 4 -3
media 111 1 5 -4
boundary 5 32 32
' Unit 145 is a copy of unit 11
unit 145
com="Unit 11"
cylinder 1 0.60579
cylinder 2 0.62103
cylinder 3 0.71501
cylinder 4 0.78501
cuboid 5 0.93726 -0.93726 0.93726 -0.93726
media 116 1 1
media 225 1 2 -1
media 205 1 3 -2
media 215 1 4 -3
media 215 1 5 -4
boundary 5 32 32
' Unit 429 is a copy of unit 11
unit 429
com="Unit 11"
cylinder 1 0.60579
cylinder 2 0.62103
cylinder 3 0.71501
cylinder 4 0.78501
cuboid 5 0.93726 -0.93726 0.93726 -0.93726
media 115 1 1
media 224 1 2 -1
media 204 1 3 -2
media 214 1 4 -3
media 214 1 5 -4
```

## Appendix C

```
boundary 5 32 32
' Unit 15 is a copy of unit 11
unit 15
com="Unit 11"
cylinder 1 0.60579
cylinder 2 0.62103
cylinder 3 0.71501
cylinder 4 0.78501
cuboid 5 0.93726 -0.93726 0.93726 -0.93726
media 114 1 1
media 223 1 2 -1
media 203 1 3 -2
media 213 1 4 -3
media 213 1 5 -4
boundary 5 32 32
' Unit 34 is a copy of unit 11
unit 34
com="Unit 11"
cylinder 1 0.60579
cylinder 2 0.62103
cylinder 3 0.71501
cylinder 4 0.78501
cuboid 5 0.93726 -0.93726 0.93726 -0.93726
media 113 1 1
media 222 1 2 -1
media 202 1 3 -2
media 212 1 4 -3
media 212 1 5 -4
boundary 5 32 32
' Unit 209 is a copy of unit 11
unit 209
com="Unit 11"
cylinder 1 0.60579
cylinder 2 0.62103
cylinder 3 0.71501
cylinder 4 0.78501
cuboid 5 0.93726 -0.93726 0.93726 -0.93726
media 112 1 1
media 221 1 2 -1
media 201 1 3 -2
media 211 1 4 -3
media 211 1 5 -4
boundary 5 32 32
unit 33
com="Unit 33"
cylinder 1 0.21418
```

## Appendix C

```
cylinder 2 0.3029
cylinder 3 0.37097
cylinder 4 0.42836
cylinder 5 0.47892
cylinder 6 0.52463
cylinder 7 0.56666
cylinder 8 0.60579
cylinder 9 0.62103
cylinder 10 0.71501
cylinder 11 0.74501
cylinder 12 0.77501
cylinder 13 0.80501
cuboid 14 0.93726 -0.93726 0.93726 -0.93726
media 33 1 1
media 331 1 2 -1
media 332 1 3 -2
media 333 1 4 -3
media 334 1 5 -4
media 335 1 6 -5
media 336 1 7 -6
media 337 1 8 -7
media 314 1 9 -8
media 301 1 10 -9
media 311 1 11 -10
media 311 1 12 -11
media 311 1 13 -12
media 311 1 14 -13
boundary 14 32 32
unit 200
com="control wing half-pellet"
cylinder 10 0.17526 chord -y=0
cylinder 20 0.23876 chord -y=0
cuboid 40 0.23876 -0.23876 0 -0.254
media 656 1 10
media 655 1 -10 20
media 620 1 -20 40
boundary 40 2 1
unit 201
com="control wing half-pellet"
cylinder 10 0.17526 chord +x=0
cylinder 20 0.23876 chord +x=0
cuboid 40 0.254 0 0.23876 -0.23876
media 656 1 10
media 655 1 -10 20
media 620 1 -20 40
boundary 40 1 2
```

## Appendix C

```
unit 202
com="control blade wing"
cuboid 10 10.17016 0 0 -0.39625
array 200 10 place 1 1 0.23876 0
media 655 1 10
boundary 10
unit 203
com="control blade wing"
cuboid 10 0.39625 0 0 -10.17016
array 201 10 place 1 1 0 -9.78916
media 655 1 10
boundary 10
unit 205
com="control blade central support"
cuboid 10 2.21234 0 0 -0.39625
media 655 1 10
boundary 10
unit 206
com="control blade central support - vertical part"
cuboid 10 0.39625 0 -0.39625 -2.21234
media 655 1 10
boundary 10
global unit 100
com="Global Unit 100 references Array 1"
cuboid 1 6.94182 -6.4643 6.4643 -6.94182
array 1 1 place 4 4 0.23876 -0.23876
cuboid 2 7.14502 -6.6675 6.6675 -7.14502
cuboid 10 7.62 -7.62 7.62 -7.62
hole 202 origin x=-5.40766 y=7.62
hole 203 origin x=-7.62 y=5.40766
hole 205 origin x=-7.62 y=7.62
hole 206 origin x=-7.62 y=7.62
media 111 1 1
media 630 1 2 -1
media 620 1 10 -2
boundary 10 24 24
end geometry
read array
ara=1 nux=7 nuy=7 pinpow=yes typ=square
fill
429 15 15 15 15 15 209
145 34 33 34 34 34 15
145 34 34 34 33 34 15
145 34 34 34 34 34 15
145 34 33 34 34 33 15
145 34 34 34 34 34 15
```



Appendix C

143 111 4.62655e-02 -33 32 U=11 tmp=4.8079e-08 imp:n=1 \$ h2o zirc4 inconel  
144 111 4.62655e-02 33 U=11 tmp=4.8079e-08 imp:n=1 \$ h2o zirc4 inconel

C

C Universe 15

90 114 6.90667e-02 -30 U=15 tmp=8.1728e-08 imp:n=1 vol=230.5813 \$ uo2  
91 223 3.34283e-05 -31 30 U=15 tmp=6.128e-08 imp:n=1 \$ he  
92 203 4.32414e-02 -32 31 U=15 tmp=4.9867e-08 imp:n=1 \$ zirc2  
93 213 4.62655e-02 -33 32 U=15 tmp=4.8079e-08 imp:n=1 \$ h2o zirc4 inconel  
94 213 4.62655e-02 33 U=15 tmp=4.8079e-08 imp:n=1 \$ h2o zirc4 inconel

C

C Universe 33

150 33 6.86901e-02 -30 U=33 tmp=8.1728e-08 imp:n=1 vol=8.23252 \$ uo2 gd2o3  
C 151 331 6.86901e-02 -151 150 U=33 tmp=8.1728e-08 imp:n=1 \$ uo2 gd2o3  
C 152 332 6.86901e-02 -152 151 U=33 tmp=8.1728e-08 imp:n=1 \$ uo2 gd2o3  
C 153 333 6.86901e-02 -153 152 U=33 tmp=8.1728e-08 imp:n=1 \$ uo2 gd2o3  
C 154 334 6.86901e-02 -154 153 U=33 tmp=8.1728e-08 imp:n=1 \$ uo2 gd2o3  
C 155 335 6.86901e-02 -155 154 U=33 tmp=8.1728e-08 imp:n=1 \$ uo2 gd2o3  
C 156 336 6.86901e-02 -156 155 U=33 tmp=8.1728e-08 imp:n=1 \$ uo2 gd2o3  
C 157 337 6.86901e-02 -30 156 U=33 tmp=8.1728e-08 imp:n=1 \$ uo2 gd2o3  
158 314 4.62655e-02 -31 30 U=33 tmp=4.8079e-08 imp:n=1 \$ h2o zirc4 inconel  
159 301 4.32414e-02 -32 31 U=33 tmp=4.9867e-08 imp:n=1 \$ zirc2  
160 311 4.62655e-02 32 U=33 tmp=4.8079e-08 imp:n=1 \$ h2o zirc4 inconel  
C 161 311 4.62655e-02 -161 160 U=33 tmp=4.8079e-08 imp:n=1 \$ h2o zirc4 inconel  
C 162 311 4.62655e-02 -162 161 U=33 tmp=4.8079e-08 imp:n=1 \$ h2o zirc4 inconel  
C 163 311 4.62655e-02 162 U=33 tmp=4.8079e-08 imp:n=1 \$ h2o zirc4 inconel

C

C Universe 34

110 113 6.90667e-02 -30 U=34 tmp=8.1728e-08 imp:n=1 vol=484.2207 \$ uo2  
111 222 3.34283e-05 -31 30 U=34 tmp=6.128e-08 imp:n=1 \$ he  
112 202 4.32414e-02 -32 31 U=34 tmp=4.9867e-08 imp:n=1 \$ zirc2  
113 212 4.62655e-02 -33 32 U=34 tmp=4.8079e-08 imp:n=1 \$ h2o zirc4 inconel  
114 212 4.62655e-02 33 U=34 tmp=4.8079e-08 imp:n=1 \$ h2o zirc4 inconel

C

C Universe 330 - The fuel array which will be placed in Universe 100

C Remember that the macrobody being filled (114) is the size of a unit cell!!!

330 0 -41 40 -43 42 LAT=1 imp:n=1 trcl=(0.23876 -0.23876 0)

FILL=-3:3 -3:3 0:0

429 15 15 15 15 15 209  
145 34 33 34 34 34 15  
145 34 34 34 33 34 15  
145 34 34 34 34 34 15  
145 34 33 34 34 33 15  
145 34 34 34 34 34 15  
11 145 145 145 145 145 429 U=330

C

C !!!

Appendix C

C Universe 100

C THIS WAS THE GLOBAL UNIT IN KENO

C

230 0 -50 51 -52 53 u=100 fill=330 imp:n=1 \$ This is for the fuel lattice in universe 330

231 111 4.62655e-02 -60 61 -62 63 (50:-53:-51:52)

U=100 tmp=4.8079e-08 imp:n=1 \$ h2o zirc4 inconel

232 630 4.32487e-02 -70 71 -72 73 (60:-63:-61:62)

U=100 tmp=4.8079e-08 imp:n=1 \$ zirc4

233 620 7.40368e-02 -1 16 -14 4 (70:-73:-71:72)

U=100 tmp=4.8079e-08 imp:n=1 \$ h2o

1233 620 7.40368e-02 -1 11 -3 14 U=100 tmp=4.8079e-08 imp:n=1 \$ h2o

1234 620 7.40368e-02 -16 2 -17 4 U=100 tmp=4.8079e-08 imp:n=1 \$ h2o

C

3420 656 7.40368e-02 -11 2 -3 14 u=100 tmp=4.8079e-08 imp:n=1 \$ Horizontal part of blade

3421 656 7.40368e-02 -16 2 -14 17 u=100 tmp=4.8079e-08 imp:n=1 \$ Vertical part of blade

C

C

250 0 -1 2 -3 4 -5 6 fill=100 imp:n=1 \$ The real world!

251 0 1:-4:-2:3:5:-6 imp:n=0 \$void

C !!!

C

C Universe 145

400 116 6.90667e-02 -30 U=145 tmp=8.1728e-08 imp:n=1 vol=230.5813 \$ uo2

401 225 3.34283e-05 -31 30 U=145 tmp=6.128e-08 imp:n=1 \$ he

402 205 4.32414e-02 -32 31 U=145 tmp=4.9867e-08 imp:n=1 \$ zirc2

403 215 4.62655e-02 -33 32 U=145 tmp=4.8079e-08 imp:n=1 \$ h2o zirc4 inconel

404 215 4.62655e-02 33 U=145 tmp=4.8079e-08 imp:n=1 \$ h2o zirc4 inconel

C

2420 655 7.40368e-02 -12 2 -3 14 -5 6 U=202 tmp=4.8079e-08 imp:n=1 \$ h2o

2421 655 7.40368e-02 -11 12 -13 14 -5 6 U=202 tmp=4.8079e-08 imp:n=1 \$ h2o

C

C Universe 209

130 112 6.90667e-02 -30 U=209 tmp=8.1728e-08 imp:n=1 vol=23.05813 \$ uo2

131 221 3.34283e-05 -31 30 U=209 tmp=6.128e-08 imp:n=1 \$ he

132 201 4.32414e-02 -32 31 U=209 tmp=4.9867e-08 imp:n=1 \$ zirc2

133 211 4.62655e-02 -33 32 U=209 tmp=4.8079e-08 imp:n=1 \$ h2o zirc4 inconel

134 211 4.62655e-02 33 U=209 tmp=4.8079e-08 imp:n=1 \$ h2o zirc4 inconel

C

C Universe 429

70 115 6.90667e-02 -30 U=429 tmp=8.1728e-08 imp:n=1 vol=46.11626 \$ uo2

71 224 3.34283e-05 -31 30 U=429 tmp=6.128e-08 imp:n=1 \$ he

72 204 4.32414e-02 -32 31 U=429 tmp=4.9867e-08 imp:n=1 \$ zirc2

73 214 4.62655e-02 -33 32 U=429 tmp=4.8079e-08 imp:n=1 \$ h2o zirc4 inconel

74 214 4.62655e-02 33 U=429 tmp=4.8079e-08 imp:n=1 \$ h2o zirc4 inconel

C

C !!!1

## Appendix C

\*1 px 7.62  
\*2 px -7.62 \$ This is to make the chord at x=0  
\*3 py 7.62 \$ This is to make the chord at y=0  
\*4 py -7.62  
\*5 pz 10.0  
\*6 pz -10.0  
C 1240 rpp -5.40766 4.6026 7.366 7.62 -10.0 10.0  
C 1240 -11 12 -3 13 -5 6  
C Horizontal Portion  
11 px 4.6026  
12 px -5.40766  
13 py 7.366  
C 2420 rpp -7.62 4.6026 7.22375 7.62 -10.0 10.0  
C 2420 -11 2 -1 14 -5 6  
14 py 7.22375  
C 172 rpp -5.40766 -4.93014 7.366 7.62 -10.0 10.0  
C 172 -15 12 -3 13 -5 6  
15 px -4.93014  
16 px -7.22375  
17 py -4.6026  
C 1241 rpp -7.62 -7.366 -4.62026 5.40766 -10.0 10.0  
C  
18 px -7.366  
C  
30 cz 0.60579  
31 cz 0.62103  
32 cz 0.71501  
33 cz 0.78501  
C  
150 cz 0.21418  
151 cz 0.3029  
152 cz 0.37097  
153 cz 0.42836  
154 cz 0.47892  
155 cz 0.52463  
156 cz 0.56666  
C Now 30  
C Now 31  
C Now 32  
160 cz 0.74501  
161 cz 0.77501  
162 cz 0.80501  
C  
C 163 rpp -0.93726 0.93726 -0.93726 0.93726 -10.0 10.0  
40 px -0.93726  
41 px 0.93726



## Appendix C

42 py -0.93726  
43 py 0.93726  
C  
C Macrobodyes for universe 100  
C 230 rpp -6.32206 6.79958 -6.79958 6.32206 -10.0 10.0  
50 px 6.79958  
51 px -6.32206  
52 py 6.32206  
53 py -6.79958  
C 231 rpp -6.4643 6.94182 -6.94182 6.4643 -10.0 10.0  
60 px 6.94182  
61 px -6.4643  
62 py 6.4643  
63 py -6.94182  
C 232 rpp -6.6675 7.14502 -7.14502 6.6675 -10.0 10.0  
70 px 7.14502  
71 px -6.6675  
72 py 6.6675  
73 py -7.14502  
C

mode n  
kcode 1000000 1.1 100 600  
ksrc 0.23876 -0.23876 0.0  
0.0 0.0 0.0

c  
m11 8016.72c 0.0460444  
92234.72c 6.10942e-06  
92235.72c 0.000682921  
92236.72c 3.13321e-06  
92238.72c 0.0223301

C  
C Dummies for m11  
m1105 92235.72c 0.000682921  
m1108 92238.72c 0.0223301

C  
m33 64160.72c 0.00022204  
92234.72c 5.85149e-06  
92235.72c 0.000654088  
92236.72c 3.00093e-06  
92238.72c 0.0213873  
8016.72c 0.0456241  
64152.72c 2.03151e-06  
64154.72c 2.21431e-05  
64155.72c 0.000150329  
64156.72c 0.000207922

## Appendix C

64157.72c 0.000158963

64158.72c 0.000252309

C

C Dummies for m11

m335 92235.72c 1.0

m338 92238.72c 1.0

m337 64157.72c 1.0

C

m101 40090.71c 0.021891

40091.71c 0.00477389

40092.71c 0.007297

28058.71c 2.52016e-05

40094.71c 0.00739486

40096.71c 0.00119135

26054.71c 5.58197e-06

28060.71c 9.70762e-06

72178.71c 6.03806e-07

28061.71c 4.21983e-07

26056.71c 8.7625e-05

28062.71c 1.34547e-06

72180.71c 7.76449e-07

26058.71c 2.6931e-07

50112.71c 4.68066e-06

28064.71c 3.42651e-07

50114.71c 3.18478e-06

50115.71c 1.64064e-06

50116.71c 7.01616e-05

50117.71c 3.70592e-05

50118.71c 0.000116872

50119.71c 4.14504e-05

50120.71c 0.000157212

26057.71c 2.02364e-06

50122.71c 2.23417e-05

50124.71c 2.79392e-05

72174.71c 3.54138e-09

72176.71c 1.16423e-07

72177.71c 4.11686e-07

24050.71c 3.30121e-06

72179.71c 3.0146e-07

24052.71c 6.36606e-05

24053.71c 7.2186e-06

24054.71c 1.79686e-06

C

m111 40090.71c 0.000155101

40091.71c 3.38237e-05

40092.71c 5.17003e-05

## Appendix C

28058.71c 4.5376e-05  
40094.71c 5.23936e-05  
22047.71c 2.07635e-07  
40096.71c 8.44086e-06  
22049.71c 1.50982e-07  
22050.71c 1.44563e-07  
14028.71c 4.3865e-06  
26054.71c 4.56715e-07  
28060.71c 1.73475e-05  
72178.71c 4.27892e-09  
28061.71c 7.51059e-07  
26056.71c 7.10934e-06  
28062.71c 2.38611e-06  
72180.71c 5.50237e-09  
22046.71c 2.3024e-07  
26058.71c 2.17231e-08  
50112.71c 3.31699e-08  
28064.71c 6.04836e-07  
50114.71c 2.25692e-08  
50115.71c 1.16266e-08  
50116.71c 4.97206e-07  
50117.71c 2.62623e-07  
50118.71c 8.28221e-07  
50119.71c 2.93742e-07  
50120.71c 1.1141e-06  
26057.71c 1.62966e-07  
50122.71c 1.58326e-07  
50124.71c 1.97993e-07  
14029.71c 2.22838e-07  
14030.71c 1.47068e-07  
8016.71c 0.0246789  
1001.71c 0.0493579  
72174.71c 2.50963e-11  
72176.71c 8.25042e-10  
72177.71c 2.91745e-09  
24050.71c 6.93173e-07  
72179.71c 2.13632e-09  
24052.71c 1.33673e-05  
24053.71c 1.51557e-06  
24054.71c 3.77297e-07  
22048.71c 2.05737e-06  
mt111 lwtr.15t \$ h2o S(a,b) scattering kernel at 550K  
C  
m112 8016.72c 0.0460444  
92234.72c 6.10942e-06  
92235.72c 0.000682921

## Appendix C

92236.72c 3.13321e-06

92238.72c 0.0223301

### C Dummies for m112

m1125 92235.72c 1.0

m1128 92238.72c 1.0

### C Dummies for m113

m1135 92235.72c 1.0

m1138 92238.72c 1.0

### C Dummies for m114

m1145 92235.72c 1.0

m1148 92238.72c 1.0

### C Dummies for m115

m1155 92235.72c 1.0

m1158 92238.72c 1.0

### C Dummies for m116

m1165 92235.72c 1.0

m1168 92238.72c 1.0

### C

m113 8016.72c 0.0460444

92234.72c 6.10942e-06

92235.72c 0.000682921

92236.72c 3.13321e-06

92238.72c 0.0223301

### C

m114 8016.72c 0.0460444

92234.72c 6.10942e-06

92235.72c 0.000682921

92236.72c 3.13321e-06

92238.72c 0.0223301

### C

m115 8016.72c 0.0460444

92234.72c 6.10942e-06

92235.72c 0.000682921

92236.72c 3.13321e-06

92238.72c 0.0223301

### C

m116 8016.72c 0.0460444

92234.72c 6.10942e-06

92235.72c 0.000682921

92236.72c 3.13321e-06

92238.72c 0.0223301

### C

m121 2004.71c 3.34283e-05

### C

m201 40090.71c 0.021891

40091.71c 0.00477389

Appendix C

40092.71c 0.007297  
28058.71c 2.52016e-05  
40094.71c 0.00739486  
40096.71c 0.00119135  
26054.71c 5.58197e-06  
28060.71c 9.70762e-06  
72178.71c 6.03806e-07  
28061.71c 4.21983e-07  
26056.71c 8.7625e-05  
28062.71c 1.34547e-06  
72180.71c 7.76449e-07  
26058.71c 2.6931e-07  
50112.71c 4.68066e-06  
28064.71c 3.42651e-07  
50114.71c 3.18478e-06  
50115.71c 1.64064e-06  
50116.71c 7.01616e-05  
50117.71c 3.70592e-05  
50118.71c 0.000116872  
50119.71c 4.14504e-05  
50120.71c 0.000157212  
26057.71c 2.02364e-06  
50122.71c 2.23417e-05  
50124.71c 2.79392e-05  
72174.71c 3.54138e-09  
72176.71c 1.16423e-07  
72177.71c 4.11686e-07  
24050.71c 3.30121e-06  
72179.71c 3.0146e-07  
24052.71c 6.36606e-05  
24053.71c 7.2186e-06  
24054.71c 1.79686e-06

C

m202 40090.71c 0.021891  
40091.71c 0.00477389  
40092.71c 0.007297  
28058.71c 2.52016e-05  
40094.71c 0.00739486  
40096.71c 0.00119135  
26054.71c 5.58197e-06  
28060.71c 9.70762e-06  
72178.71c 6.03806e-07  
28061.71c 4.21983e-07  
26056.71c 8.7625e-05  
28062.71c 1.34547e-06  
72180.71c 7.76449e-07

## Appendix C

26058.71c 2.6931e-07  
50112.71c 4.68066e-06  
28064.71c 3.42651e-07  
50114.71c 3.18478e-06  
50115.71c 1.64064e-06  
50116.71c 7.01616e-05  
50117.71c 3.70592e-05  
50118.71c 0.000116872  
50119.71c 4.14504e-05  
50120.71c 0.000157212  
26057.71c 2.02364e-06  
50122.71c 2.23417e-05  
50124.71c 2.79392e-05  
72174.71c 3.54138e-09  
72176.71c 1.16423e-07  
72177.71c 4.11686e-07  
24050.71c 3.30121e-06  
72179.71c 3.0146e-07  
24052.71c 6.36606e-05  
24053.71c 7.2186e-06  
24054.71c 1.79686e-06

C

m203 40090.71c 0.021891

40091.71c 0.00477389  
40092.71c 0.007297  
28058.71c 2.52016e-05  
40094.71c 0.00739486  
40096.71c 0.00119135  
26054.71c 5.58197e-06  
28060.71c 9.70762e-06  
72178.71c 6.03806e-07  
28061.71c 4.21983e-07  
26056.71c 8.7625e-05  
28062.71c 1.34547e-06  
72180.71c 7.76449e-07  
26058.71c 2.6931e-07  
50112.71c 4.68066e-06  
28064.71c 3.42651e-07  
50114.71c 3.18478e-06  
50115.71c 1.64064e-06  
50116.71c 7.01616e-05  
50117.71c 3.70592e-05  
50118.71c 0.000116872  
50119.71c 4.14504e-05  
50120.71c 0.000157212  
26057.71c 2.02364e-06

Appendix C

50122.71c 2.23417e-05  
50124.71c 2.79392e-05  
72174.71c 3.54138e-09  
72176.71c 1.16423e-07  
72177.71c 4.11686e-07  
24050.71c 3.30121e-06  
72179.71c 3.0146e-07  
24052.71c 6.36606e-05  
24053.71c 7.2186e-06  
24054.71c 1.79686e-06

C

m204 40090.71c 0.021891

40091.71c 0.00477389  
40092.71c 0.007297  
28058.71c 2.52016e-05  
40094.71c 0.00739486  
40096.71c 0.00119135  
26054.71c 5.58197e-06  
28060.71c 9.70762e-06  
72178.71c 6.03806e-07  
28061.71c 4.21983e-07  
26056.71c 8.7625e-05  
28062.71c 1.34547e-06  
72180.71c 7.76449e-07  
26058.71c 2.6931e-07  
50112.71c 4.68066e-06  
28064.71c 3.42651e-07  
50114.71c 3.18478e-06  
50115.71c 1.64064e-06  
50116.71c 7.01616e-05  
50117.71c 3.70592e-05  
50118.71c 0.000116872  
50119.71c 4.14504e-05  
50120.71c 0.000157212  
26057.71c 2.02364e-06  
50122.71c 2.23417e-05  
50124.71c 2.79392e-05  
72174.71c 3.54138e-09  
72176.71c 1.16423e-07  
72177.71c 4.11686e-07  
24050.71c 3.30121e-06  
72179.71c 3.0146e-07  
24052.71c 6.36606e-05  
24053.71c 7.2186e-06  
24054.71c 1.79686e-06

C

## Appendix C

m205 40090.71c 0.021891

40091.71c 0.00477389

40092.71c 0.007297

28058.71c 2.52016e-05

40094.71c 0.00739486

40096.71c 0.00119135

26054.71c 5.58197e-06

28060.71c 9.70762e-06

72178.71c 6.03806e-07

28061.71c 4.21983e-07

26056.71c 8.7625e-05

28062.71c 1.34547e-06

72180.71c 7.76449e-07

26058.71c 2.6931e-07

50112.71c 4.68066e-06

28064.71c 3.42651e-07

50114.71c 3.18478e-06

50115.71c 1.64064e-06

50116.71c 7.01616e-05

50117.71c 3.70592e-05

50118.71c 0.000116872

50119.71c 4.14504e-05

50120.71c 0.000157212

26057.71c 2.02364e-06

50122.71c 2.23417e-05

50124.71c 2.79392e-05

72174.71c 3.54138e-09

72176.71c 1.16423e-07

72177.71c 4.11686e-07

24050.71c 3.30121e-06

72179.71c 3.0146e-07

24052.71c 6.36606e-05

24053.71c 7.2186e-06

24054.71c 1.79686e-06

C

m211 40090.71c 0.000155101

40091.71c 3.38237e-05

40092.71c 5.17003e-05

28058.71c 4.5376e-05

40094.71c 5.23936e-05

22047.71c 2.07635e-07

40096.71c 8.44086e-06

22049.71c 1.50982e-07

22050.71c 1.44563e-07

14028.71c 4.3865e-06

26054.71c 4.56715e-07



## Appendix C

28060.71c 1.73475e-05  
72178.71c 4.27892e-09  
28061.71c 7.51059e-07  
26056.71c 7.10934e-06  
28062.71c 2.38611e-06  
72180.71c 5.50237e-09  
22046.71c 2.3024e-07  
26058.71c 2.17231e-08  
50112.71c 3.31699e-08  
28064.71c 6.04836e-07  
50114.71c 2.25692e-08  
50115.71c 1.16266e-08  
50116.71c 4.97206e-07  
50117.71c 2.62623e-07  
50118.71c 8.28221e-07  
50119.71c 2.93742e-07  
50120.71c 1.1141e-06  
26057.71c 1.62966e-07  
50122.71c 1.58326e-07  
50124.71c 1.97993e-07  
14029.71c 2.22838e-07  
14030.71c 1.47068e-07  
8016.71c 0.0246789  
1001.71c 0.0493579  
72174.71c 2.50963e-11  
72176.71c 8.25042e-10  
72177.71c 2.91745e-09  
24050.71c 6.93173e-07  
72179.71c 2.13632e-09  
24052.71c 1.33673e-05  
24053.71c 1.51557e-06  
24054.71c 3.77297e-07  
22048.71c 2.05737e-06  
mt211 lwtr.15t \$ h2o S(a,b) scattering kernel at 550K  
C  
m212 40090.71c 0.000155101  
40091.71c 3.38237e-05  
40092.71c 5.17003e-05  
28058.71c 4.5376e-05  
40094.71c 5.23936e-05  
22047.71c 2.07635e-07  
40096.71c 8.44086e-06  
22049.71c 1.50982e-07  
22050.71c 1.44563e-07  
14028.71c 4.3865e-06  
26054.71c 4.56715e-07

## Appendix C

28060.71c 1.73475e-05  
72178.71c 4.27892e-09  
28061.71c 7.51059e-07  
26056.71c 7.10934e-06  
28062.71c 2.38611e-06  
72180.71c 5.50237e-09  
22046.71c 2.3024e-07  
26058.71c 2.17231e-08  
50112.71c 3.31699e-08  
28064.71c 6.04836e-07  
50114.71c 2.25692e-08  
50115.71c 1.16266e-08  
50116.71c 4.97206e-07  
50117.71c 2.62623e-07  
50118.71c 8.28221e-07  
50119.71c 2.93742e-07  
50120.71c 1.1141e-06  
26057.71c 1.62966e-07  
50122.71c 1.58326e-07  
50124.71c 1.97993e-07  
14029.71c 2.22838e-07  
14030.71c 1.47068e-07  
8016.71c 0.0246789  
1001.71c 0.0493579  
72174.71c 2.50963e-11  
72176.71c 8.25042e-10  
72177.71c 2.91745e-09  
24050.71c 6.93173e-07  
72179.71c 2.13632e-09  
24052.71c 1.33673e-05  
24053.71c 1.51557e-06  
24054.71c 3.77297e-07  
22048.71c 2.05737e-06

mt212 lwtr.15t \$ h2o S(a,b) scattering kernel at 550K

C

m213 40090.71c 0.000155101

40091.71c 3.38237e-05  
40092.71c 5.17003e-05  
28058.71c 4.5376e-05  
40094.71c 5.23936e-05  
22047.71c 2.07635e-07  
40096.71c 8.44086e-06  
22049.71c 1.50982e-07  
22050.71c 1.44563e-07  
14028.71c 4.3865e-06  
26054.71c 4.56715e-07

## Appendix C

28060.71c 1.73475e-05  
72178.71c 4.27892e-09  
28061.71c 7.51059e-07  
26056.71c 7.10934e-06  
28062.71c 2.38611e-06  
72180.71c 5.50237e-09  
22046.71c 2.3024e-07  
26058.71c 2.17231e-08  
50112.71c 3.31699e-08  
28064.71c 6.04836e-07  
50114.71c 2.25692e-08  
50115.71c 1.16266e-08  
50116.71c 4.97206e-07  
50117.71c 2.62623e-07  
50118.71c 8.28221e-07  
50119.71c 2.93742e-07  
50120.71c 1.1141e-06  
26057.71c 1.62966e-07  
50122.71c 1.58326e-07  
50124.71c 1.97993e-07  
14029.71c 2.22838e-07  
14030.71c 1.47068e-07  
8016.71c 0.0246789  
1001.71c 0.0493579  
72174.71c 2.50963e-11  
72176.71c 8.25042e-10  
72177.71c 2.91745e-09  
24050.71c 6.93173e-07  
72179.71c 2.13632e-09  
24052.71c 1.33673e-05  
24053.71c 1.51557e-06  
24054.71c 3.77297e-07  
22048.71c 2.05737e-06  
mt213 lwtr.15t \$ h2o S(a,b) scattering kernel at 550K  
C  
m214 40090.71c 0.000155101  
40091.71c 3.38237e-05  
40092.71c 5.17003e-05  
28058.71c 4.5376e-05  
40094.71c 5.23936e-05  
22047.71c 2.07635e-07  
40096.71c 8.44086e-06  
22049.71c 1.50982e-07  
22050.71c 1.44563e-07  
14028.71c 4.3865e-06  
26054.71c 4.56715e-07

## Appendix C

28060.71c 1.73475e-05  
72178.71c 4.27892e-09  
28061.71c 7.51059e-07  
26056.71c 7.10934e-06  
28062.71c 2.38611e-06  
72180.71c 5.50237e-09  
22046.71c 2.3024e-07  
26058.71c 2.17231e-08  
50112.71c 3.31699e-08  
28064.71c 6.04836e-07  
50114.71c 2.25692e-08  
50115.71c 1.16266e-08  
50116.71c 4.97206e-07  
50117.71c 2.62623e-07  
50118.71c 8.28221e-07  
50119.71c 2.93742e-07  
50120.71c 1.1141e-06  
26057.71c 1.62966e-07  
50122.71c 1.58326e-07  
50124.71c 1.97993e-07  
14029.71c 2.22838e-07  
14030.71c 1.47068e-07  
8016.71c 0.0246789  
1001.71c 0.0493579  
72174.71c 2.50963e-11  
72176.71c 8.25042e-10  
72177.71c 2.91745e-09  
24050.71c 6.93173e-07  
72179.71c 2.13632e-09  
24052.71c 1.33673e-05  
24053.71c 1.51557e-06  
24054.71c 3.77297e-07  
22048.71c 2.05737e-06

mt214 lwtr.15t \$ h2o S(a,b) scattering kernel at 550K

C

m215 40090.71c 0.000155101

40091.71c 3.38237e-05  
40092.71c 5.17003e-05  
28058.71c 4.5376e-05  
40094.71c 5.23936e-05  
22047.71c 2.07635e-07  
40096.71c 8.44086e-06  
22049.71c 1.50982e-07  
22050.71c 1.44563e-07  
14028.71c 4.3865e-06  
26054.71c 4.56715e-07

## Appendix C

	28060.71c	1.73475e-05
	72178.71c	4.27892e-09
	28061.71c	7.51059e-07
	26056.71c	7.10934e-06
	28062.71c	2.38611e-06
	72180.71c	5.50237e-09
	22046.71c	2.3024e-07
	26058.71c	2.17231e-08
	50112.71c	3.31699e-08
	28064.71c	6.04836e-07
	50114.71c	2.25692e-08
	50115.71c	1.16266e-08
	50116.71c	4.97206e-07
	50117.71c	2.62623e-07
	50118.71c	8.28221e-07
	50119.71c	2.93742e-07
	50120.71c	1.1141e-06
	26057.71c	1.62966e-07
	50122.71c	1.58326e-07
	50124.71c	1.97993e-07
	14029.71c	2.22838e-07
	14030.71c	1.47068e-07
	8016.71c	0.0246789
	1001.71c	0.0493579
	72174.71c	2.50963e-11
	72176.71c	8.25042e-10
	72177.71c	2.91745e-09
	24050.71c	6.93173e-07
	72179.71c	2.13632e-09
	24052.71c	1.33673e-05
	24053.71c	1.51557e-06
	24054.71c	3.77297e-07
	22048.71c	2.05737e-06
mt215	lwtr.15t	\$ h2o S(a,b) scattering kernel at 550K
C		
m221	2004.71c	3.34283e-05
C		
m222	2004.71c	3.34283e-05
C		
m223	2004.71c	3.34283e-05
C		
m224	2004.71c	3.34283e-05
C		
m225	2004.71c	3.34283e-05
C		
m301	40090.71c	0.021891

## Appendix C

40091.71c 0.00477389  
40092.71c 0.007297  
28058.71c 2.52016e-05  
40094.71c 0.00739486  
40096.71c 0.00119135  
26054.71c 5.58197e-06  
28060.71c 9.70762e-06  
72178.71c 6.03806e-07  
28061.71c 4.21983e-07  
26056.71c 8.7625e-05  
28062.71c 1.34547e-06  
72180.71c 7.76449e-07  
26058.71c 2.6931e-07  
50112.71c 4.68066e-06  
28064.71c 3.42651e-07  
50114.71c 3.18478e-06  
50115.71c 1.64064e-06  
50116.71c 7.01616e-05  
50117.71c 3.70592e-05  
50118.71c 0.000116872  
50119.71c 4.14504e-05  
50120.71c 0.000157212  
26057.71c 2.02364e-06  
50122.71c 2.23417e-05  
50124.71c 2.79392e-05  
72174.71c 3.54138e-09  
72176.71c 1.16423e-07  
72177.71c 4.11686e-07  
24050.71c 3.30121e-06  
72179.71c 3.0146e-07  
24052.71c 6.36606e-05  
24053.71c 7.2186e-06  
24054.71c 1.79686e-06

C

m311 40090.71c 0.000155101  
40091.71c 3.38237e-05  
40092.71c 5.17003e-05  
28058.71c 4.5376e-05  
40094.71c 5.23936e-05  
22047.71c 2.07635e-07  
40096.71c 8.44086e-06  
22049.71c 1.50982e-07  
22050.71c 1.44563e-07  
14028.71c 4.3865e-06  
26054.71c 4.56715e-07  
28060.71c 1.73475e-05

## Appendix C

72178.71c 4.27892e-09  
28061.71c 7.51059e-07  
26056.71c 7.10934e-06  
28062.71c 2.38611e-06  
72180.71c 5.50237e-09  
22046.71c 2.3024e-07  
26058.71c 2.17231e-08  
50112.71c 3.31699e-08  
28064.71c 6.04836e-07  
50114.71c 2.25692e-08  
50115.71c 1.16266e-08  
50116.71c 4.97206e-07  
50117.71c 2.62623e-07  
50118.71c 8.28221e-07  
50119.71c 2.93742e-07  
50120.71c 1.1141e-06  
26057.71c 1.62966e-07  
50122.71c 1.58326e-07  
50124.71c 1.97993e-07  
14029.71c 2.22838e-07  
14030.71c 1.47068e-07  
8016.71c 0.0246789  
1001.71c 0.0493579  
72174.71c 2.50963e-11  
72176.71c 8.25042e-10  
72177.71c 2.91745e-09  
24050.71c 6.93173e-07  
72179.71c 2.13632e-09  
24052.71c 1.33673e-05  
24053.71c 1.51557e-06  
24054.71c 3.77297e-07  
22048.71c 2.05737e-06  
mt311 lwtr.15t \$ h2o S(a,b) scattering kernel at 550K  
C  
m314 40090.71c 0.000155101  
40091.71c 3.38237e-05  
40092.71c 5.17003e-05  
28058.71c 4.5376e-05  
40094.71c 5.23936e-05  
22047.71c 2.07635e-07  
40096.71c 8.44086e-06  
22049.71c 1.50982e-07  
22050.71c 1.44563e-07  
14028.71c 4.3865e-06  
26054.71c 4.56715e-07  
28060.71c 1.73475e-05

## Appendix C

72178.71c 4.27892e-09  
28061.71c 7.51059e-07  
26056.71c 7.10934e-06  
28062.71c 2.38611e-06  
72180.71c 5.50237e-09  
22046.71c 2.3024e-07  
26058.71c 2.17231e-08  
50112.71c 3.31699e-08  
28064.71c 6.04836e-07  
50114.71c 2.25692e-08  
50115.71c 1.16266e-08  
50116.71c 4.97206e-07  
50117.71c 2.62623e-07  
50118.71c 8.28221e-07  
50119.71c 2.93742e-07  
50120.71c 1.1141e-06  
26057.71c 1.62966e-07  
50122.71c 1.58326e-07  
50124.71c 1.97993e-07  
14029.71c 2.22838e-07  
14030.71c 1.47068e-07  
8016.71c 0.0246789  
1001.71c 0.0493579  
72174.71c 2.50963e-11  
72176.71c 8.25042e-10  
72177.71c 2.91745e-09  
24050.71c 6.93173e-07  
72179.71c 2.13632e-09  
24052.71c 1.33673e-05  
24053.71c 1.51557e-06  
24054.71c 3.77297e-07  
22048.71c 2.05737e-06

mt314 lwtr.15t \$ h2o S(a,b) scattering kernel at 550K

C

C

m620 8016.71c 0.0246789

1001.71c 0.0493579

mt620 lwtr.15t \$ h2o S(a,b) scattering kernel at 550K

C

m630 40090.71c 0.0218865

40091.71c 0.00477292

40092.71c 0.00729551

40094.71c 0.00739335

40096.71c 0.0011911

26054.71c 8.68307e-06

72178.71c 6.03806e-07



## Appendix C

26056.71c 0.000136306  
72180.71c 7.76449e-07  
26058.71c 4.18926e-07  
50112.71c 4.68066e-06  
50114.71c 3.18478e-06  
50115.71c 1.64064e-06  
50116.71c 7.01616e-05  
50117.71c 3.70592e-05  
50118.71c 0.000116872  
50119.71c 4.14504e-05  
50120.71c 0.000157212  
26057.71c 3.14789e-06  
50122.71c 2.23417e-05  
50124.71c 2.79392e-05  
72174.71c 3.54138e-09  
72176.71c 1.16423e-07  
72177.71c 4.11686e-07  
24050.71c 3.30121e-06  
72179.71c 3.0146e-07  
24052.71c 6.36606e-05  
24053.71c 7.2186e-06  
24054.71c 1.79686e-06

C

m655 8016.71c 0.0246789  
1001.71c 0.0493579  
mt655 lwtr.15t \$ h2o S(a,b) scattering kernel at 550K

C

m656 8016.71c 0.0246789  
1001.71c 0.0493579  
mt656 lwtr.15t \$ h2o S(a,b) scattering kernel at 550K

C

C Scale 238 group neutron library energy structure

e0 1.000E-10 5.000E-10 7.500E-10 1.000E-09 1.200E-09 1.500E-09  
2.000E-09 2.500E-09 3.000E-09 4.000E-09 5.000E-09 7.500E-09 1.000E-08  
2.530E-08 3.000E-08 4.000E-08 5.000E-08 6.000E-08 7.000E-08 8.000E-08  
9.000E-08 1.000E-07 1.250E-07 1.500E-07 1.750E-07 2.000E-07 2.250E-07  
2.500E-07 2.750E-07 3.000E-07 3.250E-07 3.500E-07 3.750E-07 4.000E-07  
4.500E-07 5.000E-07 5.500E-07 6.000E-07 6.250E-07 6.500E-07 7.000E-07  
7.500E-07 8.000E-07 8.500E-07 9.000E-07 9.250E-07 9.500E-07 9.750E-07  
1.000E-06 1.010E-06 1.020E-06 1.030E-06 1.040E-06 1.050E-06 1.060E-06  
1.070E-06 1.080E-06 1.090E-06 1.100E-06 1.110E-06 1.120E-06 1.130E-06  
1.140E-06 1.150E-06 1.175E-06 1.200E-06 1.225E-06 1.250E-06 1.300E-06  
1.350E-06 1.400E-06 1.450E-06 1.500E-06 1.590E-06 1.680E-06 1.770E-06  
1.860E-06 1.940E-06 2.000E-06 2.120E-06 2.210E-06 2.300E-06 2.380E-06  
2.470E-06 2.570E-06 2.670E-06 2.770E-06 2.870E-06 2.970E-06 3.000E-06  
3.050E-06 3.150E-06 3.500E-06 3.730E-06 4.000E-06 4.750E-06 5.000E-06

Appendix C

5.400E-06 6.000E-06 6.250E-06 6.500E-06 6.750E-06 7.000E-06 7.150E-06  
8.100E-06 9.100E-06 1.000E-05 1.150E-05 1.190E-05 1.290E-05 1.375E-05  
1.440E-05 1.510E-05 1.600E-05 1.700E-05 1.850E-05 1.900E-05 2.000E-05  
2.100E-05 2.250E-05 2.500E-05 2.750E-05 3.000E-05 3.125E-05 3.175E-05  
3.325E-05 3.375E-05 3.460E-05 3.550E-05 3.700E-05 3.800E-05 3.910E-05  
3.960E-05 4.100E-05 4.240E-05 4.400E-05 4.520E-05 4.700E-05 4.830E-05  
4.920E-05 5.060E-05 5.200E-05 5.340E-05 5.900E-05 6.100E-05 6.500E-05  
6.750E-05 7.200E-05 7.600E-05 8.000E-05 8.200E-05 9.000E-05 1.000E-04  
1.080E-04 1.150E-04 1.190E-04 1.220E-04 1.860E-04 1.925E-04 2.075E-04  
2.100E-04 2.400E-04 2.850E-04 3.050E-04 5.500E-04 6.700E-04 6.830E-04  
9.500E-04 1.150E-03 1.500E-03 1.550E-03 1.800E-03 2.200E-03 2.290E-03  
2.580E-03 3.000E-03 3.740E-03 3.900E-03 6.000E-03 8.030E-03 9.500E-03  
1.300E-02 1.700E-02 2.500E-02 3.000E-02 4.500E-02 5.000E-02 5.200E-02  
6.000E-02 7.300E-02 7.500E-02 8.200E-02 8.500E-02 1.000E-01 1.283E-01  
1.500E-01 2.000E-01 2.700E-01 3.300E-01 4.000E-01 4.200E-01 4.400E-01  
4.700E-01 4.995E-01 5.500E-01 5.730E-01 6.000E-01 6.700E-01 6.790E-01  
7.500E-01 8.200E-01 8.611E-01 8.750E-01 9.000E-01 9.200E-01 1.010E+00  
1.100E+00 1.200E+00 1.250E+00 1.317E+00 1.356E+00 1.400E+00 1.500E+00  
1.850E+00 2.354E+00 2.479E+00 3.000E+00 4.304E+00 4.800E+00 6.434E+00  
8.187E+00 1.000E+01 1.284E+01 1.384E+01 1.455E+01 1.568E+01 1.733E+01  
2.000E+01

phys:n 20.0 1.0e-11

C

C Tallies

C FM4 num\_dens dum\_mat\_num RX\_num, -6(18) for fission, -2(101)for abs

C

FC4 Tally 2 is for universe 11, U-235 Absorption

F4:N 140

FM4 0.000682921 1105 -2

C

FC14 Tally 12 is for universe 11, U-235 Fission

F14:N 140

FM14 0.000682921 1105 -6

C

FC24 Tally 22 is for universe 11, U-238 Absorption

F24:N 140

FM24 0.0223301 1108 -2

C

FC34 Tally 32 is for universe 11, U-238 Fission

F34:N 140

FM34 0.0223301 1108 -6

C

C !!!!!!!!!!! Universe 33 - Has Gd !!!!!!!!!!!!!!!!!!!!!

FC44 For universe 33, U-235 Absorption

F44:N 150

FM44 0.000654088 335 -2

Appendix C

C

FC54 For universe 33, U-235 Fission

F54:N 150

FM54 0.000654088 335 -6

C

FC64 For universe 33, U-238 Absorption

F64:N 150

FM64 0.0213873 338 -2

C

FC74 For universe 33, U-238 Fission

F74:N 150

FM74 0.0213873 338 -6

C

FC84 For universe 33, Gd-157 Absorption

F84:N 150

FM84 0.000158963 337 -2

C

C !!!!!!!!!!!!! Tallies for universe 15 !!!!!!!!!!!!!!!!!!!!!

FC94 For universe 15, U-235 Absorption

F94:N 90

FM94 0.000682921 1145 -2

C

FC104 For universe 15, U-235 Fission

F104:N 90

FM104 0.000682921 1145 -6

C

FC114 For universe 15, U-238 Absorption

F114:N 90

FM114 0.0223301 1148 -2

C

FC124 For universe 15, U-238 Fission

F124:N 90

FM124 0.0223301 1148 -6

C

C !!!!!!!!!!!!! Tallies for universe 34 !!!!!!!!!!!!!!!!!!!!!

FC134 For universe 34, U-235 Absorption

F134:N 110

FM134 0.000682921 1135 -2

C

FC144 For universe 34, U-235 Fission

F144:N 110

FM144 0.000682921 1135 -6

C

FC154 For universe 34, U-238 Absorption

F154:N 110

FM154 0.0223301 1138 -2

## Appendix C

C

FC164 For universe 34, U-238 Fission

F164:N 110

FM164 0.0223301 1138 -6

C

C !!!!!!!!!!!!! Tallies for universe 209 !!!!!!!!!!!!!

FC174 For universe 209, U-235 Absorption

F174:N 130

FM174 0.000682921 1125 -2

C

FC184 For universe 209, U-235 Fission

F184:N 130

FM184 0.000682921 1125 -6

C

FC194 For universe 209, U-238 Absorption

F194:N 130

FM194 0.0223301 1128 -2

C

FC204 For universe 209, U-238 Fission

F204:N 130

FM204 0.0223301 1128 -6

C

C !!!!!!!!!!!!! Tallies for universe 429 !!!!!!!!!!!!!

FC214 For universe 429, U-235 Absorption

F214:N 70

FM214 0.000682921 1155 -2

C

FC224 For universe 429, U-235 Fission

F224:N 70

FM224 0.000682921 1155 -6

C

FC234 For universe 429, U-238 Absorption

F234:N 70

FM234 0.0223301 1158 -2

C

FC244 For universe 429, U-238 Fission

F244:N 70

FM244 0.0223301 1158 -6

C

C !!!!!!!!!!!!! Tallies for universe 145 !!!!!!!!!!!!!

FC254 For universe 145, U-235 Absorption

F254:N 400

FM254 0.000682921 1165 -2

C

FC264 For universe 145, U-235 Fission

F264:N 400

## Appendix C

FM264 0.000682921 1165 -6

C

FC274 For universe 145, U-238 Absorption

F274:N 400

FM274 0.0223301 1168 -2

C

FC284 For universe 145, U-238 Fission

F284:N 400

FM284 0.0223301 1168